



**ICEBE**  
IMAGINEERING  
NATURE

## DIPLOMARBEIT

# **Experimental investigation on SNG production from biomass gasification**

ausgeführt zum Zwecke der Erlangung des akademischen Grades eines  
Diplomingenieurs unter der Leitung von

Univ.Prof. Dipl.-Ing. Dr.techn. Hermann Hofbauer

am

Institut für Verfahrenstechnik, Umwelttechnik und Technische Biowissenschaften

betreut von

Univ.-Prof. Dipl.-Ing. Dr.techn. Hermann Hofbauer

Dipl.-Ing. Alexander Bartik

eingereicht an der Technischen Universität Wien

Fakultät für Maschinenwesen und Betriebswissenschaften

von

**Maria Giovanna Abagnale**

Matrikelnummer 11946194

Getreidemarkt 9/166

1060 Wien

Wien, am 08.09.2021

# Table of contents

<b>1</b>	<b>INTRODUCTION</b> .....	<b>1</b>
<b>2</b>	<b>STATE OF THE ART</b> .....	<b>4</b>
2.1	SNG PRODUCTION ROUTES.....	4
2.2	GASIFICATION .....	6
2.2.1	<i>Suitable reactor types</i> .....	8
2.2.2	<i>Dual Fluidized Bed technology</i> .....	12
2.3	METHANATION UPSTREAM TREATMENTS .....	15
2.4	METHANATION FUNDAMENTALS.....	19
2.4.1	<i>Thermodynamic analysis</i> .....	19
2.4.2	<i>Catalyst choice and deactivation mechanisms</i> .....	23
2.5	METHANATION PROCESSES.....	26
2.5.1	<i>Fixed bed reactor processes</i> .....	26
2.5.2	<i>Fluidized bed reactor processes</i> .....	32
2.6	FLUIDIZATION TECHNOLOGY.....	35
<b>3</b>	<b>EXPERIMENTAL SETUP</b> .....	<b>43</b>
3.1	DESCRIPTION OF THE EXPERIMENTAL RIG.....	43
3.2	CATALYST ACTIVATION BY REDUCTION .....	45
3.3	RELEVANT VARIABLES DEFINITION .....	47
<b>4</b>	<b>RESULTS</b> .....	<b>48</b>
4.1	TEST RUN 1: STOICHIOMETRIC CO METHANATION WITH $WHSV=1.3 \text{ NL}\cdot\text{H}^{-1}\cdot\text{G}_{\text{CAT}}^{-1}$ AND VARIABLE FLUIDIZATION RATIO .....	49
4.2	TEST RUN 2: STOICHIOMETRIC CO METHANATION WITH $WHSV=1.8 \text{ NL}\cdot\text{H}^{-1}\cdot\text{G}_{\text{CAT}}^{-1}$ AND VARIABLE FLUIDIZATION RATIO .....	55
4.3	TEST RUN 3: STOICHIOMETRIC CO METHANATION WITH VARIABLE TEMPERATURE .....	60
4.4	TEST RUN 4: UNDER-STOICHIOMETRIC CO <sub>2</sub> METHANATION WITH VARIABLE TEMPERATURE .....	65
4.5	TEST RUN 5: STOICHIOMETRIC CO <sub>2</sub> METHANATION WITH VARIABLE TEMPERATURE.....	70
4.6	TEST RUN 6: OVER-STOICHIOMETRIC CO <sub>2</sub> METHANATION WITH VARIABLE TEMPERATURE.....	76
4.7	TEST RUN 7: COMBINED STOICHIOMETRIC CO AND CO <sub>2</sub> METHANATION WITH VARIABLE TEMPERATURE AND $WHSV=1.2 \text{ NL}\cdot\text{H}^{-1}\cdot\text{G}_{\text{CAT}}^{-1}$ .....	81
4.8	TEST RUN 8: COMBINED STOICHIOMETRIC CO AND CO <sub>2</sub> METHANATION WITH VARIABLE TEMPERATURE AND $WHSV=1.5 \text{ NL}\cdot\text{H}^{-1}\cdot\text{G}_{\text{CAT}}^{-1}$ .....	87
<b>5</b>	<b>DISCUSSION OF RESULTS AND SUMMARY</b> .....	<b>92</b>
<b>6</b>	<b>CONCLUSION AND OUTLOOK</b> .....	<b>97</b>
	<b>NOTATION</b> .....	<b>99</b>
	SYMBOLS.....	99
	ABBREVIATIONS .....	102

LIST OF TABLES .....	103
LIST OF FIGURES .....	106
ANNEX .....	FEHLER! TEXTMARKE NICHT DEFINIERT.

## Abstract

Since Natural Gas (NG) is not an unlimited resource and greenhouse gas emissions are continuously increasing, the option to replace it with Synthetic Natural Gas (SNG) is being considered interesting. This thesis has been fully carried out at TU Wien (Austria) and focuses on the study of a concept for SNG production by thermo-chemical gasification of biogenic residues and subsequent methanation. Results of thermodynamic investigation and experimental tests are presented. Different Product Gas (PG) compositions resulting from gasification processes are fed to a bench-scale Internally Circulated Fluidized Bed reactor (ICFB), where methanation takes place. By means of research on availability, effectiveness and price, Ni/Al<sub>2</sub>O<sub>3</sub> has been identified as the optimal catalyst and the influence of parameters such as temperature and inlet flowrate on methanation efficiency has been analysed. The results obtained show that CO methanation is more favoured than CO<sub>2</sub> and combined methanations. The desired temperature level was efficiently controlled thanks to the great heat transfer ability of the fluidized bed reactor. Methane yields up to 92 % are obtained in this experimental investigation. On the basis of the obtained results, this methanation process can become a well-established downstream technology for the Dual Fluidized Bed (DFB) gasification concept developed at the TU Wien.

## Abstract (Italiano)

Poiché il gas naturale (NG) non è una risorsa illimitata e le emissioni di gas serra sono in continuo aumento, parte della ricerca internazionale si sta focalizzando sulla possibilità di sostituirlo con gas naturale sintetico (SNG). In questa tesi, interamente svolta presso la TU Wien (Austria), viene presentato un processo di produzione di SNG mediante gassificazione termochimica di residui biogenici e successiva metanazione. I risultati dell'indagine termodinamica e quelli dei test sperimentali sono presentati in questo lavoro di tesi. Diverse composizioni di gas prodotto (PG) risultanti dai processi di gassificazione sono alimentate ad un reattore a letto fluido a circolazione interna (ICFB) su scala reale, dove avviene la metanazione. Attraverso ricerche su disponibilità, efficacia e prezzo, il Ni/Al<sub>2</sub>O<sub>3</sub> è stato identificato come catalizzatore ottimale ed è stata analizzata l'influenza sull'efficienza di metanazione di parametri come la temperatura e la portata in ingresso. I risultati ottenuti mostrano che la metanazione di CO è più favorita della metanazione di CO<sub>2</sub> e di quella combinata. Il livello di temperatura desiderato è stato controllato in modo efficiente grazie alla grande capacità di trasferimento del calore del reattore a letto fluidizzato. In questa indagine sperimentale sono state ottenute rese di metano fino al 92%. Sulla base dei risultati ottenuti, la tecnologia considerata può diventare consolidata per il concetto di gassificazione a doppio letto fluido (DFB) sviluppato presso la TU Wien.

## Kurzfassung

Da Erdgas (NG) keine unbegrenzte Ressource ist und die Treibhausgasemissionen kontinuierlich zunehmen, wird die Option, es durch synthetisches Erdgas (SNG) zu ersetzen, als interessant angesehen. Diese Arbeit wurde vollständig an der TU Wien (Österreich) durchgeführt und konzentriert sich auf die Untersuchung eines Konzepts für die SNG-Produktion durch thermochemische Vergasung biogener Rückstände und anschließende Methanisierung. Ergebnisse thermodynamischer Untersuchungen und experimenteller Tests werden vorgestellt. Verschiedene Produktgaszusammensetzungen (PG), die aus Vergasungsprozessen resultieren, werden einem intern zirkulierten Wirbelschichtreaktor (ICFB) im Labormaßstab zugeführt, in dem die Methanisierung stattfindet. Durch Untersuchungen zu Verfügbarkeit, Wirksamkeit und Preis wurde Ni/Al<sub>2</sub>O<sub>3</sub> als optimaler Katalysator identifiziert und der Einfluss von Parametern wie Temperatur und Einlassdurchfluss auf die Methanisierungseffizienz analysiert. Die erhaltenen Ergebnisse zeigen, dass die CO-Methanisierung gegenüber CO<sub>2</sub> und kombinierten Methanisierungen bevorzugt ist. Das gewünschte Temperaturniveau wurde dank der großen Wärmeübertragungsfähigkeit des Fließbettreaktors effizient gesteuert. Bei dieser experimentellen Untersuchung werden Methanausbeuten von bis zu 92% erhalten. Auf der Grundlage der erzielten Ergebnisse kann dieser Methanisierungsprozess zu einer etablierten Downstream-Technologie für das an der TU Wien entwickelte Vergasungskonzept des Dual Fluidized Bed (DFB) werden.

## Acknowledgements

The results presented in this thesis are part of the project ReGas4Industry funded by the “Klima- und Energiefonds” and carried out under the “Energieforschung” program. The work has been accomplished in cooperation with “Energy and Chemical Engineering GmbH” and “SMS group Process Technologies GmbH”. Further thanks are given to Hermann Hofbauer and Alexander Bartik, members of the research platform “Future Energy Technology” at the Institute of Chemical Engineering at the TU Wien.



# 1 Introduction

In most of the countries, the production of fuels and chemicals is oil or natural gas (NG) based. Unfortunately, these reserves are not unlimited [1] and they are not equally distributed among the different countries all over the world. Being dependent on NG and oil means to be dependent on imports from other states. In particular, Austria and Italy imported 72% and 79%, respectively, of their total energy supply in 2018 [2]-[3]. Furthermore, oil and NG are fossil fuels. Their extreme usage is the main reason of the high greenhouse emissions level which is reached nowadays [4]. Greenhouse emissions results to be one of the main issues for global warming and the consequent global climate change [5].

In order to reduce these undesired phenomena, an alternative energy source should be found. In particular, it is possible to think about synthetic or substitute natural gas (SNG). SNG is a versatile energy carrier which is interchangeable with NG. Moreover, it can be produced through a high efficiency process from sustainable and domestic feedstocks such as biomass. SNG can be distributed in the already existing gas distribution infrastructures such as NG pipelines and it can be directly utilized in well-established end use technologies, e.g. heating, compressed natural gas cars (CNG), power stations, combined heat and power (CHP) [6]. These are aspects not to be overlooked when assessing its applicability in the current energy system. Replacing part of the NG with SNG, could make a great contribution in the replacement of European fossil fuels consumption with biomass derived fuels. In particular, the European Commission aims to replace up to 20% of fossil fuels [7]. Specifically, the environmental impact of SNG has been compared with the one of other biofuels and a reduction down to 30% of the greenhouse emissions of petrol without any significant penalty in other aspects has been assessed [8].

There are different ways to produce this alternative energy source. One option we have, is to convert biomass into SNG through a gasification with a subsequent methanation. This process reaches a quite high overall chemical efficiency of 65% [9]. Biomass are gasified through a thermo-chemical gasification which generates the product gas (PG), a gaseous stream mainly composed of carbon monoxide (CO) and hydrogen (H<sub>2</sub>). The PG can be used as the educt to produce different synthetic materials, e.g. methanol, Fischer-Tropsch (FT) fuels, mixed alcohols, SNG, dimethylether (DME). However, the simplest way to use PG remains its direct combustion for industrial heating and co-firing, without the necessity of cleaning or upgrading it. On the contrary, the production of synthetic products requires a specific gas composition and an ultra-clean gas. Thus, it will be necessary to operate an extensive gas cleaning and gas upgrading in the majority of the cases [10].

When the PG is sufficiently cleaned and/or upgraded, it is sent to the desired synthesis process, which in our case is the methanation one. Even if there are several plants which produce methane (CH<sub>4</sub>) from PG, this kind of process is still under investigation for many different aspects. Methanation is a strongly exothermic reaction with a large decrease in the number of moles. This feature could represent one of

the key issues of the process, because high temperatures can induce catalyst deactivation due to sintering of metal particles, carbon deposition and sulphur poisoning. Thus, heat removal is a fundamental parameter to evaluate [11].

The different SNG production routes will be illustrated through this work and an overview of the state of the art of gasification and methanation processes will be given. Particular attention will be paid to the very efficient dual fluidized bed (DFB) technology, which was developed in TU Wien for the biomass gasification. This technology, was demonstrated for the first time in Güssing (Austria) and it has been realized in other industrial plants at a scale of 8-32 MW fuel input in Austria, Germany and Sweden [12]. In particular, it is possible to think to the gasifier in Göteborg, which is based on the existing small plant of Güssing. Subsequently, methanation upstream processes will be described. Currently, there are different gas cleaning and upgrading strategy. The cleaning section includes different components removal, e.g. tar, chlorine, nitrogen, sulphur. Gas upgrading is used to get a better PG composition, in order to improve methanation performances.

Concerning the methanation step, a more detailed treatment will be done. First of all, a fundamental aspect as thermodynamic will be presented. Thermodynamic calculations are fundamental parts of a careful investigation for the SNG production. Through them, it is possible to provide a good estimation of the expected outlet gas composition [13]. Furthermore, the used catalyst will be presented, and its particular choice will be justified. Different methanation attested technologies will be later introduced. Both fixed and fluidized bed reactors processes will be illustrated. A final subchapter concerning fluidization technology will be added.

Furthermore, experimental investigations over an Internally Circulated Fluidized Bed (ICFB) methanation reactor will be operated. In this way, the different methanation parameters found in literature could be compared to the experimental obtained ones. Different operating conditions will be investigated, concerning different variables e.g. temperature,  $H_2/CO$  ratio,  $H_2/CO_2$  ratio, flowrates, fluidization ratios. All these analyses will be done starting from the theoretical evidence founded in literature. A  $Ni/Al_2O_3$  catalyst will be used, the temperature range investigated will be 250-500 °C and the different experimented PG compositions will derive from the different biomass gasification results.

The essential aim of this work is to demonstrate the suitability of the utilisation of wood or biogenic residues to produce SNG and to realize a satisfactory methanation in a newly built ICFB reactor.

## **Research questions**

Different challenges and question marks are the reason for the continuous research operated concerning the SNG production. Biomass composition could be very complicated, and they could contain different undesired heteroatoms. This could lead to the necessity of more expensive cleaning and upgrading operations. A careful trade-off analysis should be done between the gasified biomass and the

cleaning/upgrading adopted strategy.

The methanation results to be a very exothermic reaction. For this purpose, the less expensive and at the same time more efficient heat removal method should be detected. This could be one of the points to analyse in order to choose the reactor type among fixed or fluidized bed.

The usage of a fluidized bed for methanation is quite complicated. The catalyst is subject to attrition phenomena and there is the possibility of its entrainment with the gaseous product, out of the reactor. Another challenge consists in the scale-up process. Fluid-dynamics result to be strongly influenced from the reactor size. Thus, the increase of the reactor dimensions is a very complicated procedure, that requires detailed fluid-dynamics models.

Nowadays, the best active metal for the methanation catalyst results to be Nickel but nothing prevents to seek for an even better solution. In particular, the smart choice of the Nickel catalyst support could bring countless benefits. Even the catalyst particles type or dimension could influence its deactivation process and the synthesis efficiency itself. The latter parameter results to be the most important one needed to render a process commercially available and to scale up a methanation reactor, which is only at the pilot, or bench-scale.



## 2 State of the art

Despite many research and demonstration efforts have been carried out during the last four decades, there are only a few biomass gasification and methanation technologies that are available at the market so far. Concerning biomass gasification, from the 1980s to the 2000s, CHP production has been investigated and demonstrated at the industrial scale. In the last two decades, more attention is given to the cleaning and the upgrading of the PG to syngas quality [12]. Furthermore, several synthesis reactions have been studied and continuous efforts are currently done in the field of methanation.

### 2.1 SNG production routes

SNG is a versatile energy carrier, which is interchangeable with NG from fossil sources. Thus, if its methane content is higher than a certain value, e.g. higher than 96% in Austria [14], and it has been cleaned from sulphur and/or other pollutants, it can be easily injected into the existing NG grid. There are different ways to produce it and different technologies which could be employed [7]. The chosen production route is fundamental in terms of the feed methanation composition and consequently in the resulting global production efficiency. The different SNG production routes are shown in Figure 1.

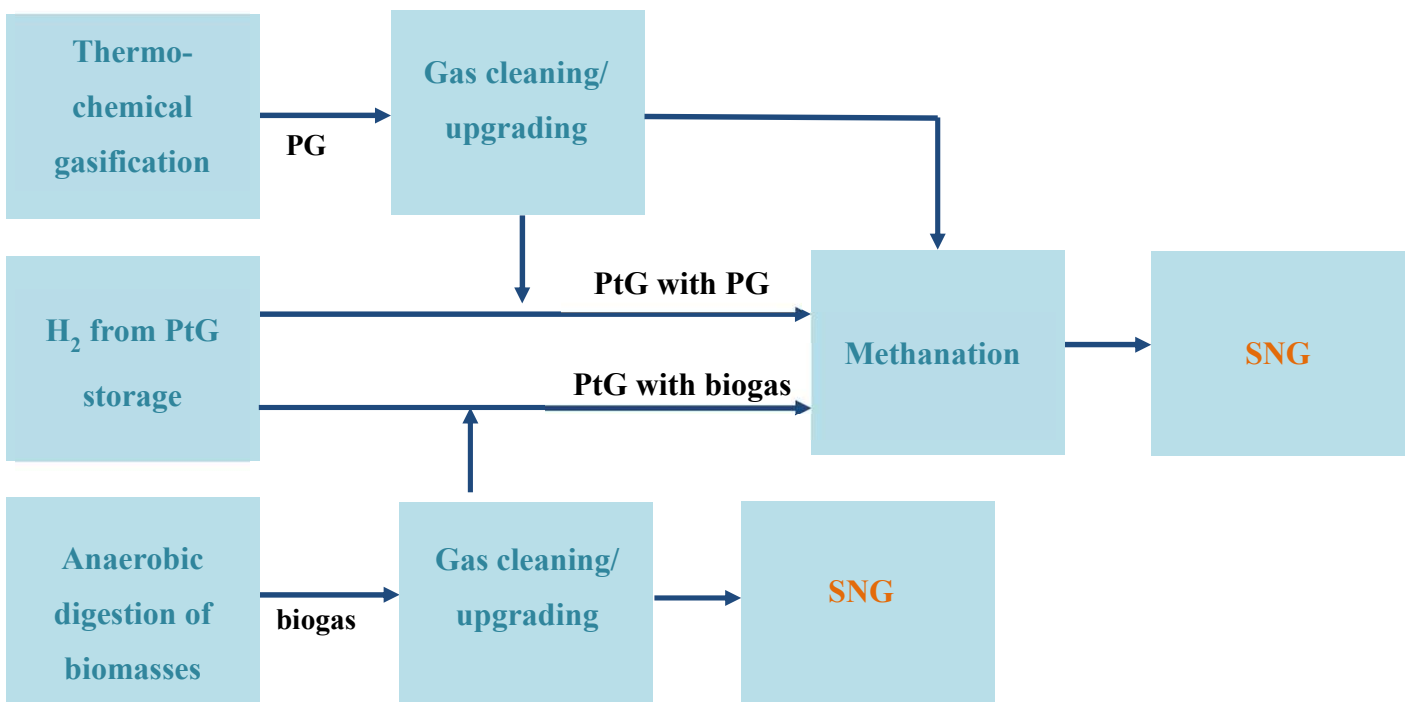
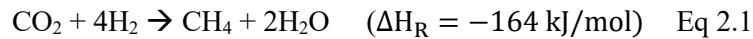


Figure 1: Different SNG production routes

Concerning biomass gasification, different biomass types should be converted with different processes. Anaerobic digestion is employed for plant-based biomass. From this procedure, a high quantity of carbon dioxide (CO<sub>2</sub>) is obtained as a by-product and this leads to a low overall chemical efficiency of about 20-40% [9]. Specifically, the biogas obtained, is usually composed approximately of 50% CH<sub>4</sub> and 50% CO<sub>2</sub> [7]. For this reason and because of the difficulty encountered in operating digestion of woody biomass, a thermo-chemical gasification is preferred for the latter ones. This kind of gasification is an endothermic reaction, and it is necessary to provide heat to power up the process [12]. The obtained PG can have different compositions, which are dependent on the heat supply method, on the gasification agent and on the gasified biomass composition.

Both the biogas and the PG can be purified and/or upgraded and further converted through the catalytical methanation step. Moreover, the cleaned and/or upgraded biogas can also be directly used as SNG without a further methanation. One fundamental reactant of methanation is hydrogen. While in the PG it is already present, in the biogas there is no hydrogen. Furthermore, in order to send the biogas stream to the methanation step, H<sub>2</sub> has to be added while its addition to the PG is just an option. The needed hydrogen can be produced through water electrolysis. The electricity employed in it could be the occasionally available excess electricity, from stochastic sources such as wind or solar power. In this power to gas (PtG) hydrogen production, electric energy is converted into chemical energy for storage [14].

For the PtG hydrogen with a biogas stream, the most observed reaction is the CO<sub>2</sub> methanation:



As we can see from its stoichiometry, an optimal H<sub>2</sub>/CO<sub>2</sub> ratio equal to 4 enhances the SNG production. Actually, the optimal H<sub>2</sub>/CO<sub>2</sub> ratio to employ is equal to 4.1. The slight excess of hydrogen is due to its beneficial action regarding both the carbon deposition on the catalyst and the selectivity to methane. Using a stream exclusively composed by CO<sub>2</sub> and H<sub>2</sub>, means to have a higher heat of reaction which is not a desired effect [7]. Furthermore, high amounts of hydrogen from stochastic sources should be added to the biogas and this constitute an additional cost.

If PG is sent to the methanation plant, both with the PtG hydrogen addition or not, the most observed reaction is the CO methanation:



CO<sub>2</sub> methanation also occur, but to a lesser extent. In this case, the stoichiometric CO/H<sub>2</sub> ratio is 3. Thus, a ratio equal to 3.1 with a slight excess of hydrogen, for the same reasons already discussed for the biogas case, is the optimal one. The stoichiometric composition in the methanation feed, has both the

disadvantage of the higher heat of reaction and the need to remove or convert all the higher hydrocarbons contained in the gasification PG [7]. This means, that a more complex purification/upgrading step should be implemented. From the thermo-chemical gasification of biomass, the standard H<sub>2</sub>/CO ratio obtained in the PG is usually between 0.3 and 2 [9]. For this reason, addition of the PtG hydrogen can be implemented to increase it. Another alternative is to send the PG to an upstream water gas shift (WGS) reactor (not shown in the figure) [15]. Building another reactor is an additional cost, but at the same time the cost of adding hydrogen will be reduced. There is also the possibility to realize the WGS simultaneously with methanation:



For this purpose, is necessary to adjust the water content before the synthesis step [7]. Another possible pathway is represented by the usage of calcite as a bed material for gasification. In this way, it is possible to realize the sorption enhanced reforming (SER). This particular type of gasification, leads to the direct production of a hydrogen-rich PG [12].

Table 1 shows the expected feed gas compositions for the different SNG production routes discussed above.

**Table 1: Typical methanation feed gas compositions [7].**

	H <sub>2</sub> /CO=3.1	Allothermal Gasification	Autothermal Gasification	H <sub>2</sub> /CO <sub>2</sub> =4.1 Power to Gas	Power to Gas with Biogas	Power to Gas with Product Gas
[mol%]						
H <sub>2</sub>	75.6	30-40	25-30	80.4	62.1-67.2	70-75
CO	24.4	20-30	16-57	0	0	10-12
CO <sub>2</sub>	0	20	2-36	19.6	15.2-16.4	10-12
CH <sub>4</sub>	0	10	5-12	0	16.4-22.7	4-5
C <sub>2</sub> H <sub>2</sub>	0	0-1	0-0.5	0	0	0-0.5
C <sub>2</sub> H <sub>4</sub>	0	1-4	0-3	0	0	1-2.5
C <sub>2</sub> H <sub>6</sub>	0	0-1	0-0.5	0	0	0-0.5

## 2.2 Gasification

Thermo-chemical gasification of biomass is potentially a great opportunity to make the energy system more sustainable. Different large-scale biomass gasification, with capacities larger than 10 MW, are nowadays commercially available [12]. One successful gasification technology is represented by the DFB reactor, developed at TU Wien [10]. A broad commercialization is still hindered by the lack of experience, some negative examples of the past years and not fully satisfactory economic performances. Nevertheless, the gasification remains a key technology which is able to generate clean energy from biomass and agricultural residues.

Before giving an overview of the different gasification processes, basic principles of thermo-chemical gasification are introduced. Basically, it is defined as a partial oxidation process and it is operated at high temperatures (400-1500 °C). The resulting product, defined as PG, is a gas consisting mainly of CO, H<sub>2</sub>, CO<sub>2</sub> and CH<sub>4</sub> [16]. A biomass particle undergoes different steps during thermo-chemical gasification. Being all endothermic processes, heat supply is needed. The heat supply could be done in two different ways: the gasification can be autothermal when the heat is generated in the reaction chamber where the gasification reaction takes place. While it is allothermal when the heat necessary for the gasification process is generated externally and delivered to the gasifier through a heat exchanger or a heat carrier media. The different endothermic steps are drying, devolatilization and gasification. During devolatilization about 80% of the biomass weight is released and only about 20% remains in the form of char. Figure 2 shows these different steps of thermo-chemical gasification [12].

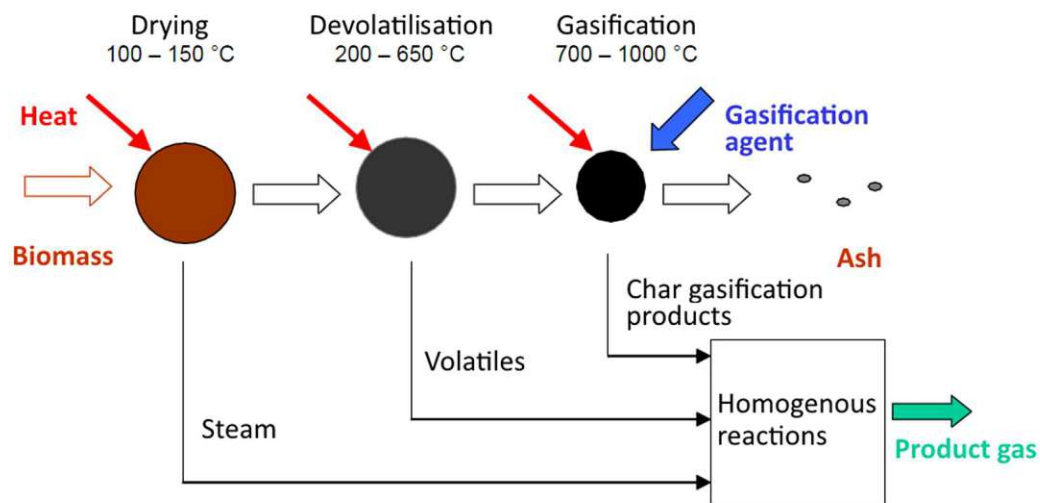


**Figure 2: Processes during gasification of a single particle [12]**

Furthermore, different gasification agents can be used. The choice of this agent influences the PG composition. The most common gasification agent remains air and it gives a PG with a high nitrogen (N<sub>2</sub>) content [12]. Other widely used gasification agents are oxygen, steam, CO<sub>2</sub>, hydrogen, oxygen-enriched air and oxygen/steam mixtures. By employing them, a lower nitrogen content in the PG can be obtained. High nitrogen content should be avoided in the PG, because it is an undesired inert agent for the synthesis steps. Employing steam as gasification agent means to have higher heating value and H<sub>2</sub> content of the PG with respect to the ones obtained when using air [17]. Autothermal gasifications, can be operated through the usage of air, oxygen or oxygen/steam mixtures as gasification agents. In these processes, a partial biomass combustion is realized inside the gasification reactor itself. Allothermal gasifications are instead carried out only with steam or CO<sub>2</sub> as gasification agents. In this case, the heat necessary for gasification is supplied indirectly through a heat exchanger or a heat carrier [12].

Table 2 shows the different PG compositions obtained with different gasification agents [18].

**Table 2: Gasification agents and the resulting PG compositions [18].**

Gasification agents	Hydrogen	Carbon monoxide	Carbon dioxide	Methane	Water	Nitrogen
O <sub>2</sub> -enriched air	26.2	31.25	10.15	1.65	7.87	22.87
Steam	48.92	35.27	5.83	0.31	7.48	0
O <sub>2</sub>	34.13	41.51	11.81	2.81	8.98	0.75
Air	19.78	23.19	8.91	0.94	7.03	39.65

We can observe that the highest value of hydrogen production is obtained when using steam as gasification agent. Specifically, the usage of steam also corresponds to the situation of maximum energetic efficiency: calorific values of the PG can be higher than 1.1 MJ/Nm<sup>3</sup> [18]. Moreover, the gasifier developed at TU Wien uses steam as gasification agent.

The main reactions of gasification and combustion observed during the process are shown in in Table 3. Most of them are endothermic and this makes the global process quite highly endothermic.

**Table 3: Most relevant reactions in the gasification process [19].**

Name of reaction		Enthalpy	
Heterogeneous reactions (gas-solid)			
Primary water-gas reaction	$C + H_2O \rightarrow CO + H_2$	131 kJ/mol	Eq. 2.4
Boudouard reaction	$C + CO_2 \rightarrow 2 CO$	172 kJ/mol	Eq. 2.5
Methane formation	$C + 2 H_2 \rightarrow CH_4$	-74.8 kJ/mol	Eq. 2.6
Homogeneous reactions (gas-gas)			
Water-gas shift	$CO + H_2O \leftrightarrow CO_2 + H_2$	-41.2 kJ/mol	Eq. 2.3
Methane steam reforming	$CH_4 + H_2O \rightarrow CO + 3 H_2$	206 kJ/mol	Eq. 2.7

### 2.2.1 Suitable reactor types

Different types of gasifiers which have been implemented for biomass gasification are presented. Their classification is based on fluid mechanical properties and thus, it is possible to distinguish between the fixed bed, the entrained flow and the fluidized bed reactors [12].

#### Fixed bed gasifiers

Fixed bed gasifiers consist of a bed of solid fuel particles, which can be typically biomass, through

which a gasification agent move either up or down. The simplest type of gasifier has a cylindrical shape. This kind of reactors are commonly classified according to the way in which the gasifying agent enters in them: in an updraft gasifier the gasifying medium moves upwards, while in a downdraft gasifier you have the opposite flow direction. Concerning the fuel bed, it moves slowly down the reactor as the gasification occurs [16]. Specifically, for large-scale gasifiers only updraft operations have been used [12].

Fixed bed gasifiers are mostly implemented using air as gasification agent and they are mainly applied for electricity production. Concerning the SNG production, the majority of the commissioned reactors consist of updraft fixed bed coal gasifiers. They use as gasification agent an oxygen/steam mixture in order to obtain a high methane amount into the PG, which results favourable for all the process chain [7]. A schematic figure of a typical fixed bed gasifiers is presented in Figure 3 [12].

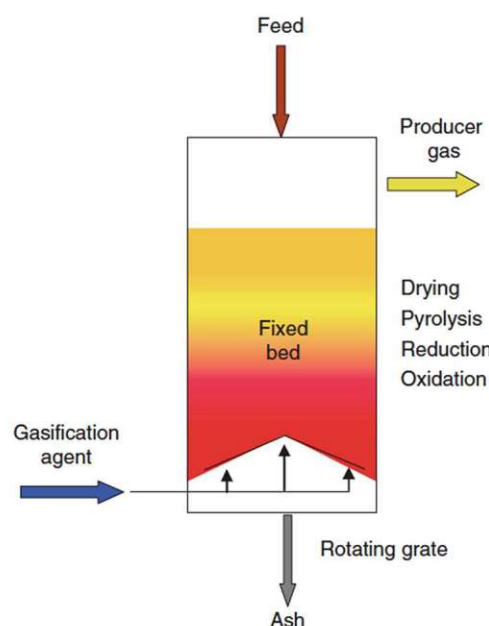


**Figure 3 : Typical arrangement for an updraft fixed bed gasifier [12].**

Coal particles, whose size goes from below 1 cm to few centimetres, are fed from the top of the reactor and they form a slowly downwards moving bed. Oxygen and steam are conversely injected from the bottom, establishing a hot combustion zone at the bottom of the reactor. The moving coal is subjected to an increasing temperature and undergo consecutively drying, pyrolysis and gasification. The resulting PG exits from the top of the reactor and it contains steam, which consists of the unreacted one and of the one derived from the drying step, tars from pyrolysis, gasification and combustion products. Among the gasification products, methane is contained in the PG at 5-10% [7]. Most gasifiers used for PG generation from coal, e.g. at Sasol, have been shut down recently, but a lot of experience is available from operation of many years [12].

### Entrained flow gasifiers

In entrained flow reactors, gasification takes place within few seconds of biomass pneumatic transport through the reactor [12]. Biomass particles with a small diameter, less than 1 mm, and a high temperature ( $>1200^{\circ}\text{C}$ ) are required in order to achieve gasification in such a short time. The feedstock and the gasification agent, which even in this case is usually a steam/oxygen mixture, are fed together from the top of the vessel and are gasified while being entrained together with the produced gas [7].

Gasification takes place in the upper part of the reactor, while in the lower part the PG is quenched with water and separated from ash particles. Ashes are collected from the bottom and PG is exiting from the side section of the gasifier. Working at these high temperatures results in having no tars and hydrocarbons production but mainly carbon monoxide, hydrogen and steam [7]. Moreover, the PG will also have a very low methane content, which can be less than 1%. This configuration is mainly implemented before synthesis steps which produce liquid fuels e.g. FT, DME. Figure 4 shows a typical configuration of an entrained flow gasifier [12].

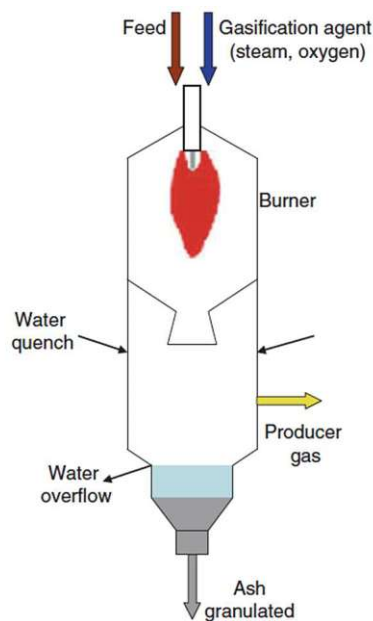


**Figure 4: Entrained flow gasifier standard configuration [12].**

### Fluidized bed gasifiers

Fluidized bed gasifiers use a bed material able to be easily and stably fluidized and that enhances the mass and heat transfer conditions. Improving the heat exchange in the reactor means that it can operate under nearly isothermal conditions [20]. The bed material can have different properties: it can be catalytically active; it can act as a  $\text{CO}_2$  carrier in case of SER gasification or even as a heat carrier for allothermal gasifiers. Furthermore, the gas which fluidizes the bed material, acts also as gasification agent. It is possible to distinguish between two types of fluidized bed reactors, which are dependent on superficial gas velocities: stationary (bubbling) and fast (circulating) fluidized beds [12]. Gas velocity in bubbling beds is relatively low, typically below 1 m/s, while in the circulating beds it is usually

between 3 and 10 m/s [20].

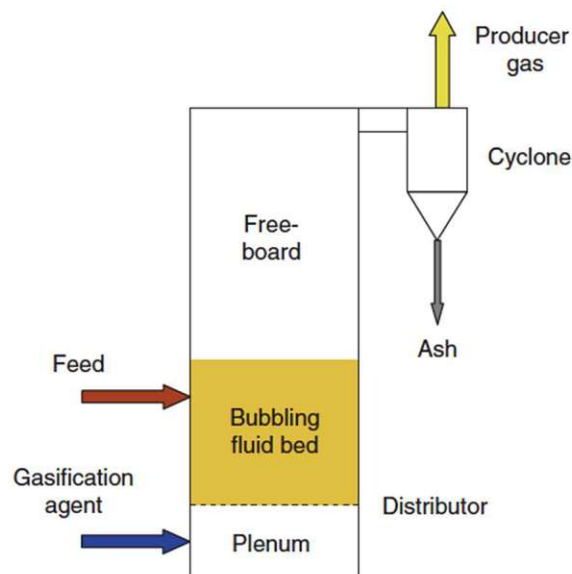


**Figure 5: Typical cross-sectional view of a bubbling fluidized bed gasifier [12].**

For stationary fluidized beds, the gasification agent most often used is a steam/oxygen mixture. The gas is typically blown into the vessel from the bottom, through a special distributor. Solid biofuel is fed directly inside the fluidized bed, where most of the reaction takes place [20]. PG leaves the reactor through the freeboard on the top, where it is cooled and separated from the ash and the entrained bed material by means of a cyclone. Figure 5 shows its usual layout [12].

Fast fluidized beds are totally filled with a gas/particle suspension whose density varies along the reactor height [12]. Due to the high gas velocities in it, the bed material particles are continuously entrained to the top of the vessel. These particles are separated from the gas in the cyclone and recirculated to the bottom of the reactor [20]. The feed layout stays the same and the gasification agent is mostly made of an oxygen/steam mixture too. A secondary cyclone is needed to counteract the high entrainment speed of the particles and to further separate the ash from the PG. A fast fluidized bed gasifier is shown in figure 6 [12].



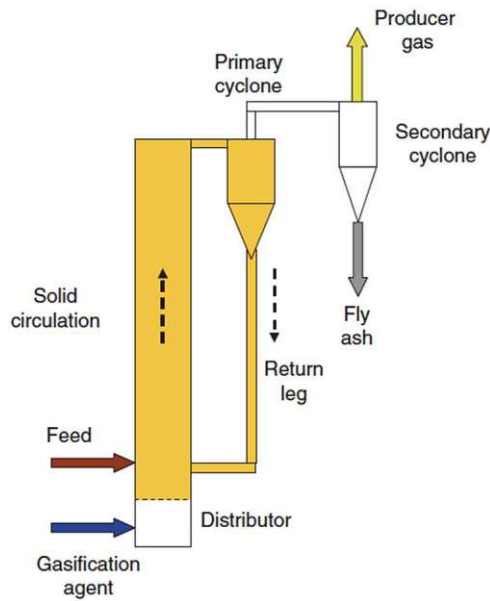


**Figure 6: Fast fluidized bed configuration [12].**

The maximum operating temperature for both the configurations is limited by the melting point of the bed material and is typically between 700 and 900 °C. At these relatively low temperatures, the chemical equilibrium is not reached and thus, the PG will inevitably contain hydrocarbons like tars and methane [20]. Furthermore, there are two configurations also in terms of heat supply. In the autothermal fluidized bed, the partial biomass combustion is realized inside the gasification reactor chamber itself, while in the allothermal fluidized bed, heat supply is done through an external heat carrier media [12]. There is not a single reactor configuration and thus, it is not possible to define a general PG composition obtained by a fluidized bed gasification reactor.

### 2.2.2 Dual Fluidized Bed technology

Dual fluidized bed (DFB) is an advanced layout of allothermal fluidized bed, and it has specific advantages especially for syngas production with biomass as feedstock. The principle of this operation is based on two interconnected reactors: one for gasification (usually fluidized with steam) and one for combustion (fluidized with air) in order to generate the heat necessary for the gasification process [12]. The bed material and the char, produced from the gasification process, are transported from the gasification reactor (GR) to the combustion reactor (CR). In the CR, the oxidation of char with air generates the heat with which the bed material is heated up. Circulating the hot bed material allows to transport the heat from the CR to the GR, powering up the gasification process [20].

The DFB is nowadays investigated in different configurations. By combining the two different fluidization states previously discussed, three different combinations are possible: two bubbling beds, one bubbling bed and one fast bed or two fast beds. In figure 7 a DFB with a bubbling fluidized bed for

the gasification reactor and a fast fluidized bed for the combustion reactor is presented [12].

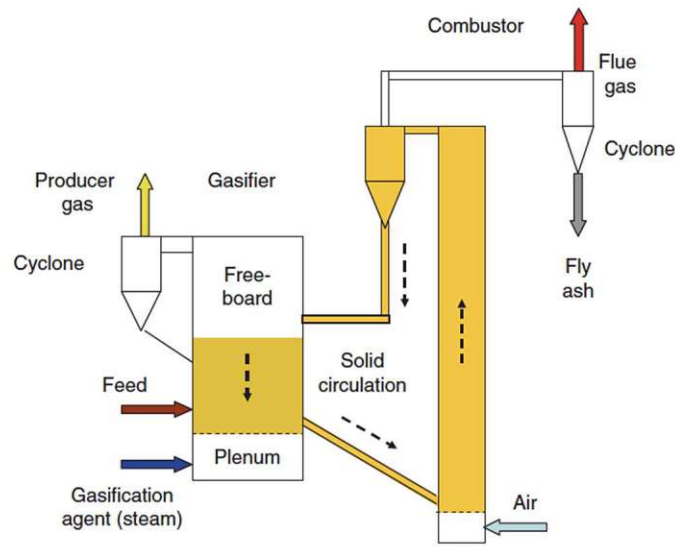


Figure 7: Dual fluidized bed scheme [12].

The basic idea is to generate a nitrogen free PG from a solid biogenic fuel without the necessity of using pure oxygen. Air separation, which is a very expensive process, can be avoided when using this kind of reactor. A steam fluidized loop seal is usually employed to circulate the bed particles between the two reactors. The basic principles of a classic DFB gasifier are shown in Figure 8 [10]. The solid fuel is fed into the GR where drying, devolatilization and gasification of particles are performed at temperatures between 750 and 850 °C. Both the remaining char and the bed material are transported to the CR which works at temperatures of around 900-970 °C. If needed, additional fuel can be introduced into the CR in order to reach a specific temperature level. After the combustion step, the heated bed material is circulated again into the GR in order to provide the heat for gasification.

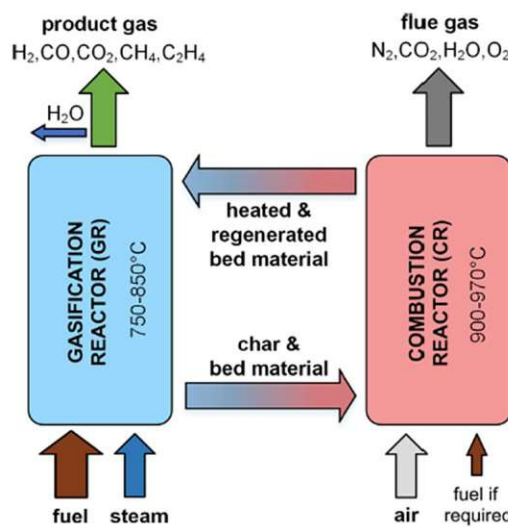
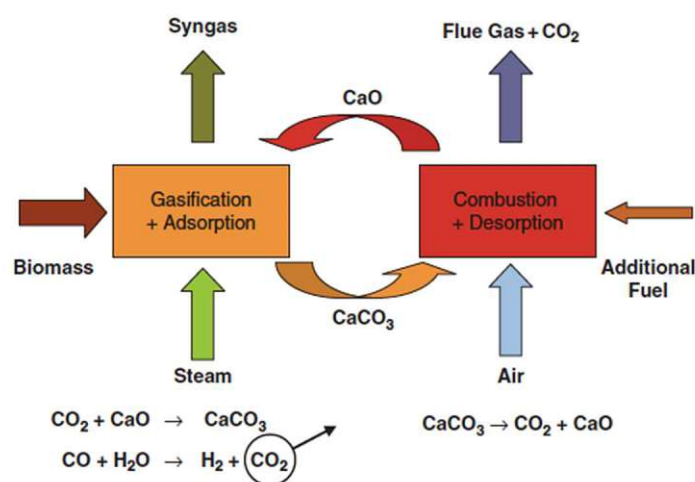


Figure 8: Basic principles of a classic DFB gasifier [10].

The PG obtained from this forefront technology does not contain nitrogen, which is an undesired inert for the downstream synthesis steps [10]. Additionally, the PG generated by the DFB reactor contains less CO<sub>2</sub> and more hydrogen and methane than autothermal fluidized bed gasification reactors. Larger amounts of H<sub>2</sub> and CH<sub>4</sub> are desired for the subsequent production of SNG [20].

The choice of the bed material is fundamental because it is used as heat carrier, as catalyst for gasification and it can be further used to capture gaseous components and transport them to the other reactor. Calcite (calcium carbonate: CaCO<sub>3</sub>) is an interesting catalyst to employ in DFB in order to realize the SER process. In the CR, CaCO<sub>3</sub> is split off in CO<sub>2</sub> and CaO. CaO is then circulated in the GR where gasification takes place and the CO<sub>2</sub> produced is captured by CaO to form again CaCO<sub>3</sub>. The CO<sub>2</sub> removal from the gasifier, enhances the WGS reaction and further hydrogen production becomes favored. For this purpose, it is necessary to operate at specific temperature levels: the temperature in the GR must be decreased to 600-700 °C, while the CR must operate at temperatures of 830-930 °C [21]. An explicative scheme of this global process is shown in figure 9 [12].



**Figure 9: SER process [12].**

SER process leads to the production of a hydrogen rich PG. Specifically, the PG obtained from SER could reach a H<sub>2</sub>/CO ratio up to five times higher with respect to the one obtained with the standard gasification process. Moreover, calcite is more active for tar removal than standard gasification catalysts as olivine and for this reason, the same tar content is obtained even if working at lower temperatures. Consequently, also the PG will be released at lower temperatures and this allows to the utilisation of fuels with low ash melting behaviour. Moreover, working at lower temperatures means also a higher process efficiency [21]. Table 4 resumes the advantages of using the SER process for biomass gasification compared to using a standard olivine gasification process. With a higher temperature level, CO<sub>2</sub> capturing is reduced and consequently also the hydrogen production [12]. The SER process also

has the advantage of being able to increase the H<sub>2</sub>/CO ratio in situ [21]. Therefore, it is possible to adapt the SER process to different syntheses used downstream.

**Table 4: Different gasification products obtained with different bed materials [12].**

Component	Conventional olivine 850 °C	SER calcite 650 °C
Hydrogen (vol%)	35-45	66-74
Carbon monoxide(vol%)	22-25	5-8
Carbon dioxide (vol%)	20-23	6-8
Methane (vol%)	9-11	10-12
Ethylene (vol%)	2-3	1.1
H <sub>2</sub> /CO	1.6-1.8	8-10

## 2.3 Methanation upstream treatments

Thermochemical biomass gasification generates a PG mainly composed by hydrogen, carbon monoxide, carbon dioxide, steam and methane but it also contains sulphur, chlorine and nitrogen, which are present as impurities in the gasification feedstock, tars, char and soot which derive from an incomplete gasification [22]. These contaminants would reduce the performance of the downstream SNG synthesis process. In order to prevent this from happening, an efficient gas cleaning is needed. On the other hand, PG will be sent to a catalytic step and thus, a specific composition is a fundamental requisite. Gas conditioning is the answer to this need, and it leads to the desired H<sub>2</sub>/CO ratio. The amount of impurities is dependent on the gasification feedstock: woody biomass have significantly less sulphur, chlorine and nitrogen than coal [7]. Furthermore, different types of gasifiers give different contaminants levels. Specifically, fluidized bed gasifiers produce less tar but more dust with respect to fixed bed ones [23].

PG unfortunately contains many different types of contaminants that need to be removed. Moreover, each contaminant has its own drawback and therefore a different reason for being removed. Sulphur contaminants are present mostly as hydrogen sulphide (H<sub>2</sub>S) and in lower amounts as carbonyl sulphide (COS). Sulphur compounds, even if present in a small amount, gives rise to three different problems: they are corrosive for metal surfaces, they are poisons for the catalyst and if burned, they are responsible for the SO<sub>2</sub> formation and consequently for acid rains [22]. Tar is a complex and sticky mixture of hydrocarbons, mostly aromatic. Being it condensable at ambient temperature, it can cause damages due to its condensation in low-temperature zones of downstream applications resulting in fouling of pipes and inhibition of the catalytically active centers [23].

Particulate matter includes solid particles which can be unconverted mass (char, soot) and inorganic

compounds (ashes) but also entrained bed material particles. They could generate fouling, erosion and corrosion of the equipment [7]. Chlorine is usually present in the form of HCl and derives from the vaporization of alkali metal salts present in the biomass and their consequent reaction with steam. Even if its amount is relatively low if compared to the other contaminants, it is very corrosive and it can react with nitrogen impurities generating compounds which are responsible of fouling and erosion. Moreover, chlorinated species are poisons for the SNG catalyst [22]. Finally, nitrogen compounds which are mainly present as  $\text{NH}_3$  but also in small amounts of HCN, give rise to  $\text{NO}_x$  if in contact with oxygen and this makes necessary a very expensive exhaust gas treatment. Furthermore, the presence of undesired ammonia, can also neutralize the acid catalysts making their action irrelevant [7].

PG cleaning technologies are classified according to the gas temperature exiting the clean-up device. It is possible to distinguish between hot gas cleaning ( $T > 400\text{ °C}$ ), cold gas cleaning ( $T < 100\text{ °C}$ ) and warm ones characterized by intermediate temperatures [7]. Cold gas cleaning technologies are already mature processes, and they are still the most widely used today. These techniques have the drawbacks of giving huge waste absorbent streams that need to be regenerated. Furthermore, cooling down the extremely hot stream resulting from the gasification process is energy intense. Hot gas cleaning techniques received great attention in the recent years. Working at higher temperatures means avoiding the wasteful cooling and the reheating necessary for the downstream methanation step. In this way, it would be possible to improve the energy efficiency of the entire process chain. Hot gas cleaning technologies are at present still under development because they have many technical difficulties [22]. Being each contaminant of different nature, it can be removed with a specific procedure.

Particulate matter is constituted by solid particles with different diameters: smaller particles are very difficult to remove while bigger ones turn out to be easily removed. The hot gas cleaning implemented for these particles is based on three different physical principles: inertial separation through cyclones, barrier filtration and electrostatic precipitation [22]. Cyclone separators can also be integrated at the exit of the gasifier [23]. On the other hand, the cold gas cleaning used to remove particulate matter consists of a wet scrubber which usually uses water as scrubbing agent. Cold gas scrubbing can be characterized by different configurations: spray scrubbers, wet dynamic scrubbers, cyclonic spray scrubbers, impactor scrubbers, venturi scrubbers and electrostatic scrubbers. They are listed with increasing removal efficiency for micro particles [22]. To achieve the complete removal of impurities by using wet scrubbers, large and expensive columns are required [7].

Tars are made of condensable organic compounds. They vary from heavier deoxygenated to lighter oxygenated and polycyclic aromatics. Thermochemical processes as gasification produce more than thousands different tar species, therefore it is very difficult to define correctly their composition. Tars content in the PG decreases with gasification temperature and residence time, thus a first method to avoid it is to operate gasification with higher temperatures and contact times [22]. Moreover, concerning

the downstream hot gas cleaning, tars are removed with three different approaches: physical separation, non-catalytic and catalytic tar removal. Physical methods aim is to cool the PG under a certain temperature level, e.g.  $T < 450\text{ }^{\circ}\text{C}$ , leading to the condensation and the formation of aerosols from tar. Devices as cyclones, electrostatic precipitators and barrier filters are implemented. Non-catalytic tar removal includes thermal cracking process, whose purpose is to decompose tars into lighter hydrocarbons through its exposition at high temperatures. Its advantage is its simplicity, but it also has several disadvantages as the loss of process efficiency, due to the need to heat, and the necessity to use expensive alloys resistant at high temperatures. Furthermore, the decomposition of tars can be initiated by reactive plasma species, which are reactive atmospheres of free radicals, ions and other excited molecules. This method is not yet applied industrially due to the high cost, the high energy demand and the operational complexity [7].

Concerning the catalytic tar removal, catalytic cracking is the most used process. Its purpose is to get closer to equilibrium conditions in order to increase the tar decomposition reaction rates [22]. Catalytic removal can be applied in situ or downstream the gasifier. In the first case, the catalytic cracking catalyst is added to the gasification bed material, while in the second case separate reactors, e.g. fixed beds and monoliths, are used. Concerning cold gas cleaning devices, wet scrubbers are implemented in order to remove tars from the PG. Lower operating temperatures of the wet scrubber means more tars condensate and easier removal. High removal efficiencies can be obtained by using venturi and vortex scrubbers [7].

Sulphur contaminants are mostly present as hydrogen sulphide ( $\text{H}_2\text{S}$ ) and sometimes as carbonyl sulphide (COS). After combustion, the sulphur exists in the form of sulphur dioxide ( $\text{SO}_2$ ) [7]. The sulphur content depends on the gasification feedstock and biomass generate a PG with less sulphur with respect to the one obtained from coal gasification. High temperature sulphur removal is performed by adsorbing  $\text{SO}_2$  and  $\text{H}_2\text{S}$  over solid materials including metal oxides based on Zn, Fe, Cu, Mn, Mo, Co and V. On the other hand, at low temperatures level physical or chemical absorption is implemented to remove acid gases as  $\text{H}_2\text{S}$  and even  $\text{CO}_2$ . The chemical absorption of acid gases is operated through the use of liquid solvents which are typically basic and the most widely used are ethanolamines, while physical absorption implements liquid methanol and dimethyl ether at cryogenic temperatures [22].

Nitrogen is contained in the PG mainly as ammonia ( $\text{NH}_3$ ), and in small amounts as hydrogen cyanide (HCN). During gasification, nitrogen is released from heterocyclic aromatics present inside the feedstocks. The amount of  $\text{NH}_3$  and HCN inside the PG is strongly dependent on the nitrogen content of the feed and on the temperature level of the gasification step. Operating gasification at higher temperatures means increasing both the  $\text{NH}_3$  and the HCN content in the PG. Hot gas cleaning of nitrogen compounds consists of ammonia decomposition rather than its removal. Thus, one possibility is to use selective catalytic oxidation to  $\text{N}_2$ ,  $\text{H}_2$  and inevitably  $\text{NO}_x$ . Another option is the thermal

catalytic decomposition in which  $\text{NH}_x$  molecules are dehydrogenated and then N and H radicals are recombined to form  $\text{H}_2$  and  $\text{N}_2$ . The most common used cold cleaning in order to remove  $\text{NH}_3$  and HCN is absorption in water. Ammonia is highly soluble in water and this makes it a common absorption liquid for ammonia removal. Even by condensing the water vapour contained in the PG it is possible to remove the nitrogen dissolved in it. In particular, partial condensation of water operated in chilled condensers results in more than 90% reduction in  $\text{NH}_3$  and a further addition of water improves the removal efficiencies [22].

Chlorides are mostly present in the form of hydrochloric acid (HCl) in the PG but they is also present in solid particles of ammonium chloride ( $\text{NH}_4\text{Cl}$ ) because of HCl reaction with  $\text{NH}_3$  [7]. HCl derives from the reaction of the vaporized alkali metal salts contained in biomass with water vapour. The evaporation of alkali metal salts results to be significant at the high temperatures of the gasifiers. Two high temperature processes are employed to reduce alkali concentrations in the PG: removal with other contaminants via condensation and hot adsorption on solid sorbents which exclusively removes HCl. Below the alkali condensation temperature, alkali vapours nucleate and agglomerate on particulate matter, thus they will be easily removed as solids simultaneously with particulate, tars and  $\text{NH}_4\text{Cl}$  in cold wet scrubbers. As solid sorbents activated carbon, alumina and common alkali oxides in fixed beds are mostly used. Being chlorine compounds water soluble, they are mainly removed at low temperatures through wet scrubbers [22].

Downstream methanation synthesis needs a  $\text{H}_2/\text{CO}$  ratio approximately equal to 3 in order to maximize the methane yields. However, PG from biomass gasifiers has usually  $\text{H}_2/\text{CO}$  ratio between 0.3 and 2. A higher ratio should be set before feeding the gas to the synthesis reactor and this is done through the gas conditioning step. The solution may be to implement SER gasification or to use a separated water gas shift reactor in order to have a higher hydrogen amount in the PG. Water gas shift reaction is shown below:



It is a slightly exothermic reaction, and it is performed between 300 °C and 400 °C. The high steam content in the gasified biomass provides already a steam source for the WGS reaction. Catalysts used for this reaction are iron/chromium oxides based ( $\text{Fe}_2\text{O}_3/\text{CrO}$ ) but also Nickel catalyses this reaction. In some cases, this reaction is running in parallel in the synthesis reactor, without the necessity of a separate step which is more expensive in terms of equipment costs. Another gas conditioning step consists in the  $\text{CO}_2$  removal. Carbon dioxide is both produced by gasification itself, due to chemical equilibrium reasons, and by WGS reaction.  $\text{CO}_2$  is removed as an acid gas with chemical or physical absorption, similarly to  $\text{H}_2\text{S}$ . Gasification PG may contain also small amounts of higher hydrocarbons, e.g. ethylene, which cause problems in the long-term stability of the catalyst and should be removed upstream the methanation step [9]. Specifically,  $\text{C}_2$  species can be converted to carbon oxides through steam

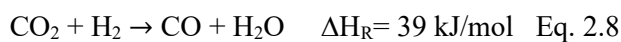
reforming over nickel or noble metals. Another possibility is the conversion of ethylene by hydrogenation into less reactive species [7].

## 2.4 Methanation fundamentals

The third step of the SNG production is the methanation reaction itself. The composition of the feed gas depends on the gasification technology, on the cleaning and on the conditioning step. Feed gas composition strongly influences the methanation efficiency: SER derived product gas, which is richer in hydrogen, leads to a higher carbon efficiency, while in PG from conventional gasification the necessity of simultaneous WGS is increased. Therefore, part of the carbon monoxide is not converted in methane but reacts through the WGS reaction which allows to reach the stoichiometric H<sub>2</sub>/CO ratio [7]. Additionally, proper management of operating parameters in the methanation reactor is essential. Varying temperature and pressure can lead to a thermodynamic optimization of the synthesis and consequently to the reduction in energy costs. In order to have a more detailed view of the synthesis step, thermodynamics and catalyst choice are analysed in special subsections.

### 2.4.1 Thermodynamic analysis

Methanation is a strongly exothermic reaction and with a reduction in number of moles, thus it is thermodynamically favoured at low temperatures and high pressures [9]. The main chemical species involved in the methanation process are CH<sub>4</sub>, H<sub>2</sub>, CO, CO<sub>2</sub> and H<sub>2</sub>O. Two reactions are the most relevant within the reactive system: CO methanation (1) and the reverse water gas shift (RWGS) (2). Moreover, CO<sub>2</sub> methanation (3) is simply the combination of reactions (1) and (2) [13].



It is observed that gas composition resulting from the methanation process is close to thermodynamic equilibrium conditions for temperatures down to about 320 °C [13]. Thus, a thermodynamic calculation provides a good estimation of the expected gas composition. Even if there are also secondary reactions in the reactive system, they are only important from the point of view of kinetics and evaluation of the amount of deposited carbon, while they do not influence thermodynamic equilibrium conditions. Therefore, thermodynamic calculations have been performed by using MATLAB, considering only CO methanation and the RWGS between 250 and 450 °C. Gas outlet composition has been calculated for



different inlet compositions: stoichiometric CO methanation, stoichiometric CO<sub>2</sub> methanation, SER gas methanation and standard PG methanation. Table 5 specifically shows the analysed input compositions.

As key process parameter, the methane yield ( $Y_{CH_4}$ ) has been evaluated for all these inlet compositions, for temperatures between 250-450 °C and for a pressure equal to 1 bar, through the following expression (Eq. 2.9). Methane yield is calculated as the methane amount obtained from carbon monoxide and dioxide, which are the carbonaceous reactants, divided by the inlet amounts of both carbon monoxide and dioxide. All the components amounts are expressed as flowrates in standard conditions [Nm<sup>3</sup>/h].

$$Y_{CH} [\%] = \frac{n_{out,CH_4} - n_{in,CH_4}}{n_{in,CO} + n_{in,CO_2}} \text{ Eq 2.9}$$

**Table 5: Analysed input methanation compositions**

	<b>Stoichiometric CO methanation H<sub>2</sub>/CO=3</b>	<b>Stoichiometric CO<sub>2</sub> methanation H<sub>2</sub>/CO<sub>2</sub>=4</b>	<b>SER gas methanation</b>	<b>Standard PG methanation</b>
<b>[mol%]</b>				
H <sub>2</sub>	75	80	64.5	41.5
CO	25	0	8	22
CO <sub>2</sub>	0	20	11	21
CH <sub>4</sub>	0	0	13	10
H <sub>2</sub> O	0	0	0	0
C <sub>2</sub> H <sub>4</sub>	0	0	1.5	2
N <sub>2</sub>	0	0	2	3.5

Gas outlet compositions at equilibrium conditions are reported, e.g. Figure 10, for each feed at each temperature:

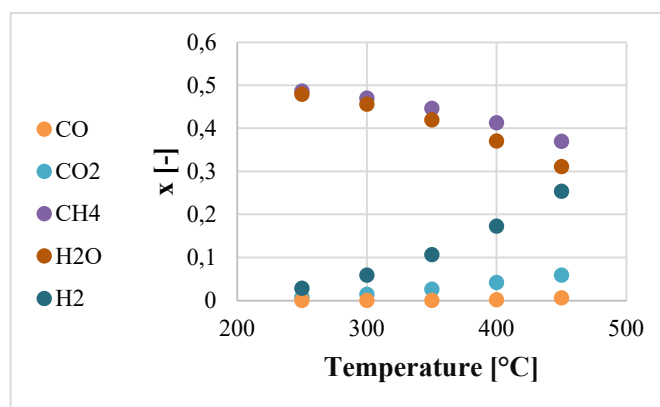


**Figure 10: Temperature vs molar fractions – stoichiometric CO methanation**

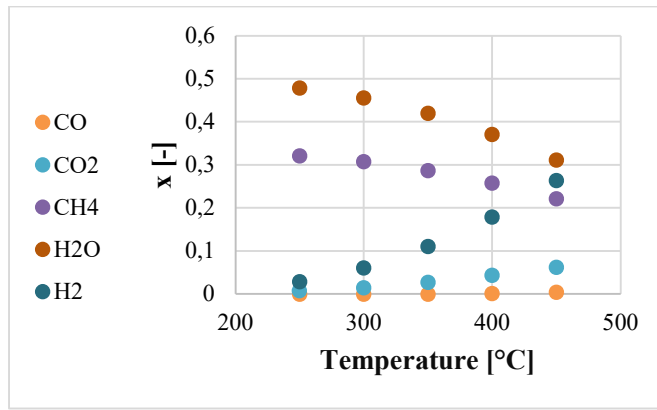


Figure 11: Temperature vs molar fractions – stoichiometric CO<sub>2</sub> methanation

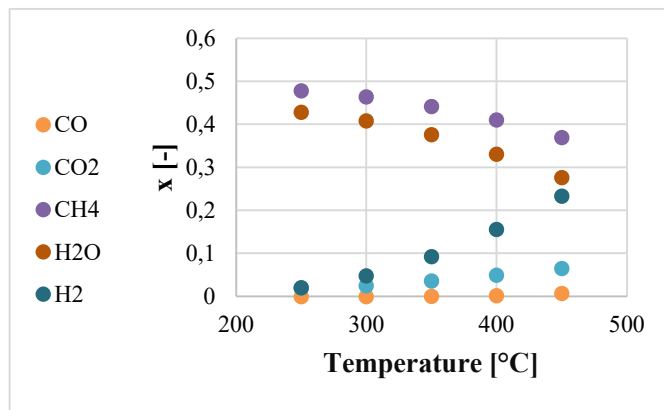


Figure 12: Temperature vs molar fractions – SER product gas methanation

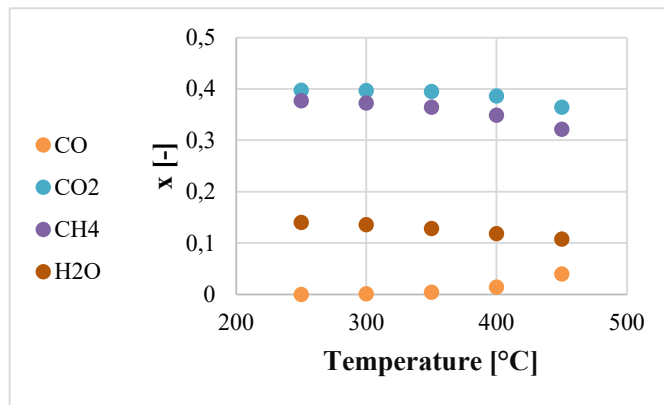
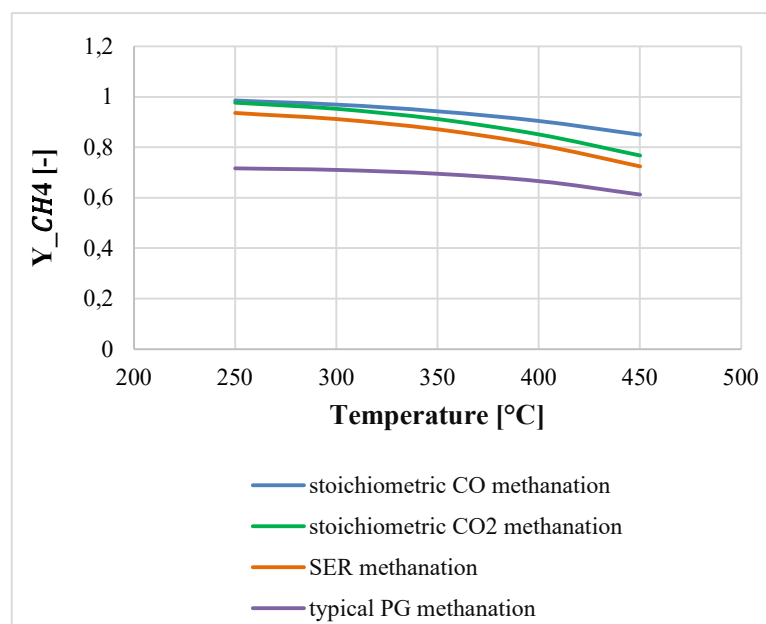


Figure 13: Temperature vs molar fractions - typical product gas methanation

Observing the plots, it is possible to identify common trends for every inlet composition: methane and water decrease with temperature while carbon monoxide, carbon dioxide and hydrogen increase with it. Methanation is exothermic and thus its extent of reaction is decreasing with increasing temperature while

the RWGS is endothermic and therefore its extent of reaction increases with higher temperatures. Methane only takes part in the first reaction and this explains its reduction with T. Carbon monoxide is reactant of the first reaction and product of the second one, being it less consumed in an exothermic reaction and more produced in an endothermic reaction, it increases with T. Water trend can be explained by the higher sensitivity to T of the first reaction: its decrease due to methanation (Eq. 2.2) is greater than the increase due to the RWGS (Eq. 2.8). This is explained by the fact that methanation (Eq. 2.2) is strongly exothermic while RWGS (Eq. 2.8) is slightly endothermic.

Concerning hydrogen and carbon monoxide contents, it is worth to look to the global reaction (Eq. 2.1). Being both reactants of a global highly exothermic reaction, they increase with the temperature level. Methane, which is the product of the exothermic global reaction (Eq. 2.1), decreases with T. Analysing the four different inlet compositions, further comments should be reported. Carbon monoxide is almost completely consumed in all the situations. Regarding carbon dioxide, we have a high leftover in the case of typical product gas methanation. Hydrogen consumption is not complete except for the typical PG feed where  $H_2/CO$  and  $H_2/CO_2$  ratios are lower and farther from stoichiometric ones. Therefore, the presence of residual  $CO_2$  in the typical PG case is due to the lack of hydrogen in that feed, which is essential for its conversion. Water production results to be higher in stoichiometric conditions and lower when there is a low  $H_2$  content. Methane yield is calculated for all the input compositions and temperatures and the results are shown in figure 15.



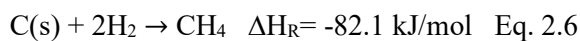
**Figure 14: Temperature vs CH<sub>4</sub> yield**

The highest methane yield is obtained for the stoichiometric feed compositions. Therefore, one might think that they represent the best situations, but it is not really the case. The very strong exothermicity

of the reaction, has to be regulated and implementing the stoichiometric composition corresponds to the situation of maximum heat production. A too high reaction heat is undesirable because it could cause damage to reactor vessel materials and catalyst. The latter would be subject to sintering, which leads to both loss of the catalytic surface and activity [24]. Furthermore, using the stoichiometric feed compositions means to realize complex gas cleaning and conditioning processes upstream of the methanation reactor because of the impossibility to directly obtain that composition from biomass gasification processes. This complexity implies also high process costs and therefore a decrease in the efficiency of the overall process chain [7]. This unattractive condition has to be avoided and thus the best option is to operate a SER gasification. The PG generated in a SER gasification, will also lead to very high methane yields between 72 and 93 %.

## 2.4.2 Catalyst choice and deactivation mechanisms

As for any catalytic process, the catalyst deactivation mechanisms and the operating conditions at which they could occur are fundamental to be known and analysed. In the case of methanation, carbon deposition is one of the major problems. Several reactions can describe the formation of carbonaceous deposits. In particular, Boudouard reaction (Eq. 2.5), also known as CO disproportionation, is mainly responsible of the decomposition of carbon monoxide in carbon and carbon dioxide. Carbon is on one hand a necessary intermediate of the reaction if it is hydrogenated to methane (Eq. 2.6) and it does not give any problem when it is gasified with steam (Eq. 2.4).



Furthermore, carbon atoms can also polymerize if their hydrogenation is not fast enough, and polymeric carbon deposits are the main causes of catalyst deactivation [6]. Reactions (Eq. 2.6) and (Eq. 2.4) show that increasing  $\text{H}_2$  and  $\text{H}_2\text{O}$  in the PG could help preventing carbon deposition [13]. This phenomenon results to be strongly dependent on temperature,  $\text{H}_2/\text{CO}$  ratio, pressure and superficial gas velocity: carbon deposits morphology and amounts are influenced by these factors. Specifically, a lower pressure, gas velocity and  $\text{H}_2/\text{CO}$  ratio favour the carbon laydown on the catalyst, while considering the variation of temperature, carbon deposition is enhanced with its increase [25]. It has been observed that also the catalyst support nature influences the carbon deposition phenomenon [7].

Other sources of catalyst deactivation are poisoning and sintering. Sintering corresponds to the coalescence of solid catalyst particles and it is favoured at high temperatures. Since methanation is strongly exothermic, the formation of hotspots on the catalyst is inevitable and thus it is necessary to efficiently remove heat in order to limit this undesired process [26]. The sintering phenomenon

decreases the catalyst surface and consequently its efficiency. Developing thermally stable catalysts or with high activities at low temperatures is one of the main challenges. Moreover, temperature peaks can be reduced by using a fluidized bed reactor for methanation: the high heat transfer coefficients achieved in it, allow to operate in isothermal conditions [9].

Considering specifically nickel (Ni) catalyst, which results to be the one mostly employed in SNG synthesis, it has to be activated by reduction. This is due to the fact that to handle the catalyst in air, a passivation procedure is needed on it. Specifically, it will be available in form of metal oxide (NiO) [27]. It has been observed that the reduction temperature influences the sintering process. In particular, nickel sintering results to be more serious at high reduction temperatures [28]. Deactivation through poisoning is due to an insufficient gas cleaning process and it consists of an irreversible adsorption of contaminant molecules on the catalyst surface [22]. The problem is that even a small amount of undesired components can cause poisoning: 10 ppm (or less) of sulphur species may be sufficient for poisoning a Nickel catalyst [29]. In particular, sulphur, chlorinated and nitrogen compounds can cause SNG catalyst poisoning. Among these three, the most abundant components in the PG, derived from biomass gasification, are sulphur containing species [22]. In particular, sulphur is a poison for different catalysts commonly implemented in the SNG synthesis, e.g. nickel (Ni), copper (Cu), cobalt (Co) or iron (Fe) [7]. Poisoning process is also influenced by the temperature: at higher temperature its effect is reduced and above 950 °C sulphur poisoning over nickel catalysts becomes nearly negligible [12].

The catalyst choice is one of the most important component in order to obtain high product yields [30]. Sabatier and Senderens found in 1902 that different transition metals are able to catalyze methanation: rhodium (Rh), ruthenium (Ru), iron (Fe), nickel (Ni), palladium (Pd), platinum (Pt) and cobalt (Co) [9]. Furthermore, other catalysts result to be active and besides the ones already mentioned, most papers discuss about copper (Cu), molybdenum (Mo), silver (Ag), gold (Au), rhenium (Re) and manganese (Mn) [31]-[32]. Noble metals, e.g. Au, Ag and Pt, have really high costs. Hence, it would be not economically feasible to use their pure form as methanation catalysts [31]. Furthermore, Pd, Pt, Rh, Re, Mo and Au catalyze simultaneously hydrogenations to CH<sub>4</sub> and methanol (CH<sub>3</sub>OH) and WGS reaction [32]. Specifically, Cu and Ag give mainly CH<sub>3</sub>OH [33].

Based on availability, effectiveness and price further analysis are carried out for Ru, Fe, Ni, Co and Mo [30]. These catalysts were defined the ones “important for methanation” by Mills and Steffgen [34]. Features as selectivity, activity, stability and cost are compared and rated from 1 to 5, where 5 is the most preferable option, for these different catalysts. Selectivity means higher CH<sub>4</sub> yields, activity is referred to the catalyst interaction with the reactants, stability quantifies the catalyst lifetime and cost is related to the price of the catalyst. Table 6 shows the catalysts scores based on these four properties. Concerning selectivity activity and stability, the most preferable option is characterized from the highest value while for costs, the 5 corresponds to the lowest price [30].

**Table 6: Catalysts ratings [30].**

	Selectivity	Activity	Stability	Costs
Catalyst				
Ru	3	5	4	1
Fe	2	4	5	5
Ni	4	3	3	4
Co	1	2	1	3
Mo	5	1	2	2

Fe is more active than Ni and it has the longest lifetime, but it presents a very low selectivity towards methane. Co has a similar activity to Ni, but it is more expensive. Mo is highly selective to methane and thus leads to high methane yields, but it has a very low activity if compared to all the others. Ru catalyst is the most chemically active and stable. Using Ru means to achieve high yields at a low temperature but an obstacle is that it has a very high price and therefore it is not suitable for wide industrial use [30]. Specifically, its price (12000 USD/kg) is 750 times higher than the one of Ni (16 USD/kg) [35]-[36]. Ni shows a good trade-off between performance and cost. As a matter of fact, it has a high activity, it operates at not too high temperatures and it is relatively cheap with respect to the other transition metals. The only drawback is that it has a very short lifetime which is caused by the blockage of the catalyst pores by way of carbon deposits. Regeneration processes, which consist in the combustion of the deposits, should be limited because it produces extra greenhouse gases. Anyway, the combination of good characteristics and low price makes nickel the most applied catalyst in commercial methanation applications [37]. As confirmed by the overall score, Ni catalysts are the leaders in the methanation field [30].

The catalyst is not only influenced by the active metal, but also by supports and promoters which give to the catalyst particular features [37]. Catalyst supports are able to improve the dispersion of the active phase and, based on their interaction with it, the reducibility of the oxides precursors is also modified [38]. Supports influence also the already analysed active metal activity since they have the main goal of enlarging the catalyst area. A larger surface area is obtained by supporting small particles of active metals on large surface supports [37]. Furthermore, the catalyst preparation methods have a great influence on the characteristics of the support. Specifically, the influence of catalyst calcination step, which is the conversion of metal salts to oxides [28], is highly relevant.

Common supports for the methanation Ni catalyst are metal oxides of large surface area, e.g. alumina ( $\text{Al}_2\text{O}_3$ ), silica ( $\text{SiO}_2$ ), titania ( $\text{TiO}_2$ ) or zirconia ( $\text{ZrO}_2$ ) [38]. Among them, alumina support is mainly implemented, especially in its  $\gamma$  configuration which has the maximum surface area [37]. Moreover,  $\alpha$ -alumina is preferred for high temperature applications [7]. A high calcination temperature leads to the

growth of Ni particles size and to the weakening of the metal-support interaction due to the decrease of the specific area and acidity of  $\text{Al}_2\text{O}_3$ . In this way, the catalyst reducibility increases and consequently also its activity and stability are promoted [39]. Unsupported catalyst could be also used, but they are less common because of their smaller surface area [37].

Furthermore, promoters are used to improve the supported catalyst qualities.  $\text{MgO}$  increases carbon resistance and thermal stability of  $\text{Ni}/\text{Al}_2\text{O}_3$  catalyst [40],  $\text{La}_2\text{O}_3$  increases its activity by increasing Ni dispersion and  $\text{H}_2$  uptake.  $\text{V}_2\text{O}_5$  improves activity, thermal stability and coke resistance of a Ni catalyst. Doping nickel supported on alumina with  $\text{CeO}_2$  means reaching a higher reducibility and long-term stability. However, promotional effects are not always positive: potassium can increase nickel selectivity to higher hydrocarbons which is undesired in a methanation reactor [37]. Additionally, adding quartz sand into the reactor also significantly promotes catalytic activity because it dilutes catalytic sites and improves the heat dissipation [40].

## 2.5 Methanation processes

For more than 100 years, different methanation processes have been developed, comprising both fixed bed and fluidized bed methanation. Originally, the main industrial applications aim of methanation was the removal of CO traces from  $\text{H}_2$  rich feed gases in ammonia plants. With the oil crisis in the late 1970s, that led to the increase in the price of fossil fuels, the interest in producing SNG in an alternative way grew and methanation became the principal synthesis step. Moreover,  $\text{CO}_2$  methanation processes gained attention in the 1980s and they were based on the production of methane in blast furnaces and coke ovens. The gases derived from these equipments require a highly intensive cleaning step and this limited the interest in the  $\text{CO}_2$  methanation. More recently, due to the increasing demand in electric storage and to the higher shares of wind and solar power productions, this process has been re-evaluated. Today,  $\text{CO}_2$  methanation is currently used in the PtG applications, in which excess electricity from wind or solar sources is implemented in the hydrogen production needed to hydrogenate  $\text{CO}_2$  [37]. For this purpose, two main reactor types have been developed: fixed bed reactors or fluidized bed reactors. Furthermore, the most important methanation industrial applications are described in this subchapter [9], [37].

### 2.5.1 Fixed bed reactor processes

Fixed bed methanation reactors are state of the art as gas cleaning before ammonia synthesis [9]. In these applications, the heat removal is not a problem due to the low concentration of CO in the treated gas. On the other hand, in the PG implemented for the production of SNG, there is a high amount of CO and therefore the heat of reaction has to be considered [9]. Thus, one of the main objectives of methanation, seen as the principal synthesis step, is to efficiently remove reaction heat in order to minimize thermal stresses, the consequent catalyst deactivation and limitations in methane yields. In

particular, reaction temperatures higher than 550 °C can cause catalyst sintering and need to be avoided [41]. In the industrial processes, heat removal is mainly achieved by using adiabatic reactors with intermediate cooling or cooled gas recycle and non-adiabatic reactors with external cooling.

## Lurgi process

In the 1970s Lurgi company, which now is the Air Liquide, developed a commercially viable methanation process based on two adiabatic fixed bed reactors with intermediate cooling and cooled product recycling [37]. These reactors work with temperatures between 300 °C and 450 °C [9]. The methanation feed of this process derives from an updraft fixed bed coal gasification [7], which was already commercially available in Germany during 1930s. Different pilot plants were built in order to investigate the process parameters: one by Lurgi and SASOL in Sasolburg (South Africa) and another by Lurgi and EL Paso Natural Gas Corporation in Schwechat (Austria) [9]. Based on their results, the first commercial SNG from coal plant was commissioned in North Dakota (United States) and it is run for 35 years by the Dakota Gas Company. The plant consists of 14 coal lignite gasifiers in parallel, which operate in counter-current and implement an oxygen and steam mixture as gasification agent [7].

Gasifiers are followed by a WGS conversion and CO<sub>2</sub> and sulphur removal via Rectisol scrubbing. Methanation section is followed by product compression, water condensation, a further CO<sub>2</sub> removal and finally the produced SNG can be distributed in the national gas grid. The CO<sub>2</sub> from the gas upgrading step is used for enhanced oil recovery in a neighbouring oil field. The plant delivered since 1992, up to 4.81 millions m<sup>3</sup>/day of SNG [9]. This technology, still commercially available from Air Liquide, is shown in Figure 15 [42]. Lurgi process is currently active in further developing with regard to the PtG applications and biomass gasification [7].

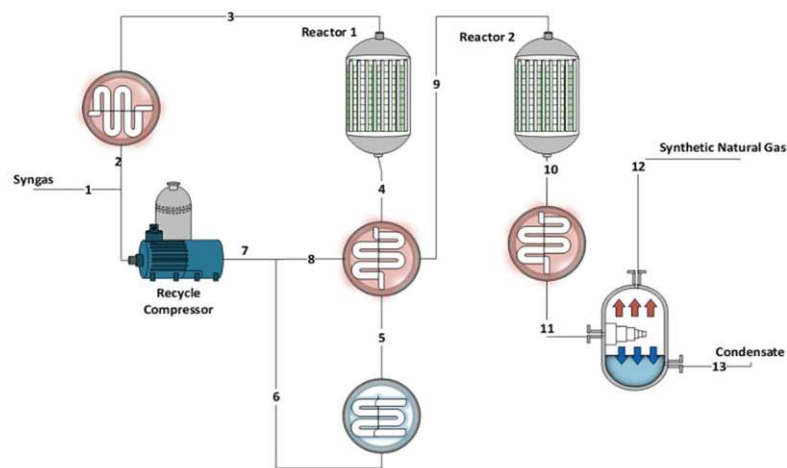


Figure 15: Lurgi methanation process scheme [42].



## TREMP process

Another methanation concept, which is still commercially available, was developed by the Danish company of Haldor Topsøe. This process is named TREMP (Topsøe Recycle Energy-efficient Methanation Process) and it is similar to Lurgi process but with 3-4 fixed adiabatic beds [37]. Haldor Topsøe developed a new methanation catalyst with higher temperature stability (around 700 °C) than the standard ones. This catalyst results to be more active at the lower temperatures suitable for methanation, e.g. reaction inlet 300 °C [7]. The overall cyclic process involves syngas methanation alternating with the methane steam reforming, which is the reverse methanation reaction and thus it is strongly endothermic. The purpose of this cyclical process is to store and distribute the process heat derived from nuclear high temperatures reactors: methane is reformed using nuclear energy and the derived syngas is converted to methane to produce heat in the form of high pressure superheated steam. The methanation section contains three adiabatic fixed bed reactors with intermediate cooling and cooled gas recycle and it is shown in Figure 16 [42].

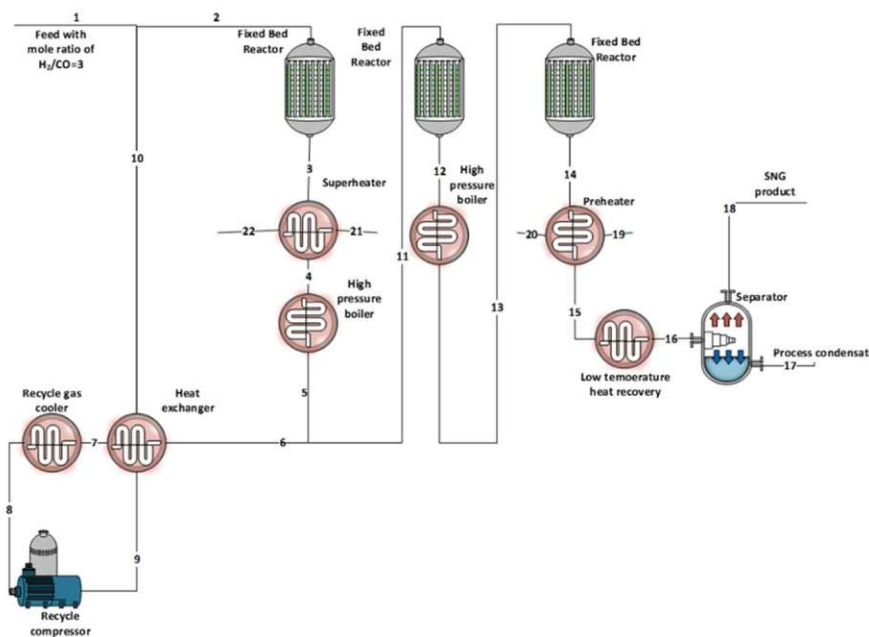


Figure 16: TREMP methanation process scheme [42].

The feed gas entering the system contains  $H_2$  and  $CO_x$ . It enters the first adiabatic fixed bed reactor and after passing the superheater and high-pressure boiler, is split into 2 different paths. A fraction of the fluid is cooled, compressed and then recycled to the first reactor. The other fraction flows in the second reactor, then enters another high-pressure boiler before entering in the third reactor. All the reactors are adiabatic fixed bed. After the third reactor, the fluid heat is recovered in a preheater and a low temperature heat recovery. Thereafter, the stream enters in a separator where the condensate is removed. The final product contains 94-98% methane [42].

## HICOM process

A further methanation development, realized by the British Gas Corporation is the HICOM (High Combined Shift Methanation) process in which methanation and WGS are combined. With this technology, a thermal efficiency of the 70 % from coal to SNG can be reached. The PG implemented derives from coal gasification. After gasification, it is cooled and desulphurised and then sent to the methanation section. The purified PG is saturated with steam and then passes through a series of fixed bed methanation reactors in which the temperature control is done by means of the cooled product recycle [9]. The HICOM process uses a Ni catalyst and additional steam is added to the feed gas in order to reduce carbon deposition on the catalyst [42].

After the main methanation reactors, one part of methane is recycled, and the other part is sent to one or more low temperature methanation reactors where recycling is not carried out because of the very low exothermicity. HICOM process appears in Figure 17 [9]. A gas upgrading step, which consists in CO<sub>2</sub> removal, follows the SNG synthesis step. In this case, the CO<sub>2</sub> is removed after methanation and therefore the unit does not need to handle any sulphur component. The semi-commercial plant built at the Westfield Development Centre (Scotland) converts 5300 m<sup>3</sup>/h of purified syngas to SNG.

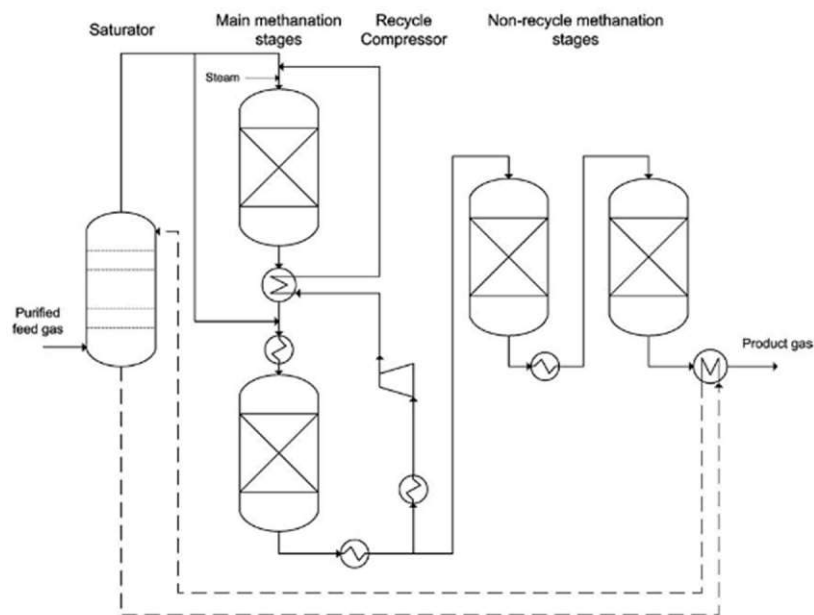
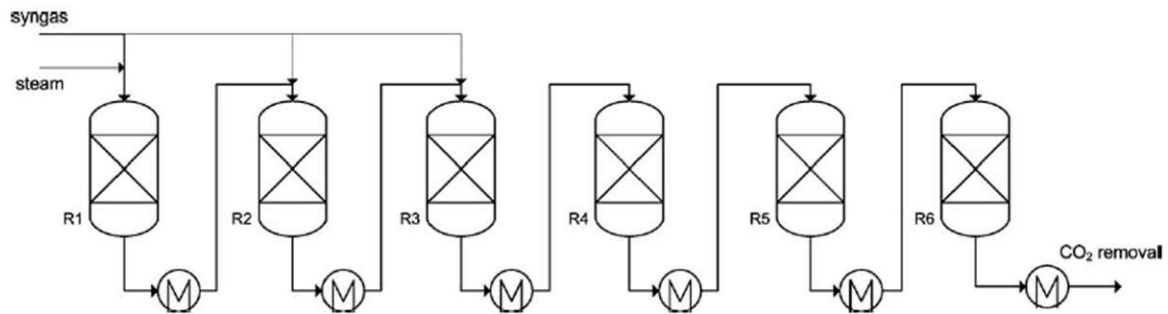


Figure 17: HICOM methanation process scheme [9].

## RMP process

To avoid gas recycling and internal reactor cooling, Ralph M. Parsons company invented a methanation process with 4-6 adiabatic fixed bed reactors in series [37]. Moreover, this process avoids a separate WGS unit. Temperature was controlled through intermediate cooling. Furthermore, the fresh syngas can be added in different distribution ratios into the first three reactors. In this way, the potential

exothermicity derived from the reaction of the whole feed, is split in different reactors. Steam is fed into the first reactor in order to reduce carbon deposition over the catalyst and to increase the hydrogen content. Moreover, steam addition limits the temperature increase. In the first reactor, CO is mainly converted to CO<sub>2</sub> and H<sub>2</sub> by WGS and only minimally to methane [9].



**Figure 18: RMP methanation process scheme [9].**

In the subsequent reactors, not fresh gas is fed. This is not a problem because most of the reaction has already taken place and therefore the exothermicity results to be low. The temperature of the process is between 318 and 538 °C. The PG sent to this process has typically a H<sub>2</sub>/CO ratio equal to 1 [42]. Nevertheless, no commercial plants of this technology were realized. The RMP process scheme is depicted in Figure 18 [9].

### ICI/Koppers process

ICI and Koppers process, whose name derives from the creators of the Imperial Chemical Industries and from the Koppers-Totzek coal gasifier, is another once-through methanation process [37]. Similarly to RMP process, it implements three adiabatic fixed-bed reactors in series with intermediate cooling. The inlet temperature of the first reactor is set to 400 °C. Steam is added to the first reactor, in order to reduce the temperature increase and to not exceed 750 °C. Figure 19 depicts this process [9].

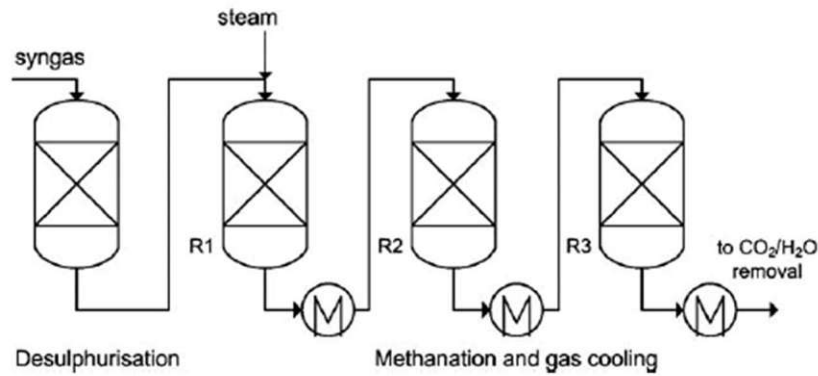


Figure 19: ICI/Koppers methanation process scheme [9].

## Linde process

In 1970s, Linde AG company developed a methanation process with a cooled fixed-bed reactor with an integrated twisted heat exchanger and a second adiabatic reactor in which only part of the first reactor product is sent [37]. The first reactor is cooled through an indirect heat exchange and thus its temperature is almost constant. Cooling tubes are grouped together within a catalyst bed [42]. Using water as external fluid, Linde reactor is able to produce steam thanks to the high exothermicity of methanation. Even in this case, part of the steam is added to the PG feed in order to minimize carbon deposition risk. The aim of the second adiabatic reactor is to increase the methane yield. This concept was not brought to the commercial application; however Linde developers continued their work on isothermal reactors, which operate commercially for methanol synthesis [9]. Figure 20 [9] shows the Linde methanation scheme.

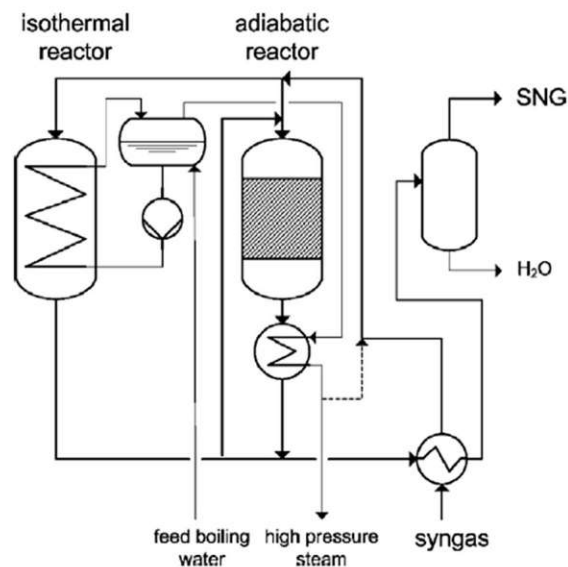


Figure 20: Linde methanation process [9].

## 2.5.2 Fluidized bed reactor processes

As an alternative to fixed bed methanation, fluidized bed reactors are also used for large-scale operations [41]. They are usually implemented for reactive systems heterogeneously catalysed and with high exothermicity [9]. The main advantage of this reactor configuration is related to the heat and mass transfer characteristics [42]. Specifically, it has much higher transfer properties with respect to fixed bed reactors. In this kind of reactor, the fluidized solids are continuously mixed in the reaction chamber and this leads to almost isothermal conditions. Furthermore, it is also possible to continuously remove and regenerate the catalyst during the operation [9]. The intensive catalyst mixing and the particles collisions help also in preventing the carbon deposition problem [43], [44]. In particular, it has been observed that, thanks to the movement of solid it is possible to have regeneration of the catalyst also inside the reactor [44].

Moreover, it has been found out that under the same space velocity, in the range 5000-25000 h<sup>-1</sup>, fluidized bed reactors give higher methane yields, lower coke content and lower bed temperature than fixed bed reactors [43]. Nevertheless, there are the catalyst attrition and entrainment problems which are absent in the fixed bed configuration [9] and the fluidized bed has a greater construction difficulty explained through the challenging fluidization theory in the next subchapter. In fixed bed reactors there is also the advantage of being able to control the residence time [43]. Several examples of fluidized bed reactors methanation processes are depicted.

### Bureau of Mines

Fluidized bed conditions require a sophisticated process control and therefore they are primarily investigated by research institutions [37]. The Bureau of Mines institution, formerly known as the United States Department of Interior, had the aim to produce high purity SNG from coal [42]. Within this research project, one fixed bed and two fluidized bed reactors were built. A much higher temperature change was detected for the fixed bed with respect to the standard fluidized bed, but the latter had a temperature difference still too high (100 K). The second fluidized bed was built in order to further minimize this difference and it has been designed as a multiple feed inlets reactor [9]. The experiments results showed that this kind of reactor was able to realize the best temperature control and its innovative scheme is depicted in Figure 21 [9]. In particular, this reactor has an operating temperature between 200 and 400 °C [42].

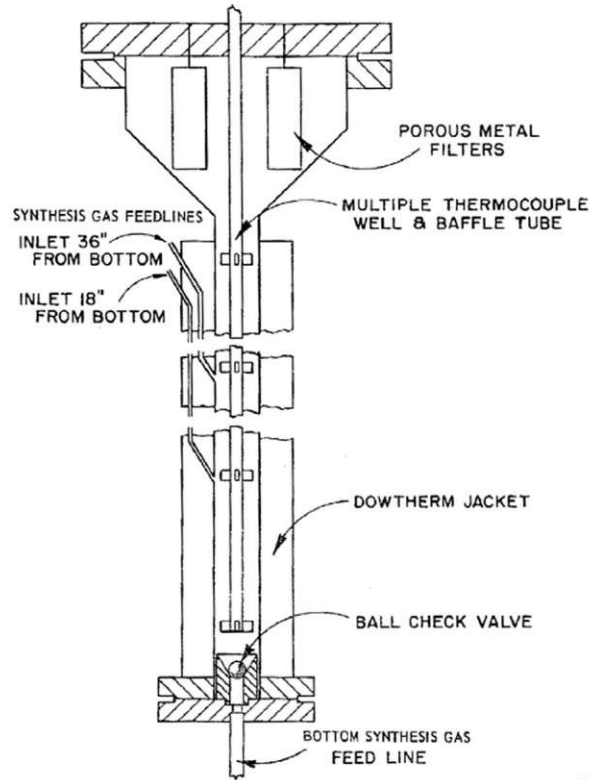


**Figure 21: multiple feed Bureau of Mines fluidized reactor [9].**

### **Bi-gas project**

One of the first fluidized bed methanation developed by an industry is the Bi-Gas project of Bituminous Coal Research Inc, initiated in 1963 [9], [37]. Even in this case, the principal aim was the SNG production starting from coal. The overall process includes a double stage entrained flow gasifier and a fluidized bed methanation reactor. Concerning methanation reactor, it was built on the template of Bureau of Mines project: it is a gas-solid fluidized bed, it includes two different feed inlet and two heat exchanger bundles [9]. The two feed injection points are one at the bottom and one between the first and the second heat exchanger [7]. The gas inlet zone is cone shaped and surrounded by a cooling jacket that uses mineral oil [9]. Furthermore, this reactor can be considered a strongly bubbling fluidized bed. Bi-gas reactor has not external jackets, but internal heat exchangers. Typical reaction conditions of this process include temperatures from 430 to 530 °C [7]. This particular reactor configuration is shown in Figure 22 [9].

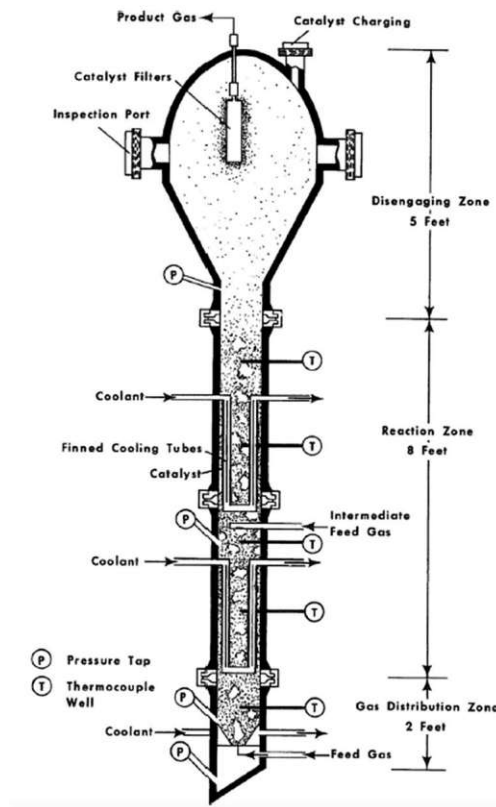


**Figure 22: Bi-gas fluidized bed methanation reactor [9].**

### COMFLUX process

The biggest fluidized bed methanation reactors have been developed by Thyssengas GmbH and the University of Karlsruhe (Germany). The aim of the project, named COMFLUX, is to produce SNG at 10% lower cost than fixed bed methanation processes, by applying a single reactor for combined WGS and methanation [7]. For this purpose, steam is added to the PG feed. The PG used in this reactor derives from coal gasification [9]. It is a standard reactor with a single feed entrance, but it is cooled through an internal heat exchanger as the Bi-Gas one. The first pilot plant was erected by Didier Engineering GmbH and it showed good results. Furthermore, after a pre-commercial reactor, the COMFLUX process was demonstrated at the industrial scale at the site of Ruhrchemie Oberhausen (Germany) [9]. The PG is desulphurised and then added to a steam stream. The feed of steam and PG is then pre-heated to facilitate the reaction occurring. Due to the exothermicity of the reaction, it is then necessary to cool the product exiting the reactor [42]. The process scheme is shown in Figure 23 [9].

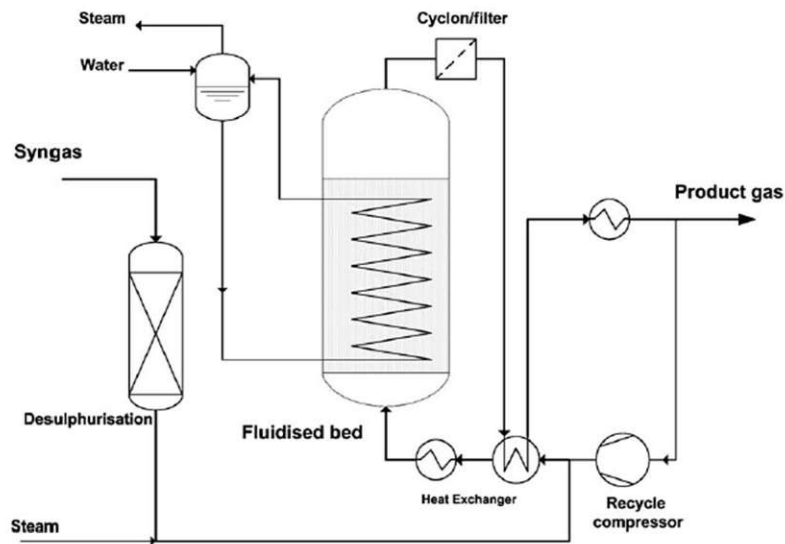


Figure 23: COMFLUX methanation process scheme [9].

## 2.6 Fluidization technology

The fluidization is defined as the operation by which solid particles are transformed into a fluidlike state through suspension in gas or liquid [45]. Particles become fluidized when an upward flowing fluid imposes a drag force that overcomes the downward gravity force. The drag force is the friction imposed by the fluid on the particles [46]. When a fluid flows upward through a granular solid material, depending on the fluid velocity, different regimes are possible and they are shown in Figure 24 [45]. If the fluid velocity is low, the solid particles have fixed positions and this situation corresponds to a fixed bed (Figure 24.a). By slightly increasing the fluid velocity, the fixed particles start to move and the minimum fluidization state (Figure 24.b) is achieved [47]. This situation is reached when the drag force increases in such a way that is equal to the weight of the particles [46]. Particles are just suspended by the upward flowing gas or liquid [45]. Up to the situation of minimum fluidization velocity, the pressure drops increase with the increase of the upward fluid velocity. Nevertheless, higher fluid velocities do not generate an increase in pressure drops [46].

Further increasing the fluid speed, in liquid-solid systems occurs a smooth and progressive expansion of the bed, which is called smoothly fluidized bed or homogeneously fluidized bed (Figure 24.c). Flow instabilities remains limited, and solids are distributed uniformly in the liquid. Generally, gas-solid systems, which are the one employed both in biomass gasification and methanation processes, behave quite differently. By exceeding the gas flowrate with respect to the minimum fluidization state, large instabilities and bubbling of the gas are observed [45], [47]. Such a bed is called bubbling fluidized bed or heterogeneously fluidized bed (Figure 24.d). An ulterior fluid velocity increase in gas-solid systems means that gas bubbles coalesce and grow as they rise. In a bed of small diameter, bubbles become large enough to spread across the vessel. Fine particles flow smoothly down close to the wall and around the rising void of gas: they give rise to the case of slugging, with axial slugs (Figure 24.e). When coarse



particles are present, the part of the bed above the bubble is pushed upward as by a piston. Moreover, the particles rain down, and the slug is disintegrated. At that moment another slug is formed, and this unstable motion is repeated again. This situation is called flat slugs (Figure 24.f). Slugging phenomenon is more relevant in narrow and long fluidized beds [45].

All these kind of fluidized bed reactors, with a distinct upper surface of the bed, are defined dense-phase fluidized beds (Figure 24 a-f). While for a higher gas flowrate, the so-called terminal velocity is overcome and consequently the upper surface of the bed disappears [45]. In particular, smaller particles have a lower terminal velocity than bigger ones [48]. Having exceeded this velocity limit, we can observe a turbulent flow of voids of gas of different sizes and shapes. Furthermore, we can observe a not negligible entrainment of particles outside the reactor. This corresponds to the turbulent fluidized bed (Figure 26.g). For even higher gas speeds, a higher amount of solid is carried out of the bed with the gas and this is the case of the lean phase fluidization with pneumatic transport of solids (Figure 26.h). In both turbulent and lean phase fluidization, large particle entrainment occurs, and this avoid the possibility to operate in steady state conditions. In order to achieve a steady state operation, solids recirculation has to be introduced [45].

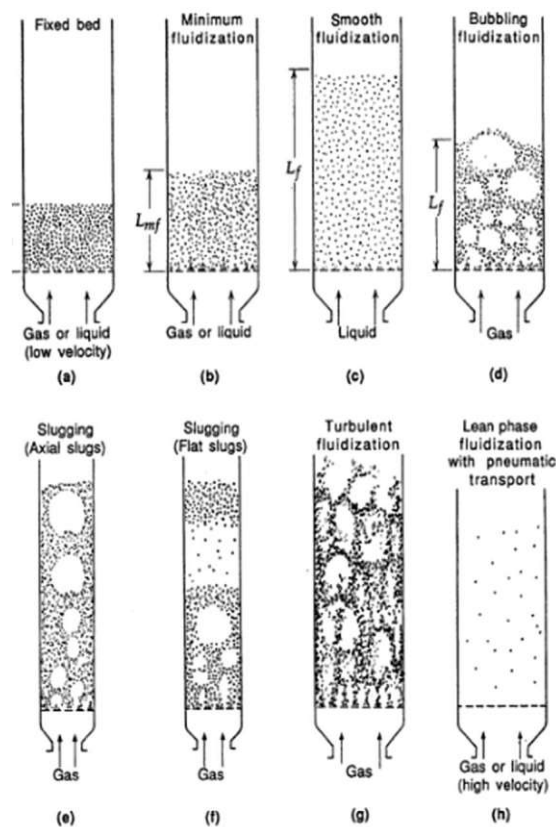
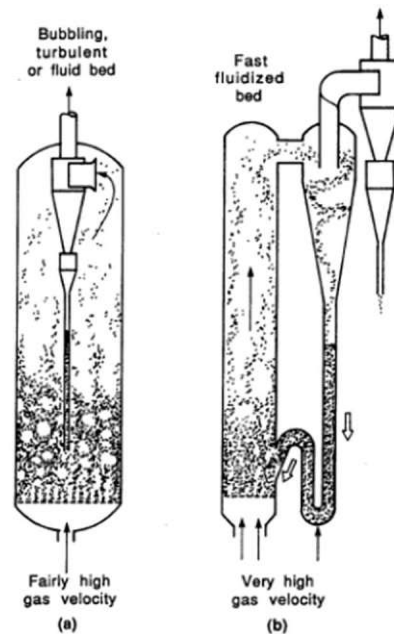


Figure 24: Possible states of a fluidized bed reactor [45].

These kinds of reactors are called circulating fluidized beds and two different configurations of them are shown in Figure 25 [45]. They typically implement gas-solid separators at the top of the unit to

collect the entrained solid particles. The recovered particles are then sent back to the bed [49]. Mainly cyclones are used as gas-solid separators. In turbulent fluidized bed, inner cyclones can deal with the moderate entrainment and this system is shown in Figure 25.a. At higher flowrates, the entrainment is much larger and external cyclone collectors are necessary. This situation corresponds to a fast fluidized bed and it is represented in Figure 25.b. Both in turbulent and fast fluidized beds, steady recirculation of solids could be achieved and this is fundamental for the reaching of good operations [45].



**Figure 25: Circulating fluidized beds [45].**

Conventional circulating fluidized beds (CFBs), as the ones shown in Figure 25, require a very tall main vessel and an additional tall cyclone. In order to reduce this height and consequently construction costs, new types of circulating beds have been realized [50]. Specifically, these reactors contain a central draft tube or flat plate to divide the bed and to permit an optimal internal solid circulation in a single vessel. This novel configuration is named Internal Circulating Fluidized Bed (ICFB) [51]. The methanation reaction in this experimental activity will be investigated in an ICFB reactor. This kind of apparatus has also the advantage to operate more flexibly [50]. Moreover, there is also the possibility to have longer residence times for the particles and this could lead to higher conversions [51]. In addition, it has been reported that particles entrainment from the reactor can be reduced if a draft tube is added to a fluidized bed reactor [50]. The gas velocities in the draft tube and the annular section are different from given gas velocities with given distributors due to gas bypassing between the draft tube and the annular section. The scheme of this reactor is depicted in Figure 26 [50].

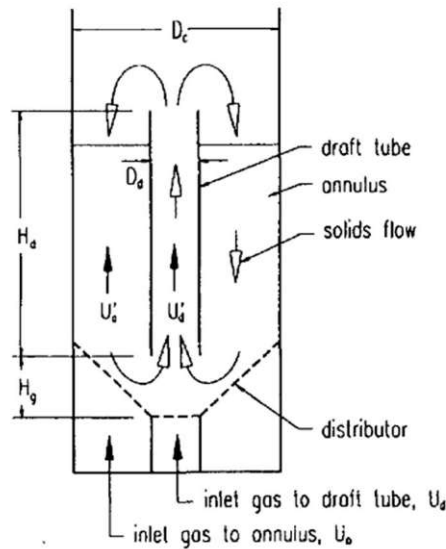


**Figure 26: Scheme of an internally circulating bed reactor [50].**

As we can notice, particles are transported upwards in the draft tube and downwards in the annular region of the reactor. Moreover, this reactor has two different inlets and two different outlet streams to the draft tube and annular section respectively. The most important parameters to model this reactor are the solid circulation rate and the gas bypassing [51]. Gas bypassing can be controlled by the inlet geometry of the draft tube and the type of gas distributor, while solid circulation rate is controlled by changing the gas velocities to the draft tube and the annulus sections independently [50]. In particular, solid circulation rate can be calculated from the following relation [51].

$$G_s = \rho_s(1 - h_{mf})V_a \quad \text{Eq. 2.10}$$

$G_s$  is the solid circulation,  $V_a$  is the particle downward velocity in the annular region,  $h_{mf}$  is the gas hold-up at the minimum fluidization velocity condition and  $\rho_s$  is the solid density, whose calculation will be analysed afterwards. From this equation, we can notice that the condition of minimum fluidization rate is also relevant as regards the circulation inside this type of reactor and therefore it is important to identify it. Its calculation will be discussed subsequently. On the other hand, the DFB reactor systems constituted by two different reactors in which the solid particles are circulated with the help of loop seals [21]. There are several configurations for the loop seals, including the so-called L-shaped tubes and U-shaped tubes. The circulation is possible because of the ability of a dense-phase gas-solid fluidized to behaves like a boiling liquid. Thus, the pressure difference between two points of the bed is calculated exactly like in a liquid, as the static head of bed between these points [45].

Specifically, Figure 27 [45] represents a solid circulation system between two fluidized beds which are connected by two U-shaped tubes. In particular, if gas is injected into the U-tube so that it is fluidized everywhere, the difference in static pressure in the two arms of the tube would be the driving force which causes the solid flow between the two fluidized reactors. A combination of two U-tubes would

be the solution that ensures the complete solid circulation between the two different vessels.

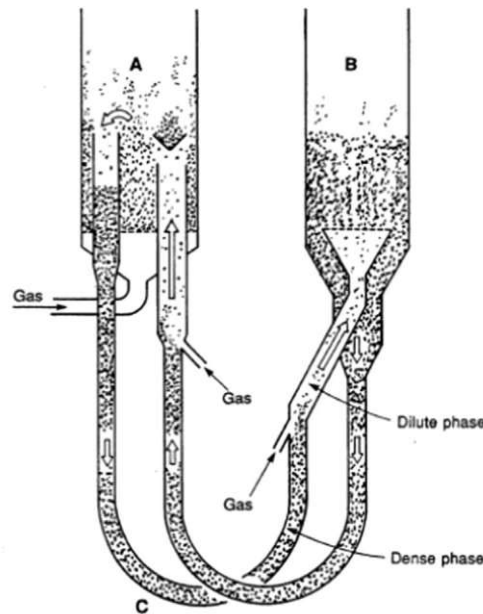


**Figure 27: Solid circulation between two beds [45].**

The ease with which particles fluidization is favoured and the range of operating conditions at which fluidization is possible (e.g. minimum fluidization velocity) are affected by many different factors. The most important one is the size and the size distribution of the solid particles. In general, fine particles could be fluidized in a wide range of gas flowrate, and this means that flexible operations could be achieved, while larger particles are able to be fluidized in a very small range of gas flowrate with resulting less flexible operations. A second important factor is the fluid-solid density ratio. Usually, liquid-solid systems are able to achieve homogeneous fluidization, while gas-solid ones originate non homogeneous systems. Deviations from this general situation are possible if there are low-density or high-density particles in the fluidized bed. Therefore, particle density corresponds to another important factor to evaluate [45].

Solid particles characterization is not a simple point. The complication derives from the non-spherical shape of particles, whose size determination results an issue. For this reason, individual particles are characterized through three different factors [47]: particle size  $d_p$ , particle shape  $\phi$  and particle density  $\rho_p$ . In a fluidized bed, there is not only an individual particle, but there is a cluster of particles to deal with. In order to characterize all the particles together, other three parameters are used: particle size distribution  $d_i$ ,  $x_i$  ( $d_m$ ,  $\sigma$ ), porosity  $\varepsilon$  and bulk density  $\rho_b$ . The individual particle size could be determined in different ways. In particular, is necessary to describe also particles whose shape is deviating from the spherical one. Thus, an equivalent diameter should be defined. There are different possible definitions,

and the most important ones are reported in Table 7 [47].

**Table 7: Possible definitions of the equivalent diameter of a particle [47].**

Symbol	Description	Explanation	Definition equation
$d_p$	Sieve diameter	Lateral length of the square through which the particle passes	$\frac{d_{\text{mesh}} + d_{\text{mesh}+1}}{2}$
$d_v$	Volume diameter	Diameter of a sphere with the same volume of the particle	$\sqrt[3]{\frac{6 \cdot V_p}{\pi}}$
$d_s$	Surface diameter	Diameter of a sphere with the same surface of the particle	$\sqrt{\frac{S_p}{\pi}}$
$d_{sv}$	Surface/Volume diameter	Diameter of a sphere with the same surface/volume ratio of the particle	$\frac{6 \cdot V_p}{S_p}$

Some of these equivalent diameters are linked between them through the shape factor  $\varphi$  which is defined as follows:

$$\varphi = \frac{\text{surface of the sphere of equal volume}}{\text{surface of the particle}} = \left(\frac{d_v}{d_s}\right)^2 \quad \text{Eq. 2.11}$$

The equivalent diameter  $d_{sv}$  can be expressed by the shape factor as:  $d_{sv} = \varphi \cdot d_v$  (Eq. 2.12). This lead to other correlations which are valid in some particular situations. For particles which do not deviate too much from the spherical shape:  $d_{sv} \cong \varphi \cdot d_p$  (Eq. 2.13). For particles significantly higher in one dimension than in the other dimensions, but not more than the double (egg-shaped):  $d_{sv} \cong d_p$  (Eq. 2.14). For particles significantly smaller in one dimension than in the other dimensions, but not less than the half (disk-shaped):  $d_{sv} \cong \varphi^2 \cdot d_p$  (Eq. 2.15). The shape factor can be determined after the separate calculation of  $d_{sv}$  and  $d_v$ , through the simple calculation of their ratio [47]. The used powder contains particles with different diameters, and this should be taken into consideration. Assuming that there  $N_1$  particles of size  $d_1$ ,  $N_2$  particles with size  $d_2$  and so on, the surface/volume average diameter is:

$$d_{sv,m} = 6 \frac{V_p}{S_p} = \frac{N_1 \frac{d_1^3 \pi}{6} + N_2 \frac{d_2^3 \pi}{6} \dots}{N_1 d_1^2 \pi + N_2 d_2^2 \pi \dots} \quad \text{Eq. 2.16}$$

Multiplying both the denominator and the numerator by the term  $\rho_p g$ , and Defining  $G_i = N_i \frac{d_i^3 \pi}{6} \rho_p g$ ,

$G_{tot} = G_1 + G_2 \dots$  and  $x_i = \frac{G_i}{G_{tot}}$ , we have that:

$$d_{sv,m} = \frac{N_1 \frac{d_1^3 \pi}{6} \rho_p g + N_2 \frac{d_2^3 \pi}{6} \rho_p g \dots}{\frac{N_1 d_1^3 \pi \rho_p g}{d_1} + \frac{N_2 d_2^3 \pi \rho_p g}{d_2} \dots} = \frac{G_1 + G_2 \dots}{\frac{G_1}{d_1} + \frac{G_2}{d_2} \dots} = \frac{x_1 + x_2 \dots}{\frac{x_1}{d_1} + \frac{x_2}{d_2} \dots} = \frac{1}{\sum \frac{x_i}{d_i}} \quad \text{Eq. 2.17}$$

This corresponds to a harmonic averaging and it reflects the great influence of small particles on fluidization. This equation cannot be used if there is an unusual (bimodal, trimodal) distribution. In order to use this formula, we should have that the relative standard deviation is less than 0.5:  $\frac{\sigma}{d_{p,modal}} < 0.5$ .

Even if a single particle can have more or less pores, in the particle density  $\rho_p$  the effect of the pores volume is not considered. In particular, the particle density is equal to the hydrodynamic density:  $\rho_p = \frac{M_p}{V_p}$  (Eq. 2.18). This is because it is based on the shape and volume that the flow “sees”. Taking into account the pores volume means to consider the absolute particle density which is equal to  $\rho_{abs,p} = \frac{M_p}{V_p - V_{pores}}$  (Eq. 2.19) which results bigger than the hydrodynamic density. We know that we are dealing with a cluster of particles. In order to characterize all the particles together, in terms of density we need to calculate the porosity and the bulk density.

The porosity results to be  $\varepsilon = \frac{\text{Void volume}}{\text{Total volume}} = \frac{V_{bed} - V_{particles}}{V_{bed}} = 1 - \frac{V_{particles}}{V_{bed}} = 1 - \frac{M_{bed}}{\rho_p V_{bed}}$  (Eq. 2.20).

The bulk density is defined as  $\rho_b = \frac{M_{bed}}{V_{bed}}$  (Eq. 2.21), so the porosity and the bulk density are linked as follows:  $\varepsilon = 1 - \frac{\rho_b}{\rho_p}$  (Eq. 2.22) [47]. The porosity depends on different parameters such as particle shape, particle size and particle size distributions. Specifically, the lower is the shape factor and the higher is porosity. Moreover, the larger are the particles and the wider is the particle size distribution, the lower is porosity [47].

Another fundamental parameter, which is dependent on all the factors already discussed, is the minimum fluidization velocity. It corresponds to the limiting speed between a fixed bed and a fluidized bed. This limit is determined by means of the pressure profiles, which result to be very different in the two beds. Figure 28 [47] shows the pressure drops as a function of velocity.

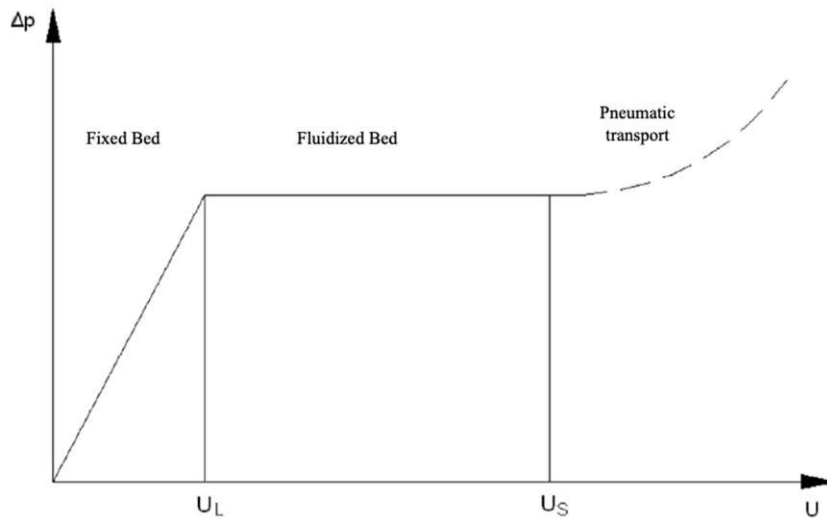


**Figure 28: Pressure – velocity diagram [47].**

While for a fixed bed the dependence of the pressure drops on velocity is linear, they remain constants in the region of the fluidized bed.  $U_L$  corresponds to the minimum fluidization velocity. After exceeding the terminal velocity  $U_S$ , pneumatic transport of particles is observed and there is a slight increase of the pressure drops [47]. The pressure drops in a fixed bed and in a fluidized bed are respectively equal to:

$$\frac{\Delta P}{H} = \frac{150(1-\varepsilon)^2}{\varepsilon^2} \cdot \frac{\mu U}{d_{sv}^2} + \frac{1.75}{\varepsilon^3} \cdot \frac{(1-\varepsilon)\rho_g U^2}{d_{sv}} \quad \text{Eq. 2.23}$$

$$\frac{\Delta P}{H} = (1 - \varepsilon) \cdot (\rho_p - \rho_g) \cdot g \quad \text{Eq. 2.24}$$

The minimum fluidization velocity can be found combining these two equations. We can put the equations together and rearrange them:

$$\frac{\rho_g d_{sv}^3 (\rho_p - \rho_g)}{\mu^2} = \frac{150(1-\varepsilon_L)}{\varepsilon_L^2} \cdot \frac{\rho_g d_{sv} U_L}{\mu} + \frac{1.75}{\varepsilon_L^3} \cdot \frac{\rho_g^2 d_{sv}^2 U_L^2}{\mu^2} \quad \text{Eq. 2.25}$$

The term on the left is the Archimedes number ( $Ar$ ) and on the right there is a dependence on the Reynolds number ( $Re = \frac{\rho_g d_{sv} U_L}{\mu}$ ). The resulting equation becomes:  $Ar = C_1 \cdot Re_L + C_2 \cdot Re_L^2$  (Eq. 2.26) and it is used in order to determine the minimum fluidization velocity, whose calculation results difficult because there are quadratic terms in the equation. Therefore, the values for  $\varepsilon_L$  are usually calculated experimentally and the  $U_L$  is consequently determined from the quadratic equation presented above (Eq. 2.25). There is also a direct expression for  $U_L$ , which is valid for Reynolds numbers between 0.01 to 4000. It has been proved for a wide variety of materials and particle size distributions [47]. According to it, the minimum fluidization velocity results:

$$U_L = \frac{\mu}{\rho_g d_{sv}} [\sqrt{33.7^2 + 0.0408 \cdot Ar} - 33.7] \quad \text{Eq. 2.27}$$

Even if the right value of the limit fluidization velocity between the fixed bed and the fluidized bed

regimes can be determined, the transition between these two states is not homogeneous for all the particles size. It starts for a very narrow distribution of particles. In particular, the particles with a smaller diameter begin to fluidize, whereas the larger ones fluidize later [47].

### 3 Experimental setup

#### 3.1 Description of the experimental rig

All the experiments have been performed in a bench-scale fluidized bed methanation reactor. Comparing fluidized bed methanation reactors with fixed bed ones, it is possible to say that the former ones have improved heat and mass transfer abilities. Furthermore, the risk of carbon deposition over the catalyst is reduced. On the other hand, a drawback of fluidized bed reactors is the high mechanical stress on the catalyst. This reactor, has been developed with the aim of experimenting methanation, using both bottled gas and outlet product gas from the 100 kW<sub>th</sub> DFB gasifier at TU Wien [52].



Figure 29: ICFB reactor in TU Wien research laboratory.



In particular, the reactor used for this experimental activity, shown in Figure 29, has an internal draft tube so that internal solid circulation is achieved. This kind of reactor is commonly named Internal Circulating Fluidized Bed (ICFB) and it has improved heat and mass transfer abilities. Moreover, thanks to the internal solid circulation, its height and construction costs are reduced with respect to the ones of the conventional circulating fluidized bed (CFB). The reaction takes place in two different regions of the reactor: the draft tube and the annular region. The diameter of the draft tube is equal to 80 mm, while the external diameter of the reactor is 164 mm. The reactor sizing is based on specific fluid dynamics calculations [52]. Above the reaction zone, there are two conical freeboards in both the regions. For the sake of clarity, P&I diagram of the whole process is shown in Figure 30.

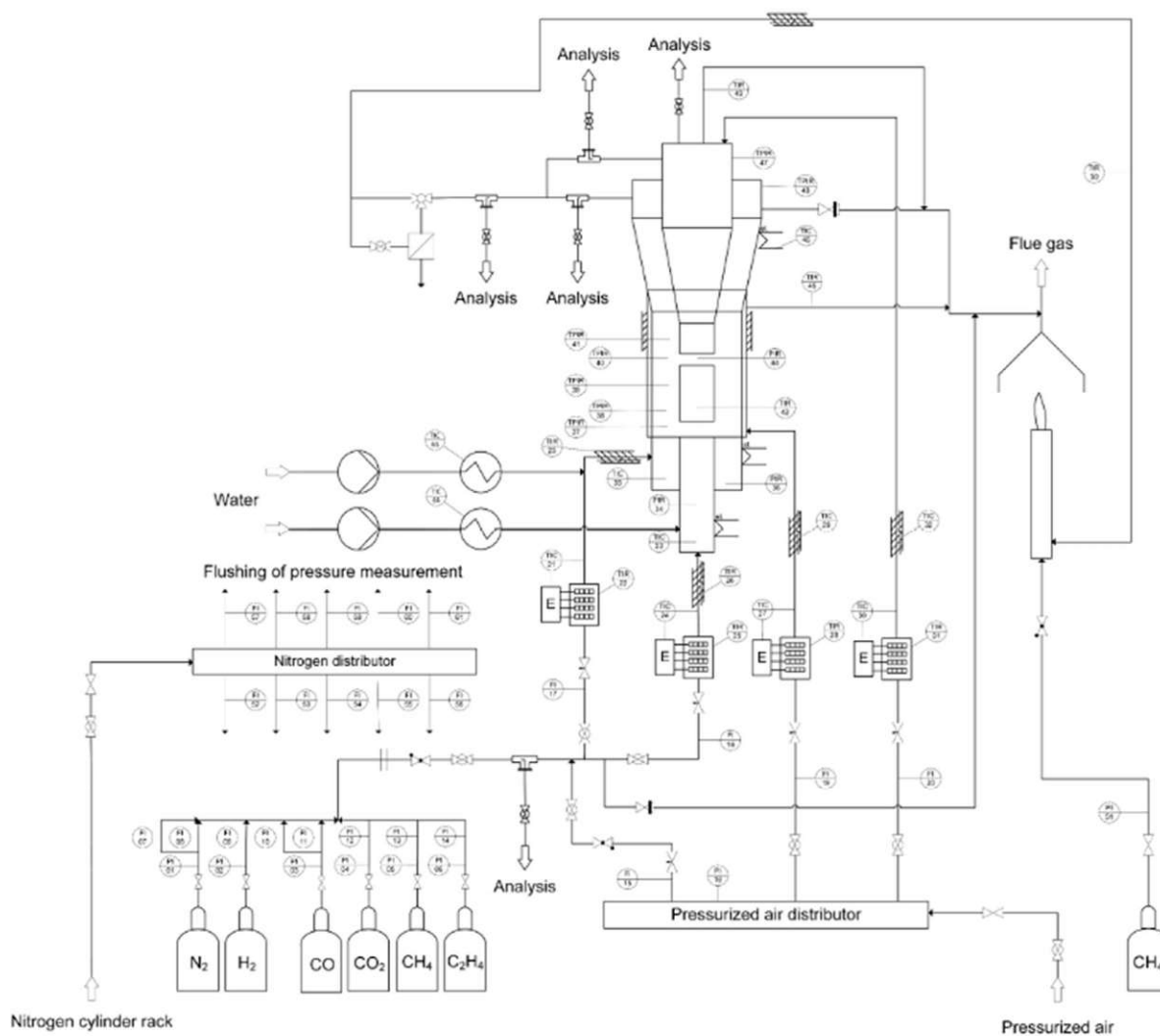


Figure 30: P&I diagram of the methanation process [52].

The feed stream derives from the gas cylinders. Single gas volume flows are detected by variable area flow meters with an integrated needle valve. The gaseous stream is split and sent separately to the draft tube and the annular region. Flow meters are also used to set this fluidization ratio. The feed gases are

then pre-heated and fed to both sections. Pressurized air is implemented both in an external jacket of the annular region and in an internal coil in the draft tube. Its flowrate is also controlled by flow meters with a needle valve. In the plant start-up phase, air is pre-heated and used to heat up the reactor in order to reach the proper temperature at which the reaction starts. Both the feeding stream and the pressurized air are pre-heated by electrical heating cartridges. Heating tapes are also present around the reactor, so that the heat losses along the pipes are compensated.

After the exothermic reaction has started, air pre-heating is turned off. In this way, it is possible to remove heat using the same pressurized air stream at about 25 °C. Moreover, two pumps are used to add water to the two reaction sections in order to prevent the carbon depositions over the catalyst and to enhance the WGS reaction. The products are exiting from the top of the reactor. Specifically, two separate pipes are present on the outlet of the two reaction sections. These two streams are then mixed and the derived stream flows to a filter stuffed with glass wool, used in order to remove the entrained catalyst particles. Among the outgoing products, which are mainly incondensable gases, there is also water that is easily removed in a dedicated condensation vessel. On the other hand, the gases leaving the reactor are sent to a natural gas operated torch.

Gas compositions are detected in five points: inlet section, top of the reactor, draft tube outlet section, annular region outlet section and overall outlet section. In particular, the gas measurements are realized via infrared spectroscopy on a dry basis. Furthermore, the plant is equipped with a maximum 10 pressure and temperature measurement points. Pressure measurements are carried out with Kalinsky DS2 pressure transmitters. All the measurement points are flushed with a small amount of nitrogen to protect the pressure transmitters and to clear the pipes from reacting gases and catalyst particles. Temperature measurements are performed by thermocouples. In the reactor, temperature, pressure and gas compositions are measured in fixed points at different heights in the annular region, in order to obtain axial profiles. For the same purpose, in the draft tube, vertically moveable pipes are used.

The catalyst implemented is nickel based on alumina ( $\text{Ni}/\text{Al}_2\text{O}_3$ ). In particular,  $\alpha$ -alumina configuration is used. Moreover, additional alumina besides the catalyst support is added to the reactor. This is done in order to reach the required filling level in the reactor. In particular, the filling level of the reactor is important for the control of the fluidization properties. Adding additional particles of alumina can improve significantly fluidization quality. This would lead to enhanced selectivity towards methane and methane yield [11].

### 3.2 Catalyst activation by reduction

The catalyst implemented in this experimental investigation is nickel based on alumina ( $\text{Ni}/\text{Al}_2\text{O}_3$ ) with  $\alpha$ -alumina configuration. In order to prevent potentially hazardous exothermic reactions during storage

and transport, transition metal catalysts are provided as metal oxides [53]. Moreover, catalysts are provided in this form also because it is difficult for manufacturers to prepare catalysts where the oxidation states are lower than those existing in air atmosphere [27]. In the case of nickel catalyst, it is provided as nickel oxide (NiO). Therefore, its activation by reduction is required before using it for reaction catalysis. This procedure can be defined as the last step of catalyst preparation and it has relevant effects on the catalyst performances. Thus, it must be done with high attention [27].

Specifically, it is realized subjecting the catalyst to a reducing environment consisting in our case of H<sub>2</sub> and N<sub>2</sub>. This reducing gaseous stream fed to the reactor, is composed of 90 % H<sub>2</sub> and 10 % N<sub>2</sub>. Before being reduced, the catalyst is heated up in a pure nitrogen stream up to 500 °C. This temperature is high enough to operate reduction [54]. Subsequently, hydrogen present at 90 % in the gaseous stream is also fed. Being reduction an exothermic reaction, an increase of temperature will be observed. If reduction is carried out at too high rates, the catalyst temperature can exceed the maximum allowable and its surface can consequently decrease [27].

It has also been observed that with an increasing reduction temperature, nickel dispersion and hydrogen chemisorption decrease, while nickel particles size increases [28]. These phenomena are all undesired, and for this reason a maximum allowable temperature equal to 500 °C is imposed. Moreover, by keeping the temperature of an exothermic reaction low, it will also be thermodynamically favoured. In the literature, a reduction time of 4 hours at 400 °C has been found to guarantee the activation of the catalyst [54]. In order to be conservative, in our case the reaction was operated for 6 h at 500 °C. The reactor temperature during time has been analysed. Figure 33 shows its trend. We can observe that there is a really fast temperature increase, from 460 °C to 485 °C when hydrogen is added to the reactor. This increase is probably due to the exothermicity of the reduction reaction and to the different properties of H<sub>2</sub> compared to N<sub>2</sub>.

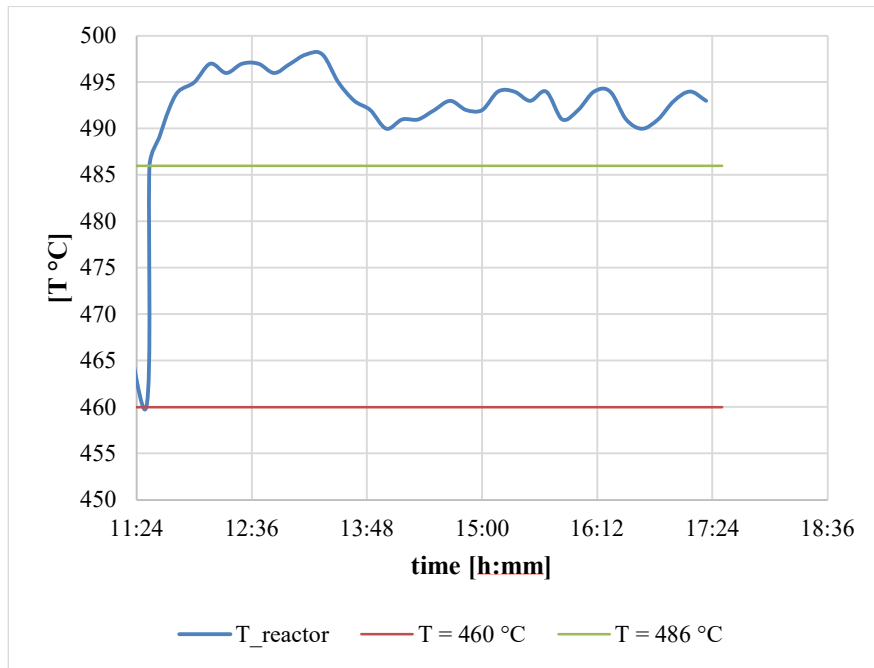


**Figure 31: time vs T during catalyst activation by reduction.**

### 3.3 Relevant variables definition

In order to evaluate the results obtained from the experimental tests and to quantify the parameters varied during the investigations, some definitions should be given. All the flowrates in these definitions, are expressed in standard conditions. The composition of the feed to the reactor can be easily classified through the definition of the Stoichiometric Number (SN). It is calculated by the ratio between the inlet hydrogen flowrate and the sum of three times the inlet carbon monoxide flowrate and four times the inlet carbon dioxide flowrate. The following equation (Eq. 4.1) shows how to calculate it.

$$SN = \frac{n_{in,H_2}}{3 \cdot n_{in,CO} + 4 \cdot n_{in,CO_2}} \quad \text{Eq 4.1}$$

Furthermore, in order to quantify the flowrate variation, the Weight Hourly Space Velocity (WHSV) on a mass basis can be considered. The WHSV [ $\text{NI} \cdot \text{h}^{-1} \cdot \text{g}_{\text{cat}}^{-1}$ ] is defined as the ratio between the inlet overall volumetric flowrate at standard conditions and the weight of the catalyst. It indicates how many gas volumes of feed can be treated in a unit of time. Another relevant parameter that is changed during this experimental investigation is the ratio between the WHSV to the draft tube and that to the annular region, defined as fluidization ratio.

Given different input conditions given by temperature, WHSV, SN and fluidization ratio, the results obtained can be evaluated through the calculation of other different parameters: methane yield ( $\chi_{CH_4}$ ), carbon monoxide conversion ( $\chi_{CO}$ ), carbon dioxide conversion ( $\chi_{CO_2}$ ), selectivity from carbon monoxide

to methane ( $S_{CO/CH_4}$ ) and selectivity from carbon dioxide to methane ( $S_{CO_2/CH_4}$ ). The following equations quantify their values.

$$Y_{CH_4}[\%] = \frac{n_{out,CH_4} - n_{in,CH_4}}{n_{in,CO} + n_{in,CO_2}} \cdot 100 \quad \text{Eq. 4.2}$$

$$\chi_{CO}[\%] = \frac{n_{in,CO} - n_{out,CO}}{n_{in,CO}} \cdot 100 \quad \text{Eq. 4.3}$$

$$\chi_{CO_2}[\%] = \frac{n_{in,CO_2} - n_{out,CO_2}}{n_{in,CO_2}} \cdot 100 \quad \text{Eq. 4.4}$$

$$S_{CO/CH_4}[\%] = \frac{n_{out,CH_4} - n_{in,CH_4}}{n_{in,CO} - n_{out,CO}} \cdot 100 \quad \text{Eq. 4.5}$$

$$S_{CO_2/CH_4}[\%] = \frac{n_{out,CH_4} - n_{in,CH_4}}{n_{in,CO_2} - n_{out,CO_2}} \cdot 100 \quad \text{Eq. 4.6}$$

In particular, the yield quantifies the product moles obtained in relation to the reactants consumption, the conversion relates the moles of reacted compound with its total inlet moles, while the selectivity from x to y is the moles of produced y with respect the moles of reacted x.

## 4 Results

Methanation reaction has been experimented in the bench-scale ICFB reactor of TU Wien. In all the experiments, the amount of Ni/Al<sub>2</sub>O<sub>3</sub> catalyst used is 1.6 kg and 1.5 kg of additional Al<sub>2</sub>O<sub>3</sub> are added, in order to reach the required filling level in the reactor so that fluidization quality will be improved. The scope of this experimental activity is to identify the optimal parameters for methanation. Relevant parameters, such as WHSV, temperature and SN are varied and the corresponding outlet compositions, methane yields, reactants conversions and selectivity are reported and discussed.

Pressure has not been varied and the reaction is operated at atmospheric pressure. The DFB gasifier of TU Wien operates at 1 bar, and thus a compression upstream of the methanation reactor is avoided. Additionally, the pressure influences only mildly the gas composition from a thermodynamic point of view [13]. Moreover, in the large-scale methanation process in Güssing (Austria), satisfying results have

been obtained by operating the fluidized bed reactor at a pressure of 1 bar [52].

#### 4.1 Test run 1: Stoichiometric CO methanation with $WHSV=1.3 \text{ NI}\cdot\text{h}^{-1}\cdot\text{g}_{\text{cat}}^{-1}$ and variable fluidization ratio

In this test run, methanation reaction is investigated with an inlet constant ratio  $\text{H}_2/\text{CO}$  equal to 3 which corresponds to an  $\text{SN}=1$ . This inlet composition corresponds to the stoichiometric one for CO methanation. The  $WHSV$  in this first set of experimental tests is equal to  $1.3 \text{ NI}\cdot\text{h}^{-1}\cdot\text{g}_{\text{cat}}^{-1}$ , which corresponds to a total inlet flowrate equal to  $2 \text{ Nm}^3/\text{h}$ . The reaction is operated with an approximately constant temperature of  $320 \text{ }^\circ\text{C}$ . The ratio between the  $WHSV$  to the draft tube and that to the annular region, defined as fluidization ratio is considered as a varying parameter. Table 8 shows the inlet composition, reported as percentage by volume.

**Table 8: Inlet composition test run 1.**

$F_{\text{in,draft}}/F_{\text{in,annular}}=$	
Component	[vol-%]
CO	24.4
H <sub>2</sub>	75.6
CO <sub>2</sub>	0
CH <sub>4</sub>	0
H <sub>2</sub> O	0

With this inlet feed composition, the most observed reaction is the CO methanation (Eq. 2.2) from which methane and water are produced. Moreover, we can observe CO<sub>2</sub> production, and this means that CO and H<sub>2</sub>O are also involved in the WGS (Eq. 2.3) reaction which generates carbon dioxide and additional hydrogen. In this test run, three values for the fluidization ratio are analysed. The outlet composition is measured in three different points: draft tube outlet section, annular region outlet section and overall outlet section. The overall outlet compositions are reported in Table 9. The molar fractions are reported as percentage by volume.

**Table 9: Overall outlet composition of test run 1.**

Fluidization ratio	0.84	2.4	4.3
Component	[vol-%]	[vol-%]	[vol-%]
CO	0.59	0.47	1.633
H <sub>2</sub>	19.90	19.22	24.43
CO <sub>2</sub>	3.46	3.37	3.85
CH <sub>4</sub>	39.79	40.19	37.00
H <sub>2</sub> O	36.25	36.74	33.1

We can notice that CO and H<sub>2</sub> have a trend with a minimum. Their minimum value, which corresponds to their maximum consumption, is obtained for the intermedium fluidization ratio equal to 2.4. The opposite is observed for CH<sub>4</sub> and H<sub>2</sub>O production, they have a maximum value for the same intermedium fluidization ratio. The maximum amount of products corresponds to the maximum consumption of the reactants. Moreover, we can observe that CO<sub>2</sub> is produced, and this means that WGS reaction is happening, CO<sub>2</sub> has a trend with a minimum with increasing fluidization ratio. Specifically, its minimum amount is obtained with fluidization ratio equal to 2.4. The minimum of CO<sub>2</sub> corresponds to the maximum of methane and water. It is probably due to the fact that minimum CO<sub>2</sub> production means minimum consumption of CO in the WGS reaction and consequently to the maximum CH<sub>4</sub> production.

Moreover, the composition is also analysed at the outlet of the draft tube and at the one of the annular region. From Table 10 we can see the comparison between the outlet compositions of the two sections.

**Table 10: Outlet compositions of test run 1 for the two different outlet sections.**

Reactor section	Annular region	Annular region	Annular region	Draft tube	Draft tube	Draft tube
Fluidization ratio	0.84	2.4	4.3	0.84	2.4	4.3
Component	[vol-%]	[vol-%]	[vol-%]	[vol-%]	[vol-%]	[vol-%]
CO	0.68	0.08	0.07	0.60	0.79	2.22
H <sub>2</sub>	20.80	13.62	11.71	20.61	23.28	29.71
CO <sub>2</sub>	3.63	2.23	1.75	3.64	4.18	4.77
CH <sub>4</sub>	39.29	43.19	44.15	39.43	38.00	34.07
H <sub>2</sub> O	35.59	40.88	42.32	35.72	33.75	29.23

In the annular region, with an increasing fluidization ratio CO and H<sub>2</sub> amounts decrease. This corresponds to the increase of CH<sub>4</sub> and H<sub>2</sub>O. In the draft tube, the trend is the opposite: CO and H<sub>2</sub> amounts increase while CH<sub>4</sub> and H<sub>2</sub>O amounts decrease. This is probably because an increase of the fluidization ratio means that the inlet flowrate in the annular region decreases, and therefore there is less flowrate to treat and more CH<sub>4</sub> production. At the same time, an increase of the fluidization ratio corresponds to the increase of the flowrate to treat in the draft tube, and thus the CH<sub>4</sub> production decreases. These two opposite trends in the two different sections of the reactor are the reason for the resulting trend with a maximum in the overall production of CH<sub>4</sub>. Concerning CO<sub>2</sub> amount, it decreases in the annular region with increasing fluidization ratio, while it increases in the draft tube. This gives the trend with a minimum in the overall section. This trend is explained by the fact that when increasing the flowrate to treat, methanation is more kinetically limited than the WGS, therefore more CO<sub>2</sub> is produced.

The methane yields,  $Y_{CH_4}[\%]$ , at the outlet of the three sections (overall, draft tube, annular) are calculated for the three fluidization ratio values. Figure 34 shows the results.

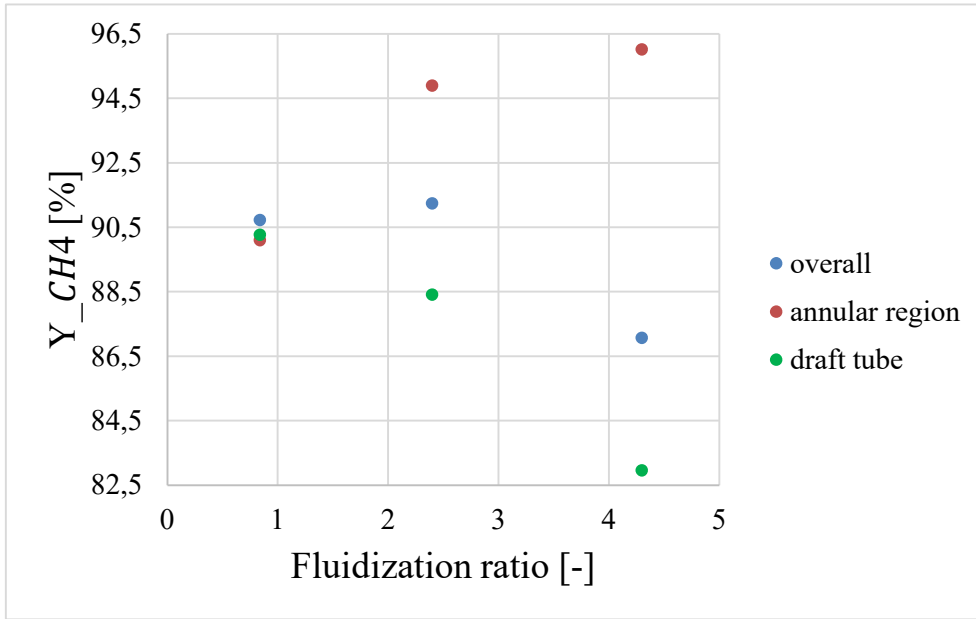


**Figure 32: fluidization ratio vs methane yield of test run 1.**

The maximum overall yield is obtained for the intermedium fluidization ratio equal to 2.4. The yields at the outlet of the annular region and of the draft tube have opposite trends: the one at the annular region increases with the fluidization ratio, while the one at the draft tube decreases with it. These two opposites trend give the trend with a maximum of the overall yield. Moreover, for the sake of clarity the values for the methane yield are reported in Table 11.

**Table 11: Methane yields for test run 1.**

Fluidization ratio	0.84	2.4	4.3
Y <sub>CH4</sub>	[%]	[%]	[%]
Overall section	90.73	91.24	87.08
Annular region	90.10	94.90	96.02
Draft tube	90.27	88.41	82.96

The maximum overall yield is obtained for fluidization ratio equal to 2.4 and it is 91.24%. The maximum



yield at the outlet of the annular region is obtained for the minimum inlet flowrate to the annular region and it is equal to 96.02%. The same is observed for the methane yield at the outlet of the draft tube: its maximum value is 90.27% and it is obtained for the lowest inlet flowrate to the draft tube.

Other two interesting parameters to analyse are carbon monoxide conversion, and selectivity from carbon monoxide to methane. Figure 35 shows how the conversion varies with the fluidization ratio and Table 12 shows all the specific values. Moreover, Figure 36 shows how the selectivity varies with the fluidization ratio and Table 13 shows all the corresponding values.

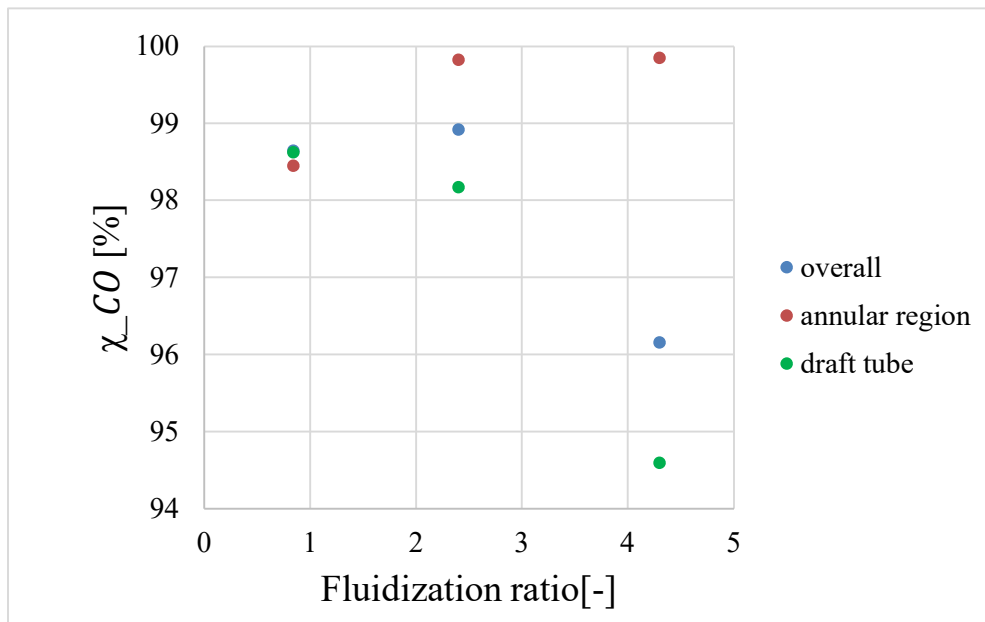
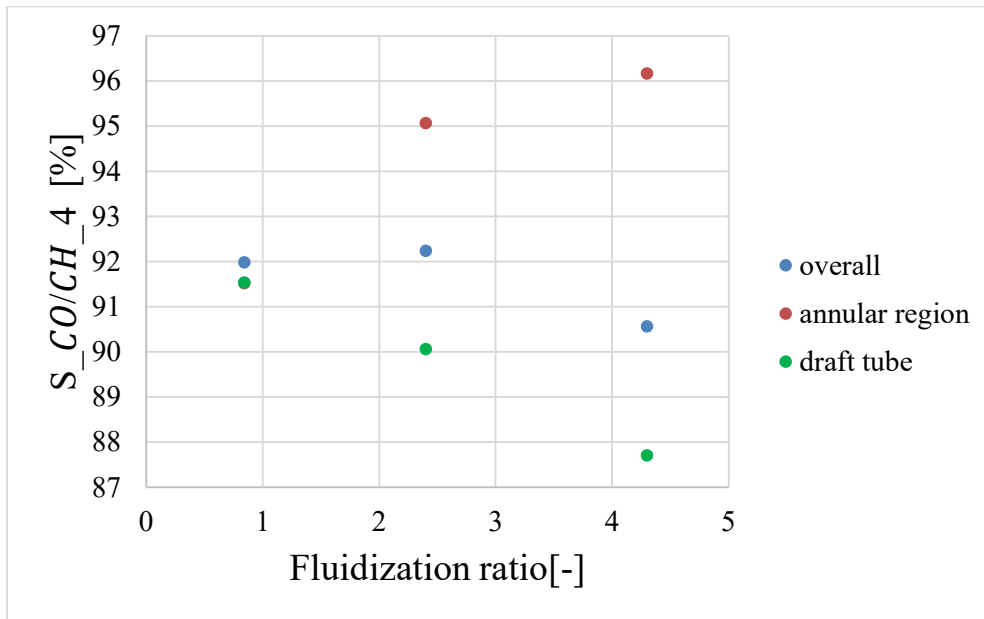


Figure 33: fluidization ratio vs CO conversion of test run 1.

Table 12: Carbon monoxide conversion for test run 1.

Fluidization ratio	0.84	2.4	4.3
$\chi_{CO}$	[%]	[%]	[%]
Overall section	98.64	98.91	96.15
Annular region	98.45	99.82	99.84
Draft tube	98.62	98.17	94.59

As we can notice, we have almost complete conversion of carbon monoxide for all the conditions. Also, for this parameter, the best overall situation is given from the fluidization ratio equal to 2.4. Specifically, the maximum overall conversion obtained is 98.81%. Moreover, the CO conversion has the same trend of the CH<sub>4</sub> yield in the two regions: it increases with fluidization ratio in the annular region, and it decreases with it in the draft tube.



**Figure 34: fluidization ratio vs selectivity to CH<sub>4</sub> of test run 1.**

**Table 13: Selectivity to methane for test run 1.**

Fluidization ratio	0.84	2.4	4.3
S <sub>CO/CH<sub>4</sub></sub>	[%]	[%]	[%]
Overall section	91.98	92.24	90.56
Annular region	91.52	95.07	96.17
Draft tube	91.54	90.07	87.70

As we can notice, the maximum overall selectivity is obtained also in this case for fluidization ratio equal to 2.4 and it is 92.24%. The same trends with the fluidization ratio in the two different regions is observed also for the selectivity.

Being methanation an exothermic reaction, from a thermodynamic point of view it is favoured at low temperatures. Furthermore, high temperatures can induce catalyst deactivation due to sintering of metal particles or carbon deposition. Thus, heat removal and the resulting temperature level are fundamental parameters to evaluate. In particular, it is fundamental to keep the temperature in the reactor as low as possible. Moreover, a homogeneous temperature in the different regions of the reactor is desired. The temperature during time in the annular region and in the draft tube are analysed. In particular, an average temperature from the various readings of the different thermocouples is calculated. The temperature profile during time is reported in Figure 37.

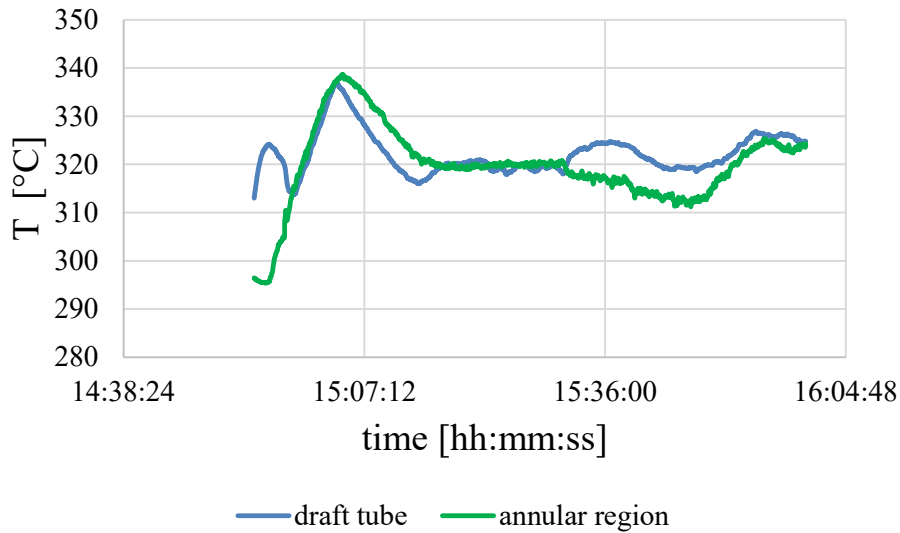


**Figure 35: time vs average temperature of test run 1.**

The temperature level is about the same in the two different regions. Specifically, it is possible to keep in this case a temperature approximately constant and equal to 320 °C using pressurized air as cooling fluid. There is a sudden temperature increase both in annular region and draft tube sections and it can represent the starting point of the exothermic reaction. When the reaction starts, temperature starts to increase really fast, and the pressurized air pre-heating is turned off manually. For this reason, it will take a while to reduce the temperature and stabilize it.

In order to analyse the temperature profile along the height of the two regions of the reactor, the single thermocouple temperatures will be reported. Specifically, in the annular region, three thermocouples are used, which are from the bottom to the top indicated by Temperature Indicator Regulator (TIR) 38, TIR 39 and TIR 40. For the draft tube, two thermocouples are used, and they are from the bottom to the top indicated by TIR 42 and TIR 44. Figure 38 shows the temperature profiles for the single thermocouples in annular region while Figure 39 shows the single thermocouple profile in the draft tube.

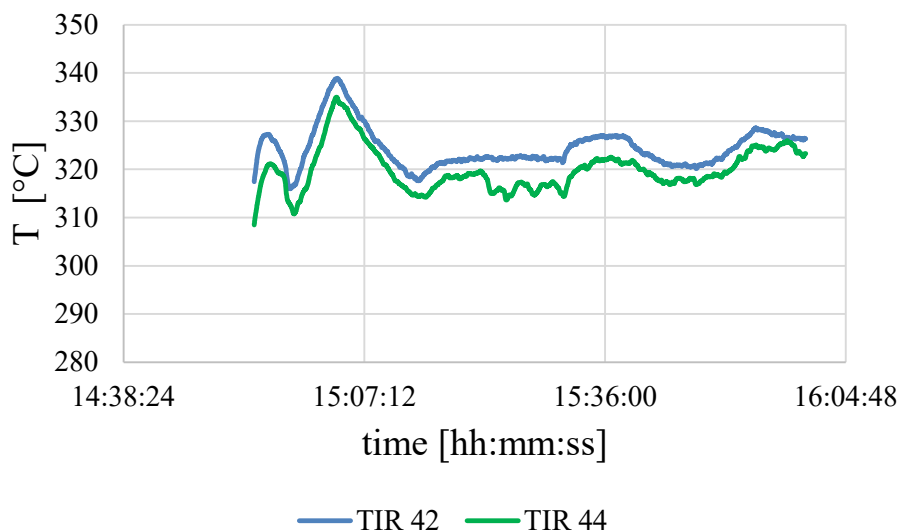


**Figure 36: time vs temperature at different height in the draft tube.**

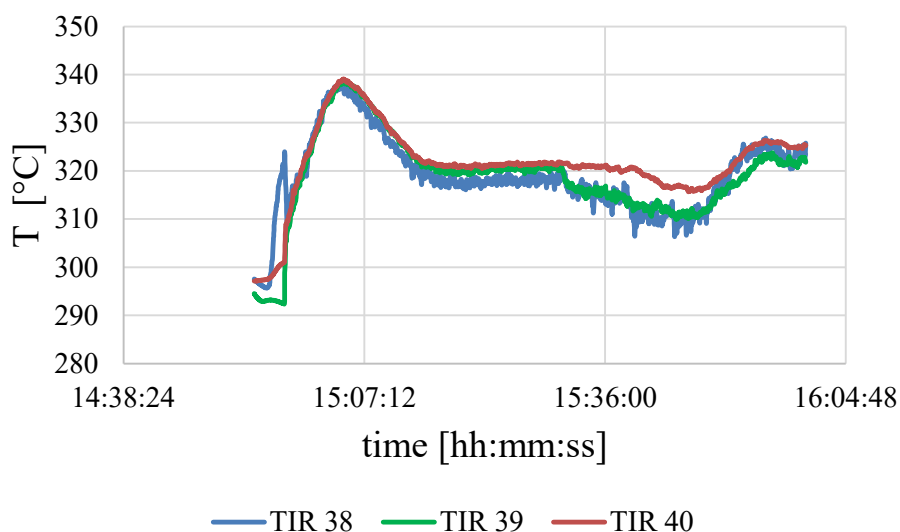


**Figure 37: time vs temperature at different height in the annular region.**

In the annular region temperature increases with the height, while in the draft tube temperature decreases along the height of the reactor.

## 4.2 Test run 2: Stoichiometric CO methanation with $WHSV = 1.8 \text{ NI}\cdot\text{h}^{-1}\cdot\text{g}_{\text{cat}}^{-1}$ and variable fluidization ratio

In this test run, methanation is investigated with an inlet  $\text{H}_2/\text{CO}$  ratio equal to 3 which means SN equal to 1. The WHSV in this experiment is equal to  $1.8 \text{ NI}\cdot\text{h}^{-1}\cdot\text{g}_{\text{cat}}^{-1}$ . Specifically, this inlet composition

corresponds to the stoichiometric CO methanation one and the total inlet flowrate is equal to 2.88 Nm<sup>3</sup>/h. The reaction is operated with an approximately constant temperature of 320 °C. The fluidization ratio is varied. Table 14 shows the inlet composition, reported as percentage by volume.

**Table 14: Inlet composition of test run 2**

Component	[vol-%]
CO	24.4
H <sub>2</sub>	75.6
CO <sub>2</sub>	0
CH <sub>4</sub>	0
H <sub>2</sub> O	0

In this case, the reactions observed are CO methanation (Eq. 2.2) and WGS (Eq. 2.3). Moreover, three values for the fluidization ratio are analysed. The outlet composition is measured at the outlet of the annular section, at the outlet of the draft tube and at the outlet of the overall section. The overall outlet compositions are reported in Table 15. The molar fractions are reported as percentage by volume.

**Table 15: Overall outlet composition of test run 2.**

Fluidization ratio	2.2	4.9	7.6
Component	[vol-%]	[vol-%]	[vol-%]
CO	2.07	2.16	6.61
H <sub>2</sub>	25.17	25.40	36.19
CO <sub>2</sub>	4.65	4.64	4.01
CH <sub>4</sub>	36.47	36.30	28.68
H <sub>2</sub> O	31.64	31.49	24.51

From the results, we can observe that the amount of CO and H<sub>2</sub> is increasing with fluidization ratio, while the amount of CH<sub>4</sub> and H<sub>2</sub>O is decreasing with this fluidization ratio. The maximum production of CH<sub>4</sub>, which corresponds to the maximum consumption of CO is obtained for a fluidization ratio equal to 2.2. Moreover, the WGS takes place and thus we have production of CO<sub>2</sub>. In particular, the CO<sub>2</sub> production decreases with the fluidization ratio.

The comparison between the outlet compositions of the draft tube and the annular region can be seen in Table 16.

**Table 16: Outlet compositions of test run 2 for the two different outlet sections.**

Reactor section	Annular region	Annular region	Annular region	Draft tube	Draft tube	Draft tube
Fluidization ratio	2.2	4.9	7.6	2.2	4.9	7.6
Component	[vol-%]	[vol-%]	[vol-%]	[vol-%]	[vol-%]	[vol-%]
CO	0.76	0.69	0.98	2.22	5.80	7.55
H <sub>2</sub>	19.34	17.04	15.04	27.27	36.81	41.39
CO <sub>2</sub>	4.18	3.65	2.93	5.07	4.77	4.61
CH <sub>4</sub>	40.04	41.22	42.08	35.34	28.77	25.60
H <sub>2</sub> O	35.68	37.39	38.96	30.10	23.84	20.84

Concerning both the products, CH<sub>4</sub> and H<sub>2</sub>O, their amount increases with the fluidization ratio in the annular region while decreases in the draft tube. Furthermore, hydrogen has an opposite trend: it decreases in the annular region and increases in the draft tube, with the increase of fluidization ratio. Concerning CO, it has a trend with a minimum along the fluidization ratio values in the annular region and it increases in the draft tube. Carbon dioxide decreases both in the annular region and in the draft tube.

The methane yield is also analysed in this test run. Figure 40 shows the trends and Table 17 the specific values.

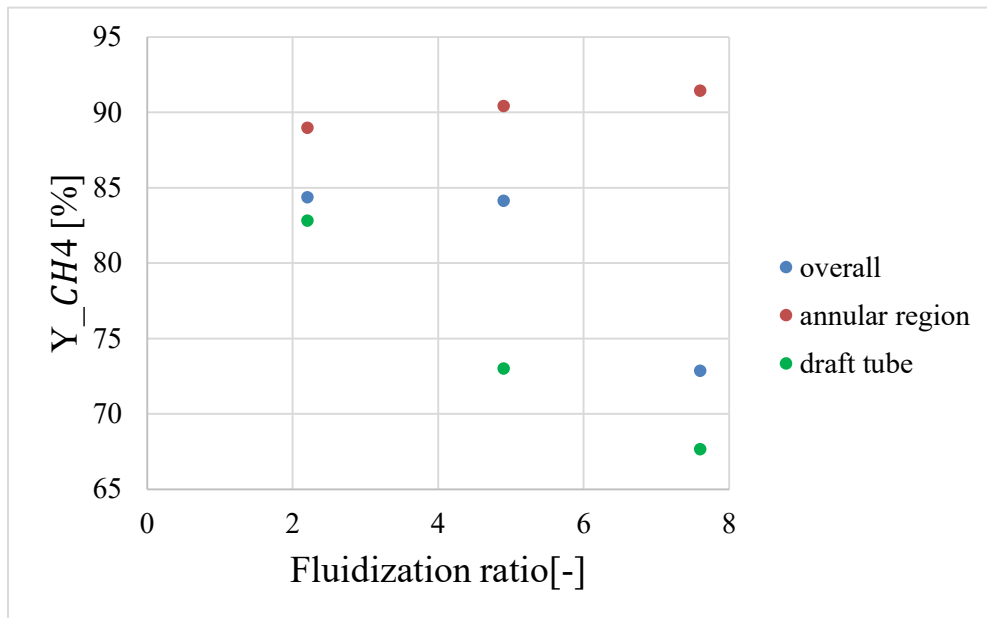


**Figure 38: fluidization ratio vs methane yield of test run 2.**

**Table 17: Methane yields for test run 2.**

Fluidization ratio	2.2	4.9	7.6
Y <sub>CH4</sub>	[%]	[%]	[%]
Overall section	84.37	84.15	72.86
Annular region	88.98	90.43	91.45
Draft tube	82.84	73.01	67.67

The yield at the outlet of the annular region increases with the fluidization ratio, while it decreases with it at the outlet of the draft tube. Moreover, the decrease is much higher than the increase. For this reason, the overall methane yield decreases with the fluidization ratio and it is maximum for a fluidization ratio equal to 2.2. The maximum overall yield reached is of 84.37%.

For completeness, the results regarding selectivity from CO to methane and CO conversion are also shown. Figure 41 shows the trends of CO conversion and Figure 42 shows the ones of selectivity. Moreover, Table 18 shows the conversion values and Table 19 the selectivity ones.

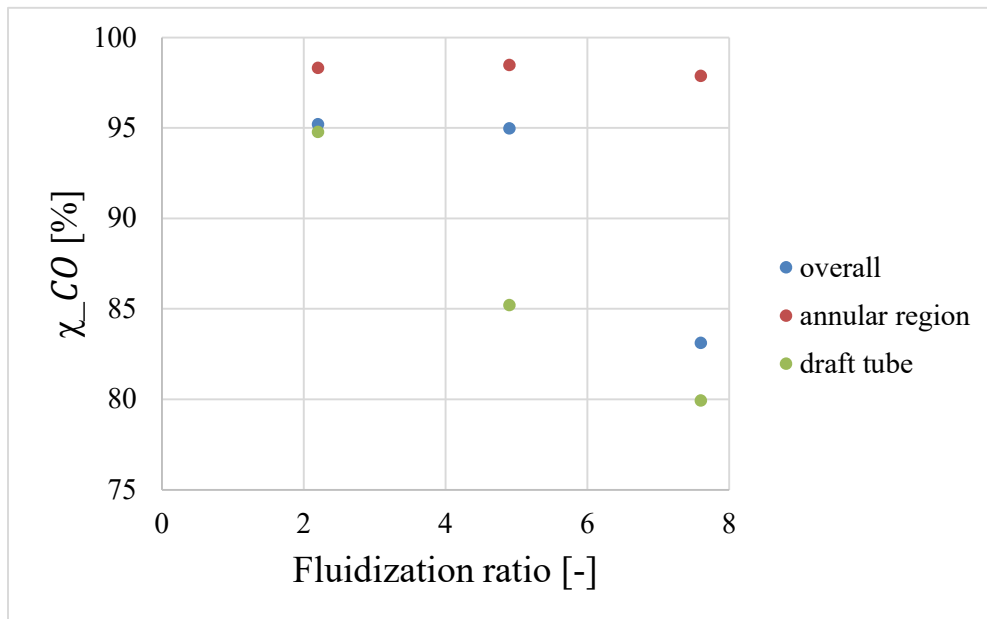


**Figure 39: fluidization ratio vs CO conversion of test run 2.**

**Table 18: Carbon monoxide conversion for test run 1.**

Fluidization ratio	2.2	4.9	7.6
χ <sub>CO</sub>	[%]	[%]	[%]
Overall section	95.19	94.96	83.18
Annular region	93.31	98.47	97.86
Draft tube	94.77	85.19	79.93

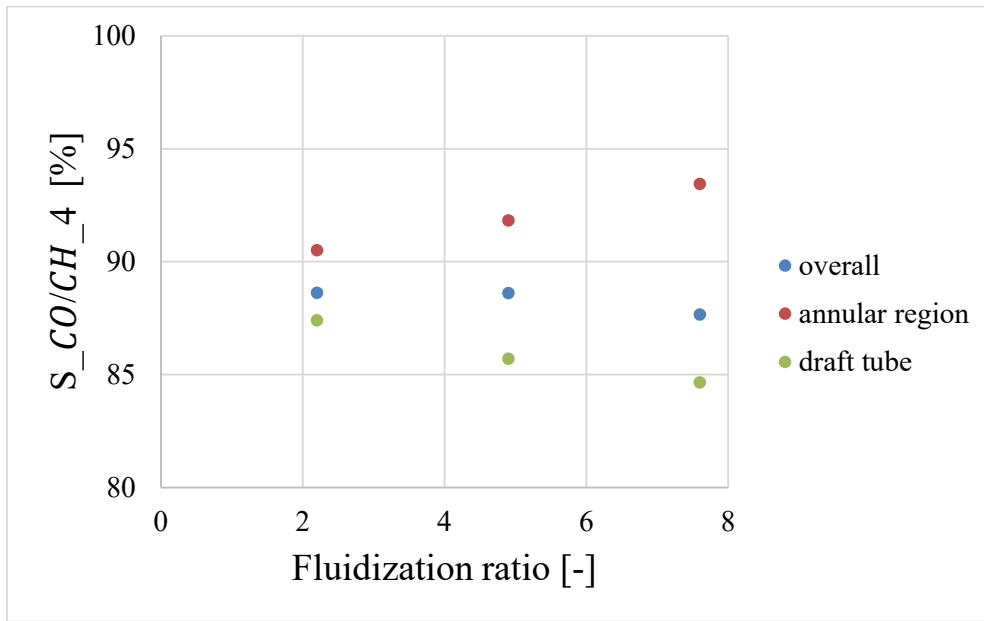


**Figure 40: fluidization ratio vs selectivity from CO to CH<sub>4</sub> of test run 2.**

**Table 19: Selectivity from carbon monoxide to methane of test run 2.**

Fluidization ratio	2.2	4.9	7.6
S <sub>CO/CH<sub>4</sub></sub>	[%]	[%]	[%]
Overall section	88.63	88.62	87.66
Annular region	90.51	91.84	93.45
Draft tube	87.41	85.71	84.66

The selectivity from carbon monoxide to methane has the same trends as the methane yield. It increases with the fluidization ratio in the annular region, and it decreases with it in the draft tube. Its overall trend has a maximum for fluidization ratio equal to 2.2 and it decreases for higher values of this ratio. The maximum selectivity reached is of 88.63%. Moreover, it is almost the same value and equal to 88.62% also for fluidization ratio equal to 4.9. Concerning CO conversion, it has the same trend for the draft tube, and it decreases with the flowrates while it has a trend with a maximum for 4.9 for the annular region. The resulting overall trend is the same as selectivity and yield: CO conversion decreases with the fluidization ratio. The maximum overall conversion reached is equal to 95.19% and it is obtained for a fluidization ratio equal to 2.2.

The temperature profile during time is reported in Figure 43. Specifically, the average temperature from the various measurement of both the annular region and the draft tube is shown.



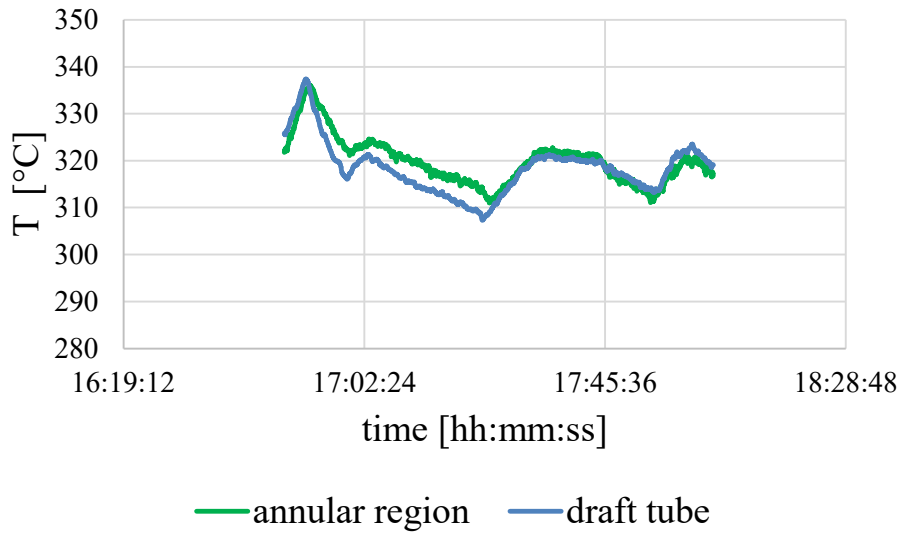


**Figure 41: time vs average temperature of test run 2.**

The temperature profile is almost identical in the two different regions of the reactor. The temperature is kept about constant and equal to 320 °C for the entire reaction time. Temperature trend is also analysed for the single thermocouples. In the annular region, as the case with a lower WHSV, the temperature increases from the bottom to the top of the reactor. For the draft tube, we have that the temperature decreases from the bottom to the top and also this trend is the same as the previous test run.

### 4.3 Test run 3: Stoichiometric CO methanation with variable temperature

In this test run, stoichiometric CO methanation is investigated. Specifically, an inlet mixture with a  $H_2/CO$  ratio equal to 3 is used as feed. In these conditions, the SN is equal to 1. The pressure is equal to 1 bar and the WHSV is  $1.2 \text{ NI}\cdot\text{h}^{-1}\cdot\text{g}_{\text{cat}}^{-1}$  which corresponds to an inlet flowrate equal to  $1.92 \text{ Nm}^3/\text{h}$ . Temperature is the varying parameter and specifically, it is varied from 280 °C to 420 °C. This experiment is operated with constant inlet volume flows to both reactor regions. Specifically, it is implemented a fluidization ratio equal to 1. In this way, fluidization results to be the same in the two sections. This is confirmed by the fact that the outlet compositions at the two sections are approximately the same. For this reason, only the overall outlet compositions are reported in the results section. Table 20 shows the input composition of this experimental test.

**Table 20: Inlet composition of test run 3.**

Component	[vol-%]
CO	24.7
H <sub>2</sub>	75.3
CO <sub>2</sub>	0
CH <sub>4</sub>	0
H <sub>2</sub> O	0

Feeding this mixture means that the most relevant reactions are CO methanation (Eq. 2.2) and WGS (Eq. 2.3). The reaction is analysed for 8 temperatures: 280 °C, 290 °C, 320 °C, 340 °C, 360 °C, 380 °C, 400 °C and 420 °C. The trend of the overall outlet composition of each component with the temperature is reported in the following figures (Figure 44-48).

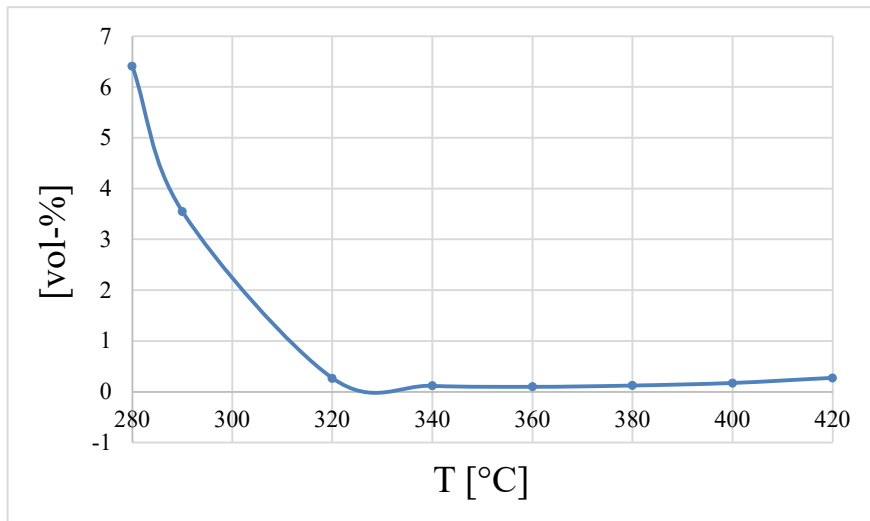


**Figure 42: temperature vs outlet CO percentage by volume of test run 3.**

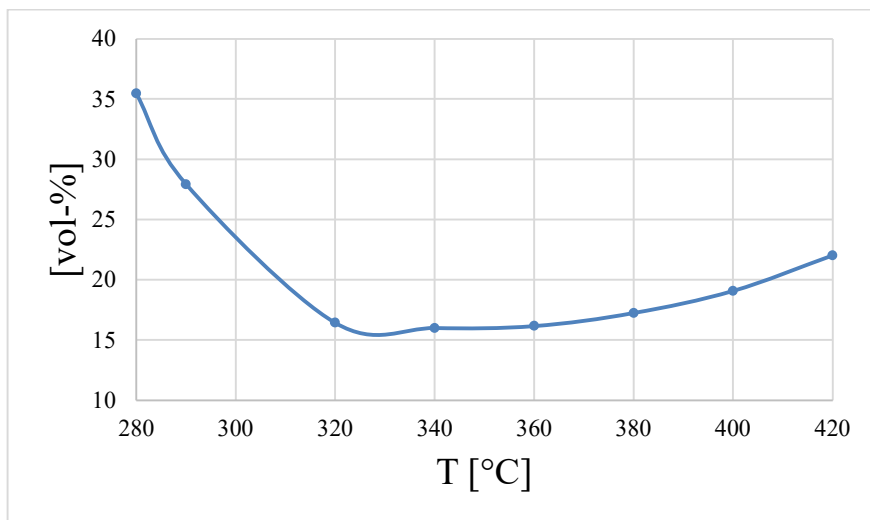


**Figure 43: temperature vs outlet H<sub>2</sub> percentage by volume of test run 3.**

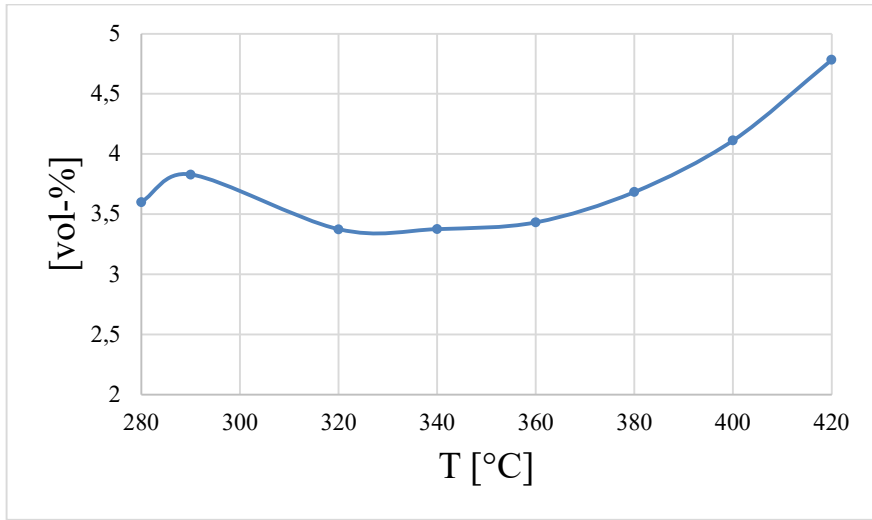


**Figure 44: temperature vs outlet CO<sub>2</sub> percentage by volume of test run 3.**

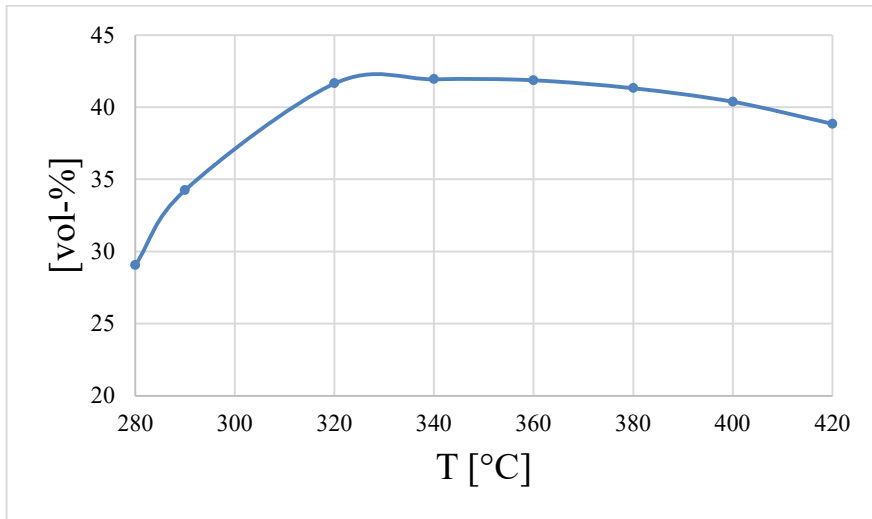


**Figure 45: temperature vs outlet CH<sub>4</sub> percentage by volume of test run 3.**

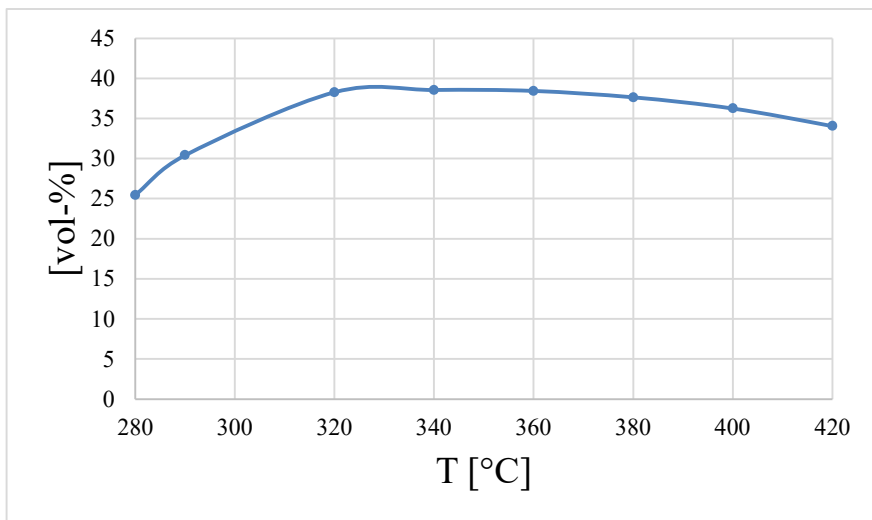


**Figure 46: temperature vs outlet H<sub>2</sub>O percentage by volume of test run 3.**

Both the reactants have a trend with a minimum. The minimum corresponds to their maximum consumption and specifically it is at 360 °C for CO and at 340 °C for H<sub>2</sub>. At the same way, the products have a trend with a maximum: CH<sub>4</sub> maximum production is reached at 360 °C and water maximum production at 340 °C. CO<sub>2</sub> is produced and this means that WGS takes place. In particular, at 360 °C we have the maximum production of CH<sub>4</sub> but not the maximum production of H<sub>2</sub>O. This probably means that WGS is also favoured at that temperature, and water is consumed in that reaction. The same reason could explain the fact that the minimum quantity of H<sub>2</sub> does not correspond to the minimum CO. Therefore, at 360 °C WGS takes place, and this reduces water amount and increases H<sub>2</sub>.

Specifically, the maximum production of CH<sub>4</sub> is at intermediate temperatures. This can be explained by the fact that methanation is an exothermic reaction and thus, it is favoured from a thermodynamic point of view at low temperatures while for a kinetic point of view, it is favoured at high temperatures. Concerning CO<sub>2</sub> trend, it increases with temperature and it has its maximum production at 420 °C. In particular WGS reaction is slightly exothermic, and it is more sensitive to kinetics than thermodynamics. This explains the maximum CO<sub>2</sub> amount at the highest experimented temperature. Moreover, methane yield, CO conversion and selectivity from CO to CH<sub>4</sub> are analysed and reported in the following Tables (21-23) and Figures (49-51).

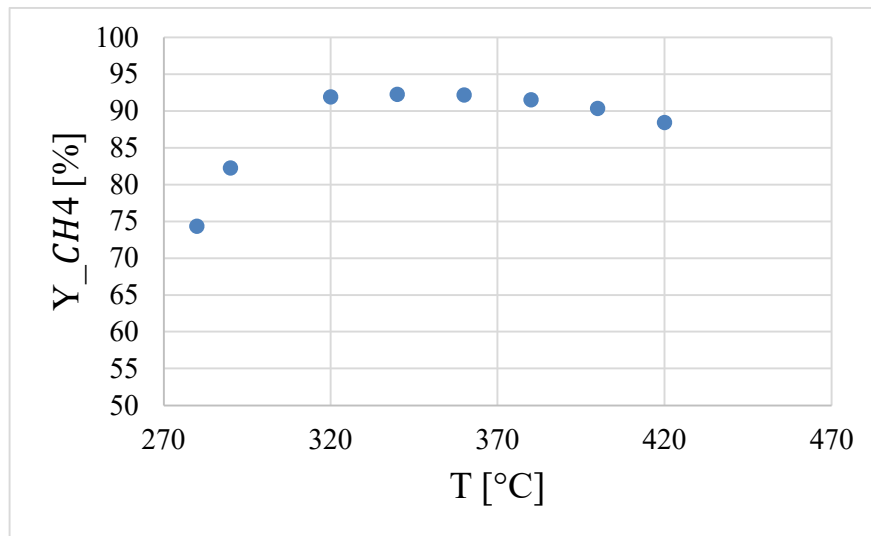


**Figure 47: temperature vs methane yield of test run 3.**

**Table 21: methane yield at different temperatures of test run 3.**

T [°C]=	280	290	320	340	360	380	400	420
Y_CH4	[%]	[%]	[%]	[%]	[%]	[%]	[%]	[%]
Overall section	74.37	82.27	91.95	92.31	92.22	91.55	90.40	88.48

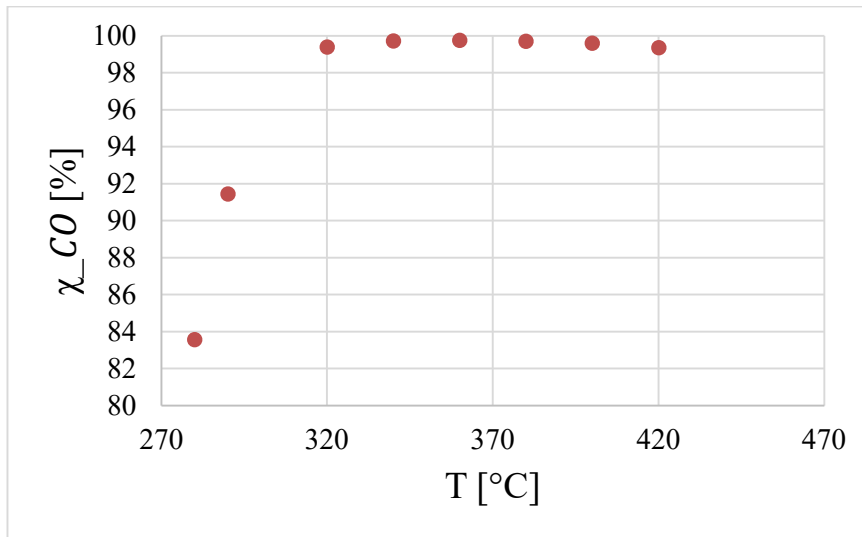


Figure 48: temperature vs carbon monoxide conversion of test run 3.

Table 22: carbon monoxide conversion at different temperatures of test run 3.

T [°C]=	280	290	320	340	360	380	400	420
χ <sub>CO</sub>	[%]	[%]	[%]	[%]	[%]	[%]	[%]	[%]
Overall section	83.59	91.47	99.67	99.74	99.72	91.55	99.61	99.37

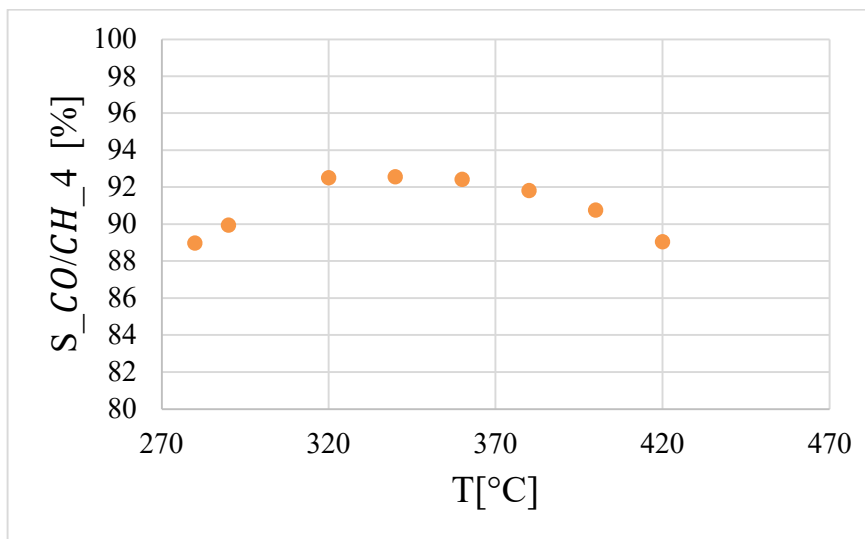


Figure 49: temperature vs selectivity from carbon monoxide to methane of test run 3.

Table 23: selectivity from carbon monoxide to methane at different temperatures of test run 3.

T [°C]=	280	290	320	340	360	380	400	420
S <sub>CO/CH<sub>4</sub></sub>	[%]	[%]	[%]	[%]	[%]	[%]	[%]	[%]
Overall section	88.97	89.94	92.50	92.55	92.42	91.81	90.75	89.03

Methane yield, carbon monoxide conversion and selectivity from carbon monoxide to methane have a trend with a maximum. The maximum values for all these parameters are reached for  $T=340\text{ }^{\circ}\text{C}$ . Specifically, the maximum methane yield is 92.30%, the maximum carbon monoxide conversion is equal to 99.74% and the maximum selectivity to methane is 92.55%. We can therefore conclude that the optimal temperature for stoichiometric CO methanation, with  $\text{WHSV}=1.2\text{ NI}\cdot\text{h}^{-1}\cdot\text{g}_{\text{cat}}^{-1}$  and a pressure equal to 1 bar, is  $340\text{ }^{\circ}\text{C}$ .

#### 4.4 Test run 4: Under-stoichiometric CO<sub>2</sub> methanation with variable temperature

In this test run, an under-stoichiometric mixture for CO<sub>2</sub> methanation is investigated. For this purpose, an inlet mixture with  $\text{SN}=0.9$  is used as feed. The pressure is equal to 1 bar and the WHSV is  $1.2\text{ NI}\cdot\text{h}^{-1}\cdot\text{g}_{\text{cat}}^{-1}$  which corresponds to an inlet volumetric flowrate of  $1.92\text{ Nm}^3/\text{h}$ . In this case temperature is the varying parameter, and it is varied from  $270\text{ }^{\circ}\text{C}$  to  $420\text{ }^{\circ}\text{C}$ . In this experiment, the inlet volume flows to the two reactor regions are constant. In particular, the fluidization ratio is equal to 1. This value is chosen because in these conditions the fluidization is the same for the two sections. For this reason, we have the same outlet compositions for the two sections and the overall section. The composition of the feed stream used in this experiment is shown in Table 24.

**Table 24: Inlet composition of test run 4.**

Component	[vol-%]
CO	0
H <sub>2</sub>	78.76
CO <sub>2</sub>	21.24
CH <sub>4</sub>	0
H <sub>2</sub> O	0

With this feed composition, the most observed reactions are CO methanation (Eq. 2.2), from which methane and water are produced, and RWGS (Eq. 2.8) which produces CO and additional water. Specifically, the combination of these two reactions is the CO<sub>2</sub> methanation (Eq. 2.1). The temperature investigated are equal to  $270\text{ }^{\circ}\text{C}$ ,  $280\text{ }^{\circ}\text{C}$ ,  $290\text{ }^{\circ}\text{C}$ ,  $300\text{ }^{\circ}\text{C}$ ,  $310\text{ }^{\circ}\text{C}$ ,  $335\text{ }^{\circ}\text{C}$ ,  $360\text{ }^{\circ}\text{C}$ ,  $375\text{ }^{\circ}\text{C}$ ,  $400\text{ }^{\circ}\text{C}$ ,  $410\text{ }^{\circ}\text{C}$  and  $420\text{ }^{\circ}\text{C}$ . The outlet composition profiles are reported in the following Figures (52 – 56) and the results are discussed below them.

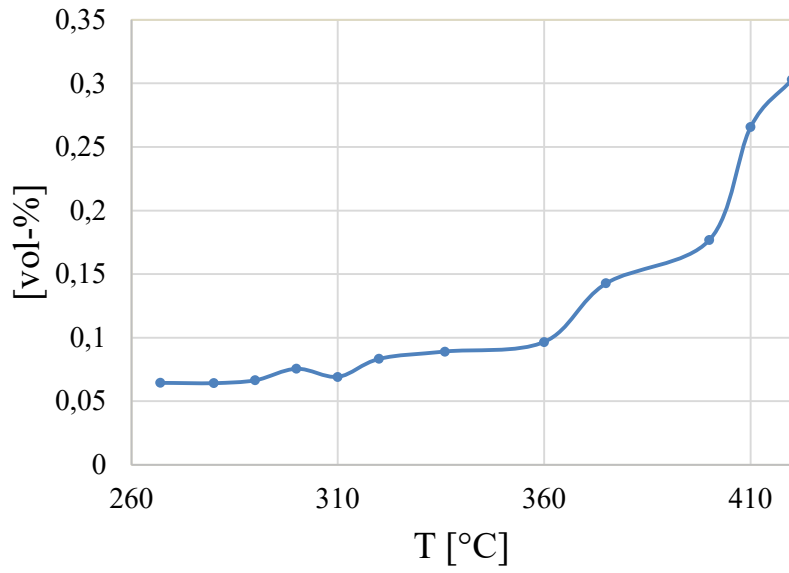


Figure 50: temperature vs outlet CO percentage by volume of test run 4.

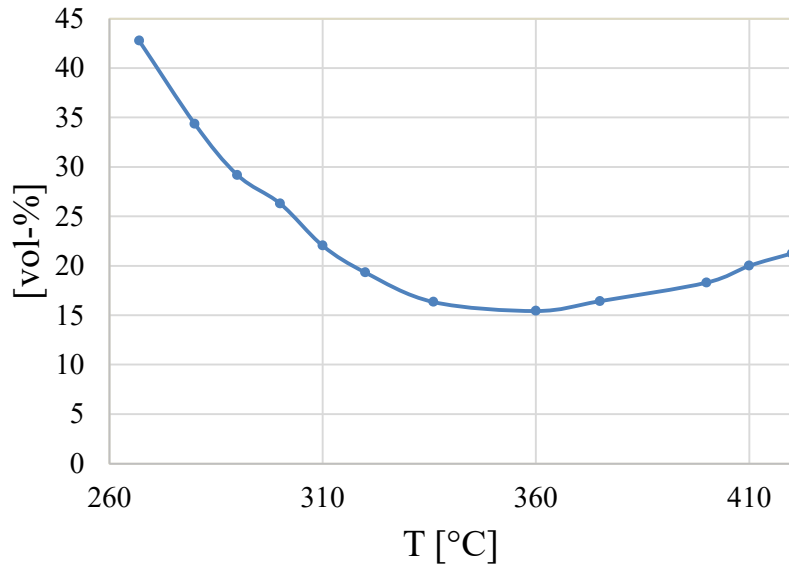
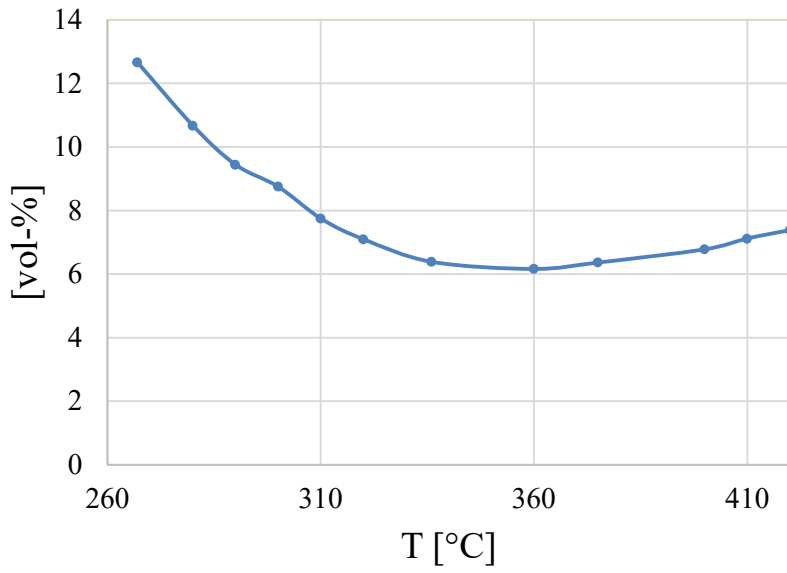
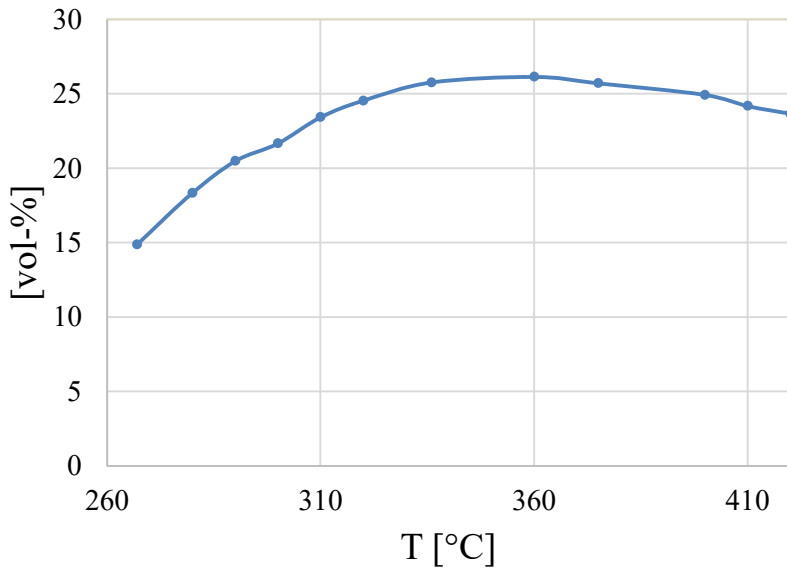


Figure 51: temperature vs outlet H<sub>2</sub> percentage by volume of test run 4.



**Figure 52: temperature vs outlet CO<sub>2</sub> percentage by volume of test run 4.**



**Figure 53: temperature vs outlet CH<sub>4</sub> percentage by volume of test run 4.**



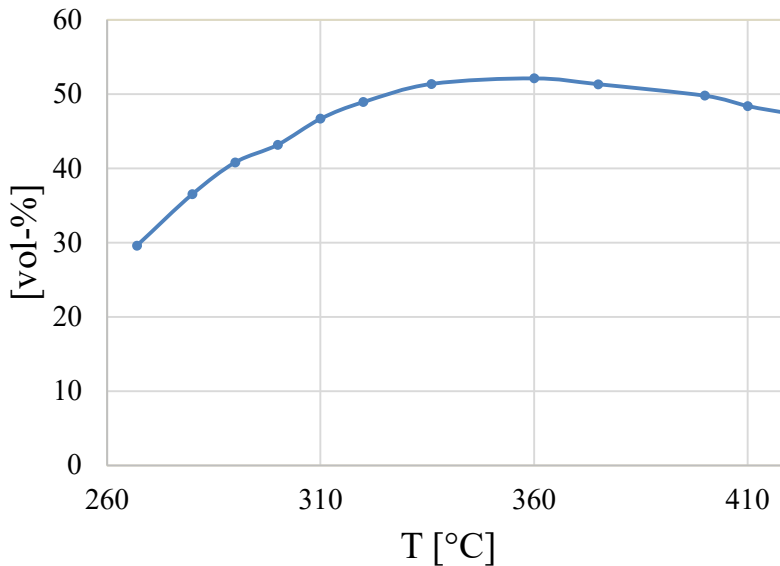


**Figure 54: temperature vs outlet H<sub>2</sub>O percentage by volume of test run 4.**

The amount of CO, which is produced by the RWGS reaction, increases with the temperature. That is probably due to the fact that the RWGS is slightly endothermic and therefore it is mainly influenced by kinetics. Therefore, the maximum production of CO is at the maximum temperature, due to the enhanced kinetics at high temperatures. Concerning H<sub>2</sub> and CO<sub>2</sub> amounts, they have a trend with a minimum. The minimum of the amounts of both components is reached at T=360 °C. Consequently, at this temperature there is also the maximum production of water and methane. For this experimental test, methane yield is also analysed.

Moreover, there are other relevant parameters to calculate because the main reactant in this case is carbon dioxide. In particular, they are CO<sub>2</sub> conversion and selectivity from CO<sub>2</sub> to CH<sub>4</sub>. These parameters are shown in Table 25, Table 26 and Table 27 for all the different temperatures investigated. Moreover, their trends with temperature are shown in Figure 57, Figure 58 and Figure 59.

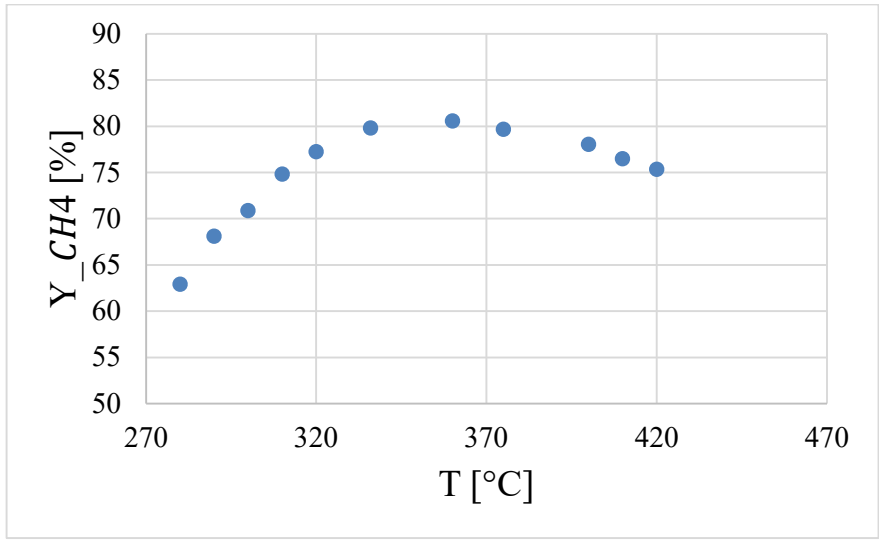
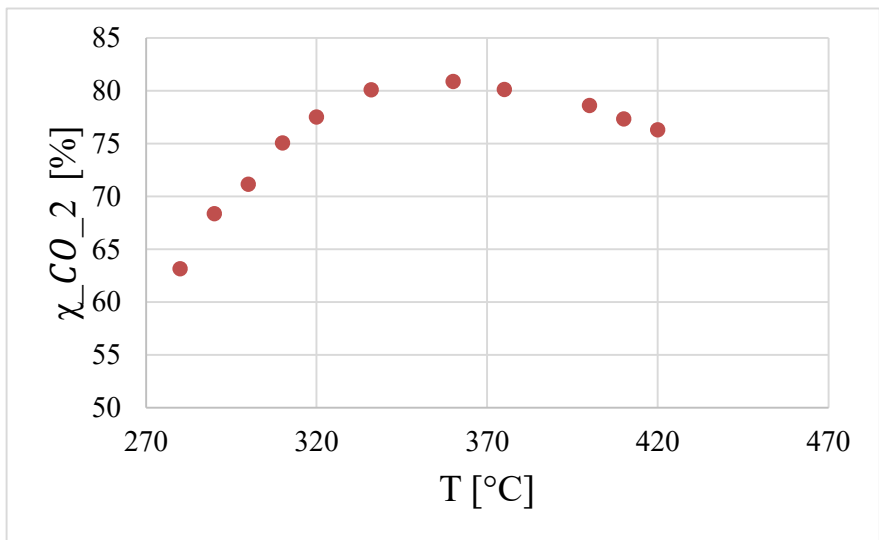


**Figure 55: temperature vs methane yield of test run 4.**

**Table 25: methane yield at different temperatures of test run 4.**

T [°C]=	270	280	290	300	310	320	335	360	375	400	410	420
Y <sub>CH4</sub>	[%]	[%]	[%]	[%]	[%]	[%]	[%]	[%]	[%]	[%]	[%]	[%]
Overall section	53.70	62.95	68.16	70.93	74.87	77.27	79.83	80.59	79.71	78.08	76.51	75.37

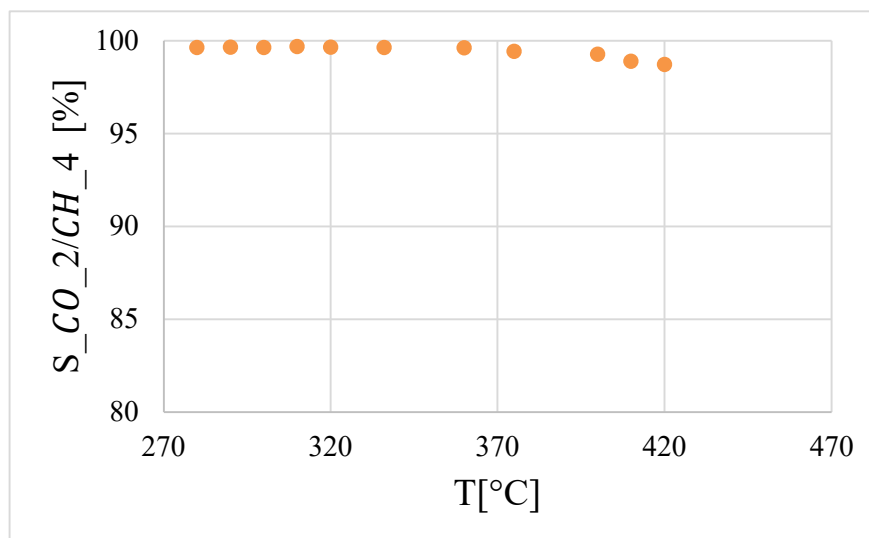
Methane yield has a trend with a maximum when temperature increases. Specifically, the maximum yield is reached at  $T=360\text{ }^{\circ}\text{C}$  and it is equal to 80.59 %. This trend could be explained by the fact that being  $\text{CO}_2$  methanation an exothermic reaction, it is favoured thermodynamically at low temperatures and kinetically at high temperatures. Therefore, the maximum methane production is observed at intermediate temperatures.



**Figure 56: temperature vs carbon dioxide conversion of test run 4.**

**Table 26: carbon dioxide conversion at different temperatures of test run 4.**

T [°C]=	270	280	290	300	310	320	335	360	375	400	410	420
$\chi_{CO_2}$	[%]	[%]	[%]	[%]	[%]	[%]	[%]	[%]	[%]	[%]	[%]	[%]
Overall section	53.93	63.17	68.38	71.18	75.09	77.54	80.11	80.89	80.16	78.64	77.36	76.34

**Figure 57: temperature vs selectivity from CO<sub>2</sub> to methane of test run 4.****Table 27: selectivity from CO<sub>2</sub> to CH<sub>4</sub> at different temperatures of test run 4.**

T [°C]=	270	280	290	300	310	320	335	360	375	400	410	420
$\chi_{CO_2}$	[%]	[%]	[%]	[%]	[%]	[%]	[%]	[%]	[%]	[%]	[%]	[%]
Overall section	99.56	99.65	99.67	99.649	99.70	99.66	99.65	99.63	99.44	99.29	98.91	98.73

Carbon dioxide conversion has a trend with a maximum. Its maximum value is equal to 80.89 % and it is reached at T=360 °C, the same value for which it is obtained the maximum methane yield. Concerning selectivity from carbon dioxide to methane, it has an almost flat profile with temperature with values around 98-99 %. This means that even if it is not observed almost complete conversion of CO<sub>2</sub>, almost all the CO<sub>2</sub> converted gives methane and only a very small part reacts in the RWGS, generating CO and H<sub>2</sub>O. This is confirmed by the very low outlet amount of CO observed. Anyhow, the maximum value for selectivity is reached for a temperature equal to 310 °C and it is equal to 99.7 %.

## 4.5 Test run 5: Stoichiometric CO<sub>2</sub> methanation with variable temperature

In this experimental test, a mixture with the ratio H<sub>2</sub>/CO<sub>2</sub> equal to 4 and an SN equal to 1 is implemented.

Specifically, this ratio corresponds to the stoichiometric condition for CO<sub>2</sub> methanation. The pressure is equal to 1 bar and the WHSV is 1.5 NI·h<sup>-1</sup>·g<sub>cat</sub><sup>-1</sup> which corresponds to an inlet volumetric flowrate of 2.4 Nm<sup>3</sup>/h. Moreover, 1.6 kg of catalyst are used. A fluidization of 1 is implemented. The temperature is varied from 280 °C to 420 °C. The inlet composition is shown in Table 28.

**Table 28: inlet composition of test run 5.**

Component	[vol-%]
CO	0
H <sub>2</sub>	80.02
CO <sub>2</sub>	19.98
CH <sub>4</sub>	0
H <sub>2</sub> O	0

With this inlet compositions, the most observed reactions are CO methanation (Eq. 2.2) and RWGS reactions (Eq. 2.8), whose combination gives the CO<sub>2</sub> methanation (Eq. 2.1). Specifically, the values of the temperatures investigated are 280 °C, 290 °C, 300 °C, 320 °C, 340 °C, 360 °C, 380 °C, 390 °C, 400 °C, 410 °C and 420 °C. The trends of the outlet compositions with the temperature are reported in Figure 60, Figure 61, Figure 62, Figure 63 and Figure 64.

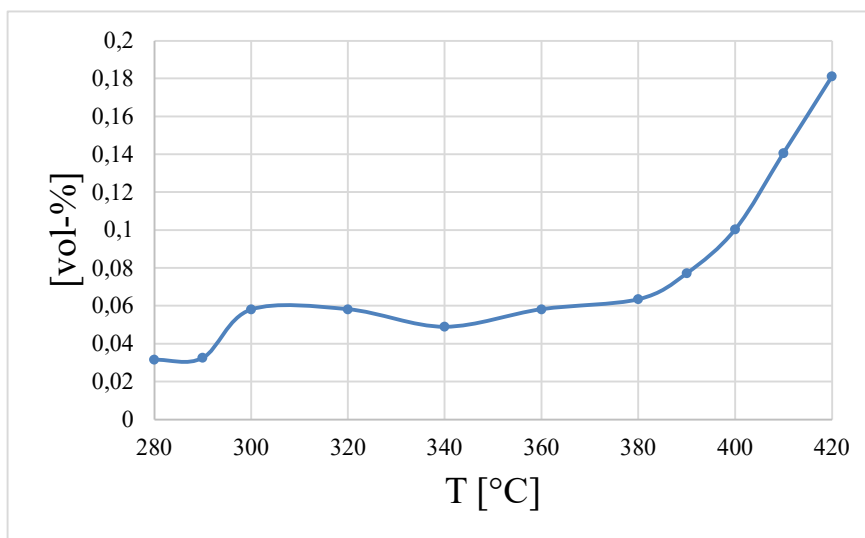


**Figure 58: temperature vs outlet CO percentage by volume of test run 5.**

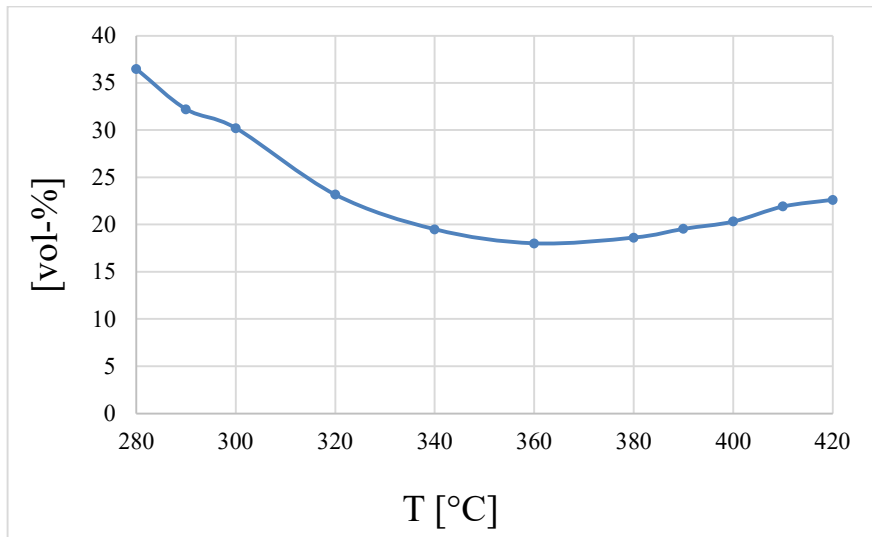


**Figure 59: temperature vs outlet H<sub>2</sub> percentage by volume of test run 5.**

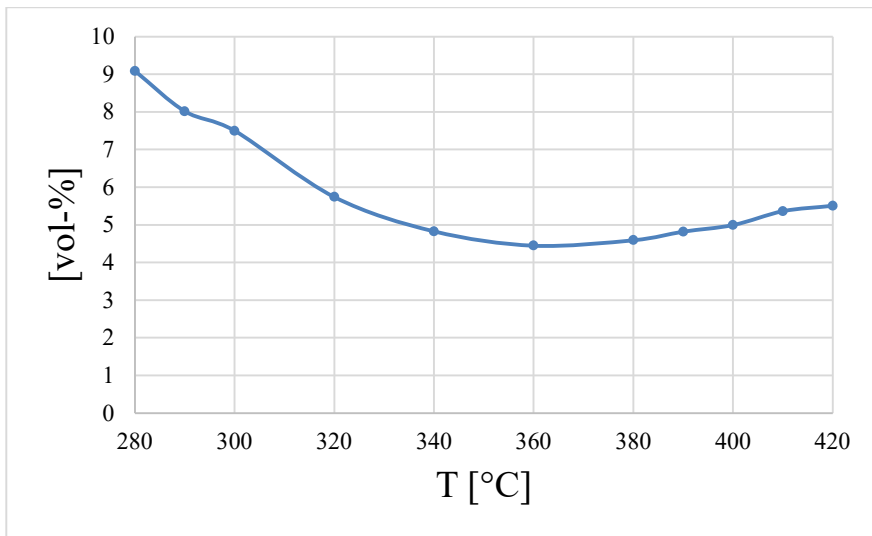


**Figure 60: temperature vs outlet CO<sub>2</sub> percentage by volume of test run 5.**

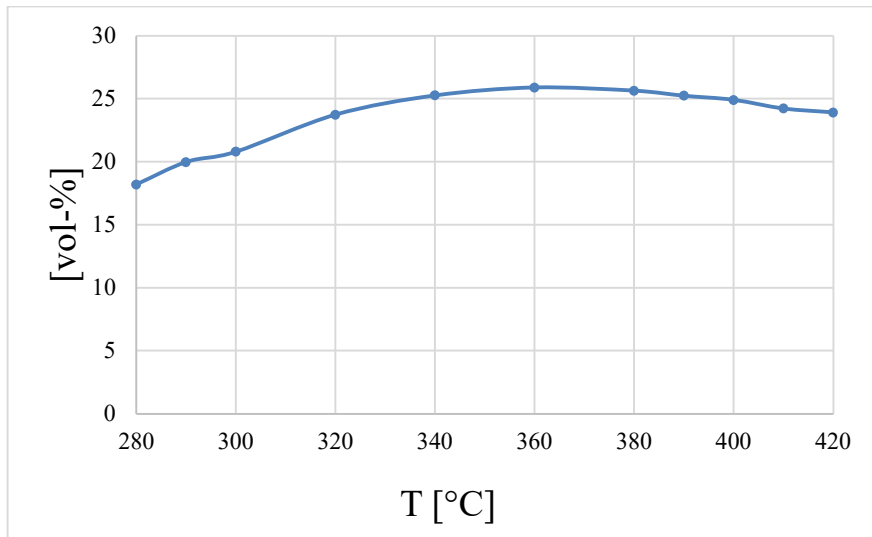


**Figure 61: temperature vs outlet CH<sub>4</sub> percentage by volume of test run 5.**

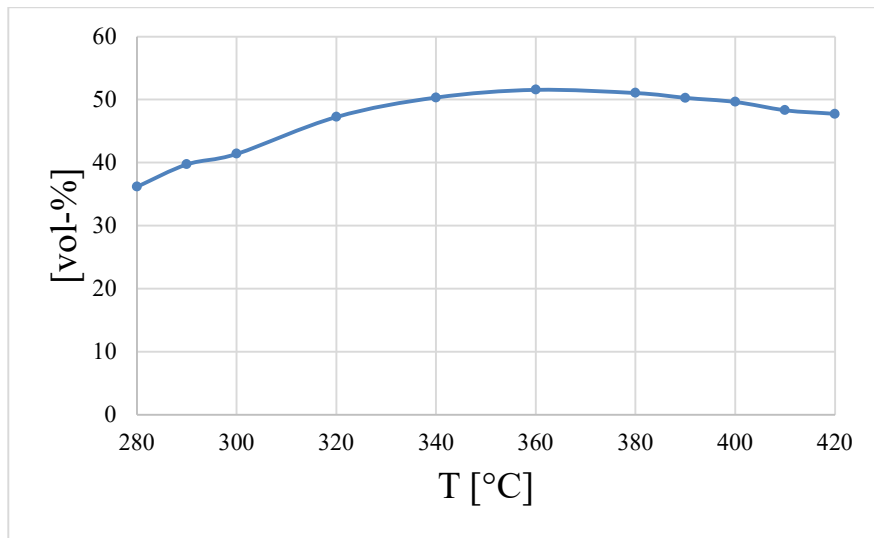


**Figure 62: temperature vs outlet H<sub>2</sub>O percentage by volume of test run 5.**

The trend of CO, which is produced by the RWGS reaction, increases with increasing temperature. This can be explained by the fact that RWGS is a slightly endothermic reaction, and it is mainly influenced by kinetics, which is favoured at high temperatures. Moreover, there is a local minimum in CO percentage by volume at T=340 °C. This is due to the fact that at that temperature, CO methanation is particularly enhanced and we have seen it from the results of stoichiometric CO methanation. Concerning the trends of CO<sub>2</sub> and H<sub>2</sub>, which are the reactants of the global reaction, they have a trend with a minimum. Their minimum amount is obtained for T= 360 °C. At the same temperature, we can observe a maximum in the amounts of CH<sub>4</sub> and H<sub>2</sub>O, which are the products of the global reaction.

This means that 360 °C is the optimal temperature which enhances CO<sub>2</sub> methanation with a WHSV equal to 1.5 NL·h<sup>-1</sup>·g<sub>cat</sub><sup>-1</sup> and a pressure equal to 1 bar. In particular, this is explained by the fact that it is

a strongly exothermic reaction. Thus, it is favoured thermodynamically at low temperature and kinetically at high temperatures. This gives the maximum products amounts at an intermediate temperature. Important parameters for the evaluation of the experiment are methane yield, CO<sub>2</sub> conversion and selectivity from CO<sub>2</sub> to CH<sub>4</sub>. Their values at the different temperatures are reported in the following Tables (29-31) and their trends with temperatures are shown in the following Figures (65-67).

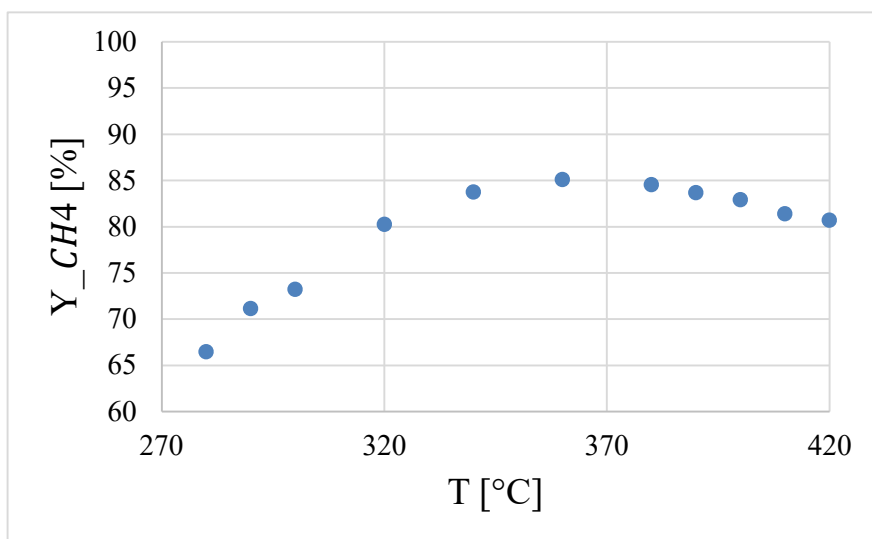
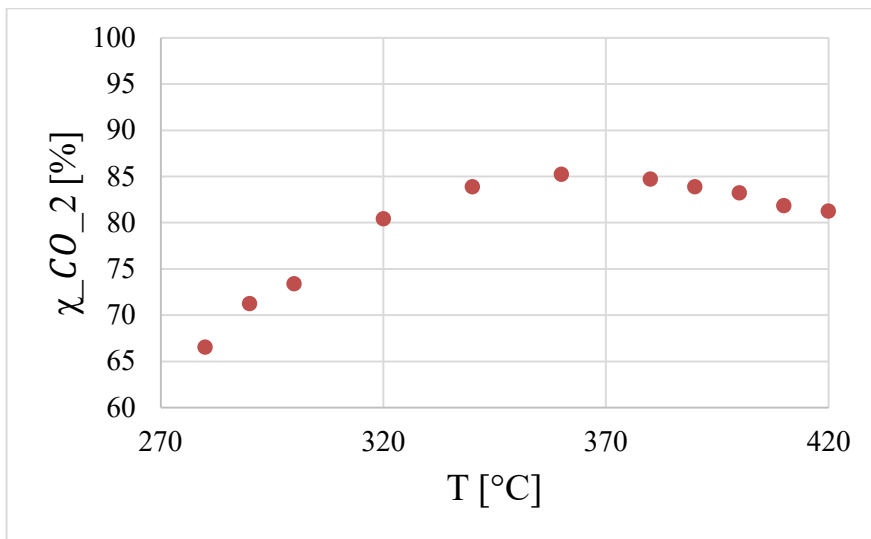


Figure 63: temperatures vs methane yield of test run 5.

Table 29: methane yield at different temperatures of test run 5.

T [°C]=	280	290	300	320	340	360	380	390	400	410	420
Y_CH4	[%]	[%]	[%]	[%]	[%]	[%]	[%]	[%]	[%]	[%]	[%]
Overall section	66.47	71.15	73.23	80.27	83.75	85.10	84.55	83.67	82.93	81.40	80.69



**Figure 64: temperatures vs carbon dioxide conversion of test run 5.**

**Table 30: carbon dioxide conversion at different temperatures of test run 5.**

T [°C]=	280	290	300	320	340	360	380	390	400	410	420
χ <sub>CO<sub>2</sub></sub>	[%]	[%]	[%]	[%]	[%]	[%]	[%]	[%]	[%]	[%]	[%]
Overall section	66.58	71.27	73.44	80.47	83.91	85.29	84.76	83.93	83.27	81.87	81.31

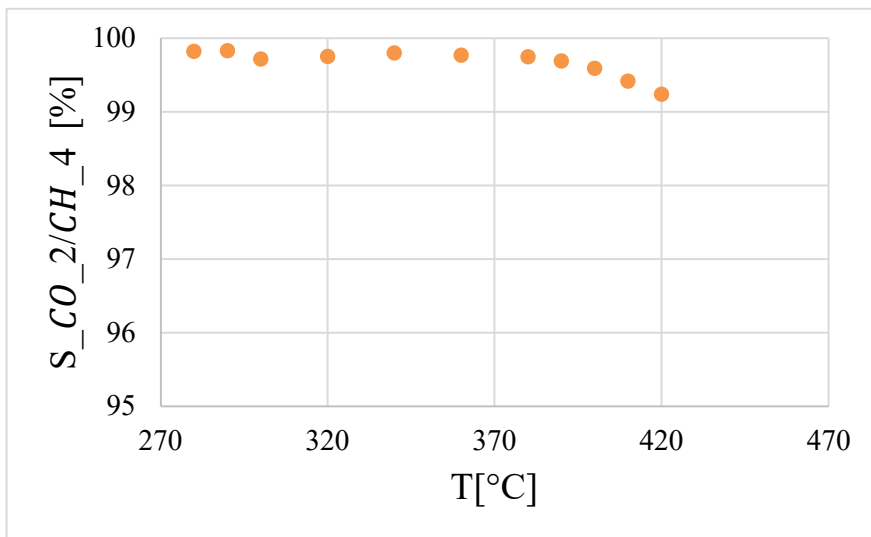


**Figure 65: temperature vs selectivity from CO<sub>2</sub> to methane of test run 5.**

**Table 31: selectivity from CO<sub>2</sub> to CH<sub>4</sub> at different temperatures of test run 5.**

T [°C]=	280	290	300	320	340	360	380	390	400	410	420
S <sub>CO<sub>2</sub>/CH<sub>4</sub></sub>	[%]	[%]	[%]	[%]	[%]	[%]	[%]	[%]	[%]	[%]	[%]



Methane yield and CO<sub>2</sub> conversion have a trend with a maximum with increasing temperatures. Their maximum is located at T= 360 °C, which is the optimal temperature of CO<sub>2</sub> stoichiometric methanation. The maximum methane yield reached is equal to 85.10% and the maximum CO<sub>2</sub> conversion is 85.29%. Concerning the methane selectivity from CO<sub>2</sub>, it has an almost flat profile. Specifically, selectivity is very high and above 99% for all the temperatures. Anyway, its maximum value is reached for T= 290 °C and it is equal to 99.83 %. This is because at low temperatures, CO production is the minimum because kinetic is not favoured.

#### 4.6 Test run 6: Over-stoichiometric CO<sub>2</sub> methanation with variable temperature

In this test run, a mixture with H<sub>2</sub>/CO<sub>2</sub> equal to 4.4 is used. This mixture has an SN equal to 1.1 and therefore it corresponds to the condition for the over-stoichiometric methanation of CO<sub>2</sub>. The pressure is kept constant and equal to 1 bar and the WHSV is 1.5 NI·h<sup>-1</sup>·g<sub>cat</sub><sup>-1</sup>. This WHSV condition corresponds to an overall flowrate equal to 2.4 Nm<sup>3</sup>/h and 1.6 kg of catalyst are used. A fluidization equal to 1 is implemented. In this case, only the temperatures with the maximum yield and conversion values were investigated. Specifically, the range of temperature investigated includes only values between 340 °C and 360 °C. The inlet composition of this test run is reported in Table 32.

**Table 32: inlet composition of test run 6.**

Component	[vol-%]
CO	0
H <sub>2</sub>	81.49
CO <sub>2</sub>	18.51
CH <sub>4</sub>	0
H <sub>2</sub> O	0

With this composition, the reactions mainly observed are CO methanation (Eq. 2.2) and RWGS (Eq. 2.8). The global reaction originated from the combination of these two, is the CO<sub>2</sub> methanation (Eq. 2.1). The values of temperatures analysed are 340 °C, 350 °C, 360 °C. The outlet compositions at these

three values of temperatures are shown in the following Figures (68-72).

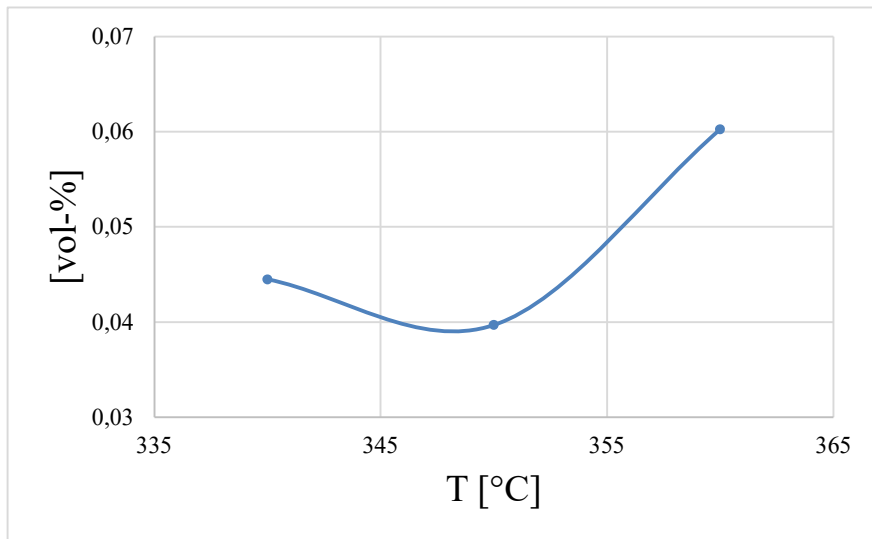


**Figure 66: temperature vs outlet CO percentage by volume of test run 6.**

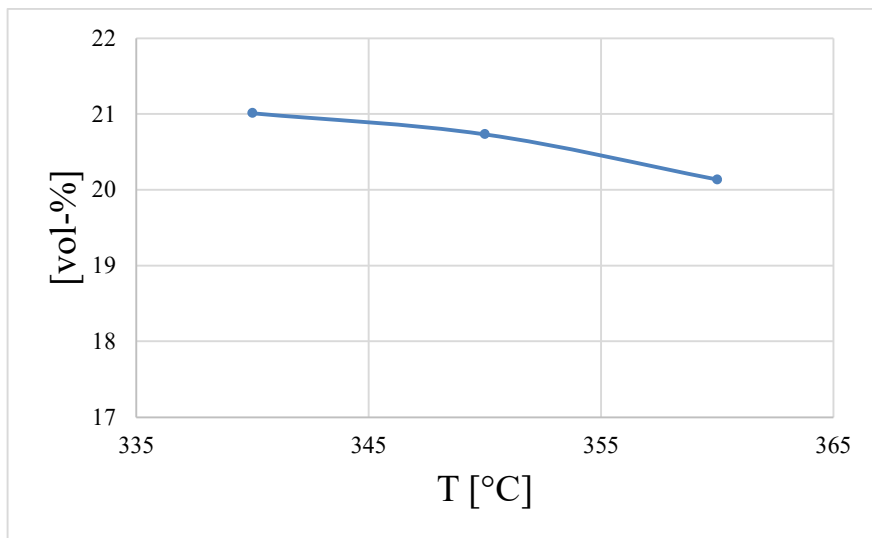


**Figure 67: temperature vs outlet H<sub>2</sub> percentage by volume of test run 6.**

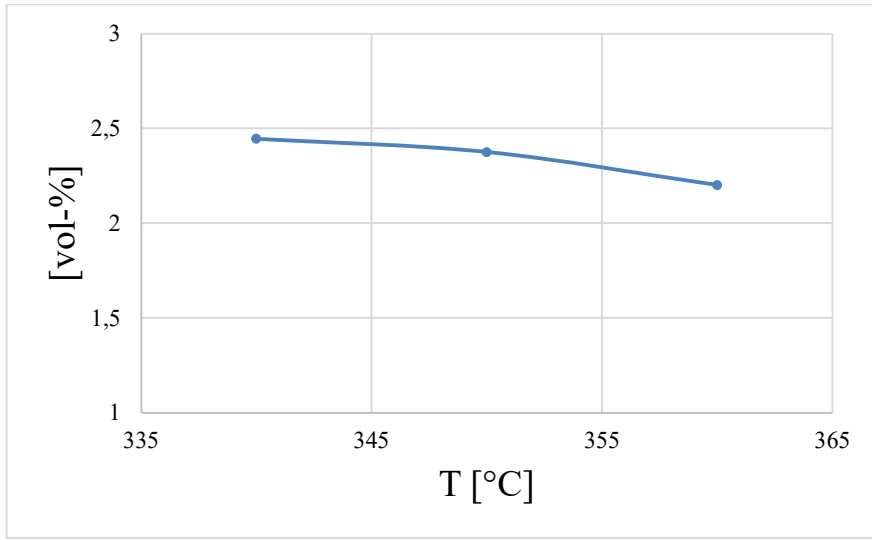


**Figure 68: temperature vs outlet CO<sub>2</sub> percentage by volume of test run 6.**

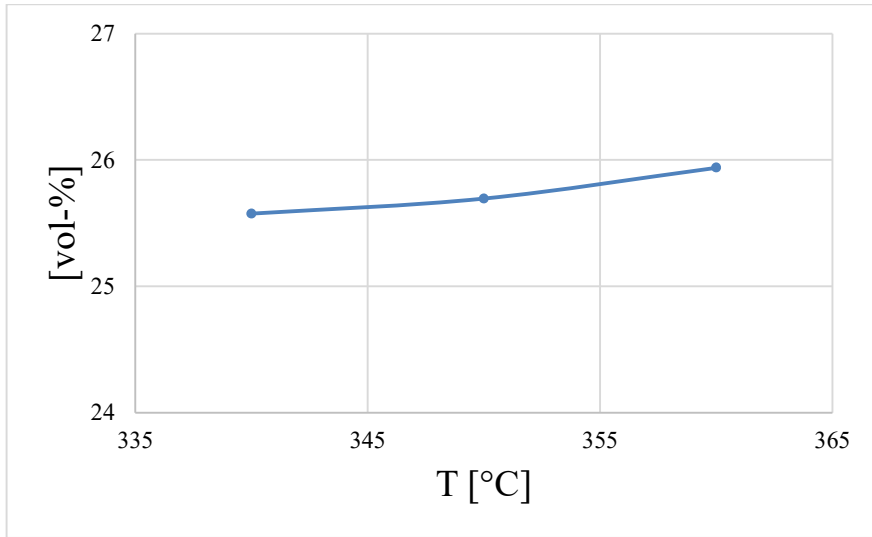


**Figure 69: temperature vs outlet CH<sub>4</sub> percentage by volume of test run 6.**

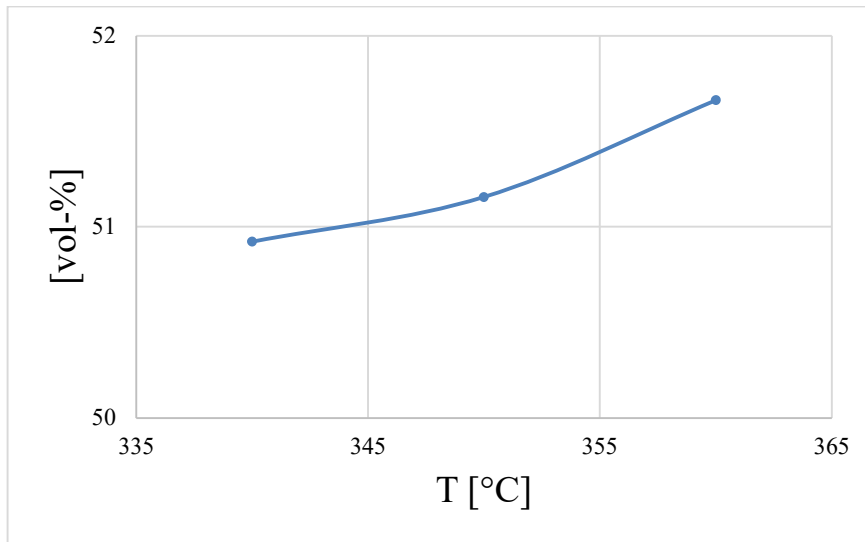


**Figure 70: temperature vs outlet H<sub>2</sub>O percentage by volume of test run 6.**

Carbon monoxide is produced by the RWGS reaction, and it increases with increasing temperature. This is because RWGS is a slightly endothermic reaction, and therefore it is influenced by kinetics. Kinetics is favoured at high temperatures and the maximum CO content is obtained at the highest temperature. For these analysed temperatures, the minimum percentage by volume of CO is observed at T=350 °C. This is probably due because at this temperature, CO methanation is enhanced. Concerning CO<sub>2</sub> and H<sub>2</sub>, which are the reactants of the global reaction, they decrease with the temperature. On the other hand, the amounts of CH<sub>4</sub> and H<sub>2</sub>O increase with increasing temperature.

This means that the CO<sub>2</sub> over-stoichiometric methanation with a WHSV=1.5 NI·h<sup>-1</sup>·g<sub>cat</sub><sup>-1</sup> and a pressure equal to 1 bar is favoured at T=360 °C. Other relevant parameters, such as CH<sub>4</sub> yield, CO<sub>2</sub> conversion and selectivity from CO<sub>2</sub> to methane are analysed. In particular, their trends with the temperature are reported in Figure 73, Figure 74 and Figure 75 and their values at the different temperatures are shown in Table 33, Table 34 and Table 35.

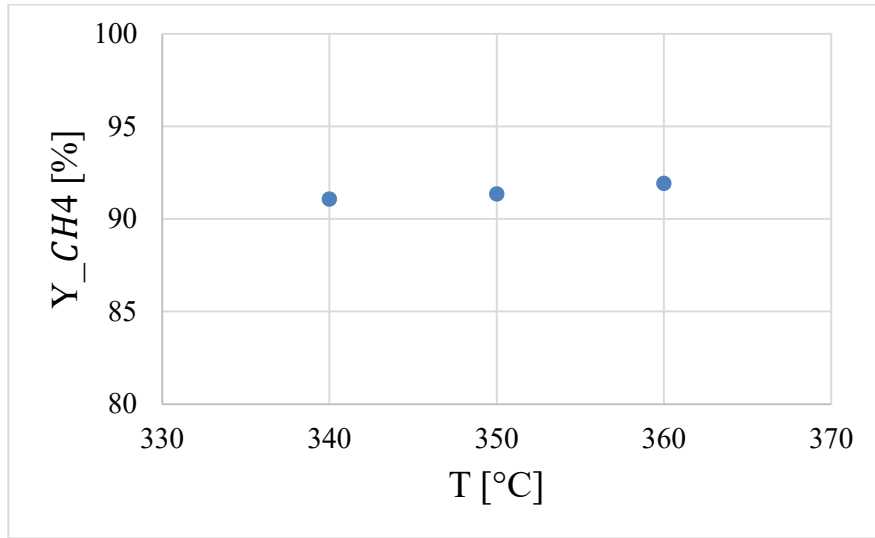


**Figure 71: temperatures vs methane yield of test run 6.**

**Table 33: : methane yield at different temperatures of test run 6.**

T [°C]=	340	350	360
Y <sub>CH4</sub>	[%]	[%]	[%]
Overall section	91.08	91.36	91.94

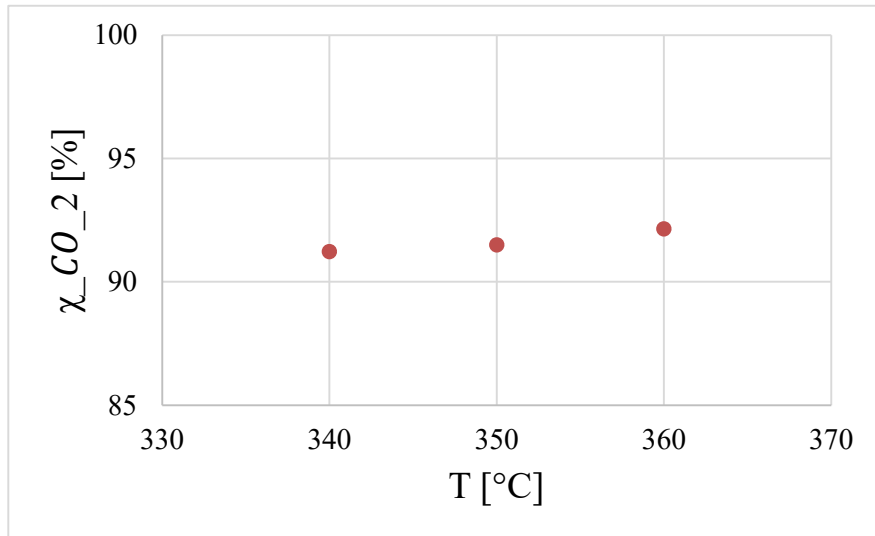


**Figure 72: temperatures vs carbon dioxide conversion of test run 6.**

**Table 34: carbon dioxide conversion at different temperatures of test run 6.**

T [°C]=	340	350	360
χ <sub>CO_2</sub>	[%]	[%]	[%]
Overall section	91.24	91.51	92.15

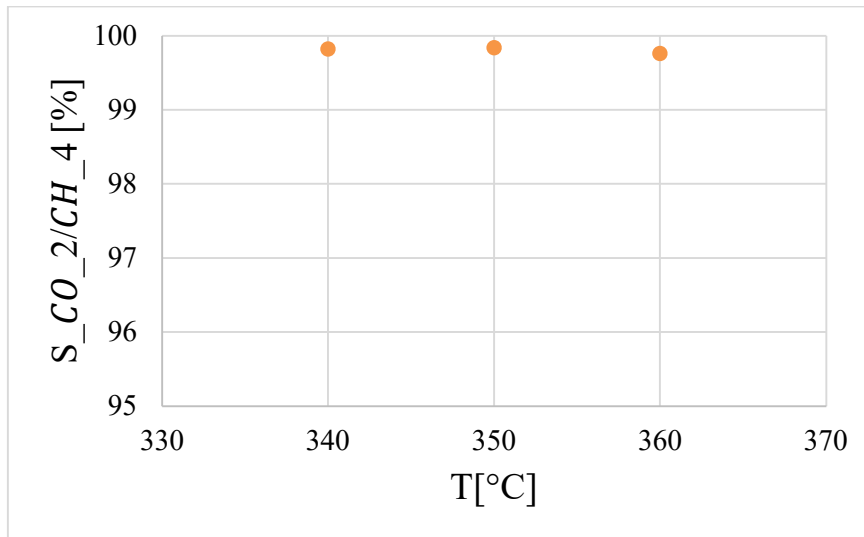


**Figure 73: temperatures vs selectivity from CO<sub>2</sub> to CH<sub>4</sub> of test run 6.**

**Table 35: selectivity from CO<sub>2</sub> to CH<sub>4</sub> at different temperatures of test run 6.**

T [°C]=	340	350	360
S <sub>CO<sub>2</sub>/CH<sub>4</sub></sub>	[%]	[%]	[%]
Overall section	99.82	99.84	99.77

Methane yield and carbon dioxide conversion increase with increasing temperatures. Their maximum is located at T= 360 °C, which is the optimal temperature of CO<sub>2</sub> over-stoichiometric methanation with WHSV=1.5 NI·h<sup>-1</sup>·g<sub>cat</sub><sup>-1</sup> and a pressure equal to 1 bar. The maximum methane yield reached is equal to 91.94% and the maximum CO<sub>2</sub> conversion is 92.15%. Concerning the methane selectivity from CO<sub>2</sub>, it has an almost flat profile. Specifically, selectivity is very high and above 99% for all the temperatures. Its maximum value is reached for T=350 °C and it is equal to 99.84 %. This means that even if at 350 °C the maximum CO<sub>2</sub> conversion is not reached, almost all the CO<sub>2</sub> reacted is involved in methanation more than in RWGS reaction.

#### 4.7 Test run 7: Combined stoichiometric CO and CO<sub>2</sub> methanation with variable temperature and WHSV=1.2 NI·h<sup>-1</sup>·g<sub>cat</sub><sup>-1</sup>

In this test run, a mixture with H<sub>2</sub>/CO/CO<sub>2</sub> equal to 7 is used. This mixture has an SN equal to 1 and therefore it corresponds to the combined stoichiometric methanation of both CO and CO<sub>2</sub>. The pressure is kept constant and equal to 1 bar and the WHSV is 1.2 NI·h<sup>-1</sup>·g<sub>cat</sub><sup>-1</sup>. A fluidization ratio equal to 1 is implemented. The temperature is varied from 280 °C to 420 °C. The inlet composition of this test run is reported in Table 36.

**Table 36: Inlet composition of test run 7.**

Component	[vol-%]
CO	10.02
H <sub>2</sub>	78.39
CO <sub>2</sub>	11.59
CH <sub>4</sub>	0
H <sub>2</sub> O	0

With this feed, the reactions mainly observed are CO methanation and RWGS (Eq. 2.8). Moreover, the combination of these two reactions gives the CO<sub>2</sub> methanation. The values of temperatures at which the reaction is investigated are 280 °C, 300 °C, 320 °C, 340 °C, 360 °C, 380 °C, 390 °C, 400 °C and 420 °C. The outlet compositions trends as function of temperature are reported in the following Figures (76-79).

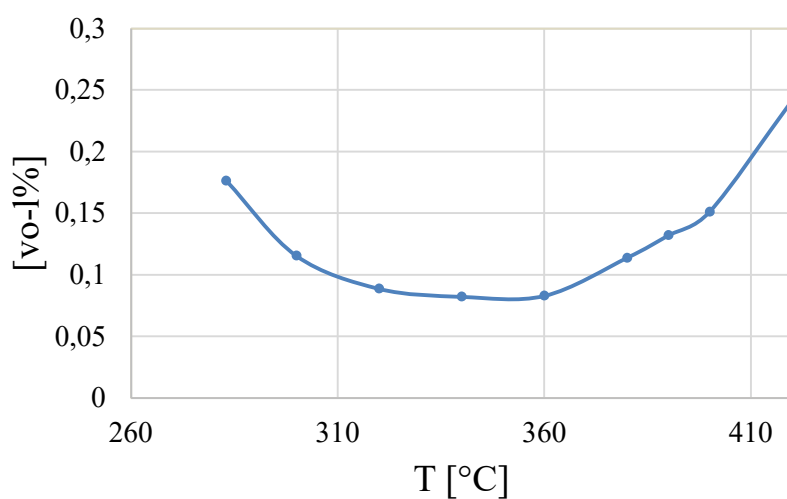


**Figure 74: temperature vs CO outlet percentage by volume of test run 7.**

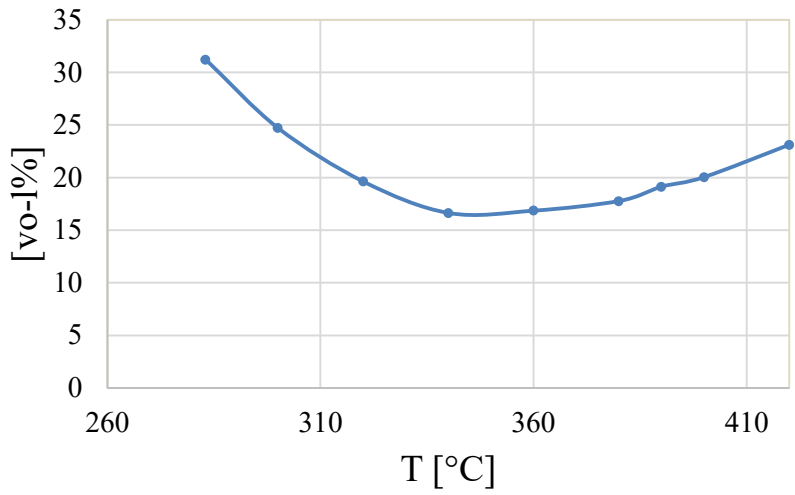


**Figure 75: temperature vs H<sub>2</sub> outlet percentage by volume of test run 7.**

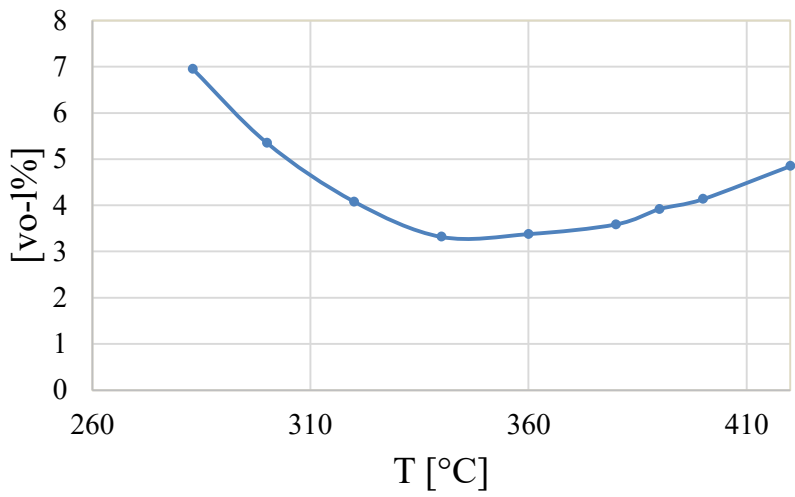


**Figure 76: temperature vs CO<sub>2</sub> outlet percentage by volume of test run 7.**



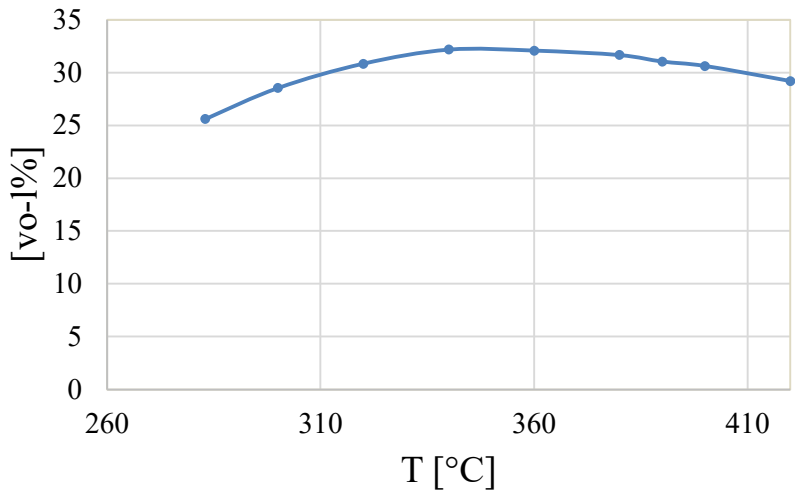


**Figure 77: temperature vs CH<sub>4</sub> outlet percentage by volume of test run 7.**

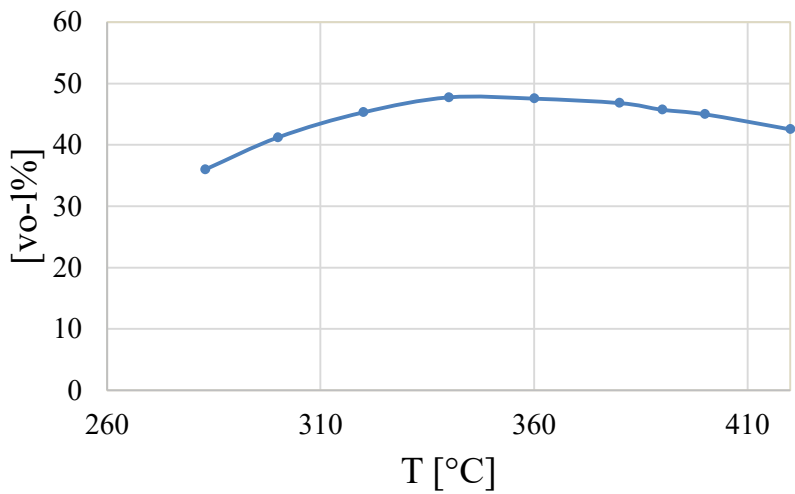


**Figure 78: temperature vs H<sub>2</sub>O outlet percentage by volume of test run 7.**

Carbon monoxide and hydrogen profiles have a minimum at intermediate temperatures. This is explained by the fact that CO methanation is an exothermic reaction and it is favoured thermodynamically at low temperatures and kinetically at high temperatures. Specifically, their minimum amount is observed at T=340 °C. On the other hand, methane and water, which are the products of methanation, have a trend with a maximum.

The explanation of this trend is the same that we reported for the profiles of the reactants. In particular, the maximum amounts for water and methane are reached for the same temperature at which the minimum for H<sub>2</sub> and CO is obtained: T=340 °C. Concerning CO<sub>2</sub> profile, it is considered also a reactant because the global reaction that takes place is the CO<sub>2</sub> methanation. Being also CO<sub>2</sub> methanation

exothermic, its amount has also a trend with a minimum in  $T=340\text{ }^{\circ}\text{C}$ .

For this feed compositions, in addition to the methane yield, both CO and CO<sub>2</sub> conversions are calculated. The specific values at all the different temperatures analysed, are reported in Table 37, Table 38 and Table 39. Moreover, their trend with temperature is shown in Figure 81, Figure 82 and Figure 83.

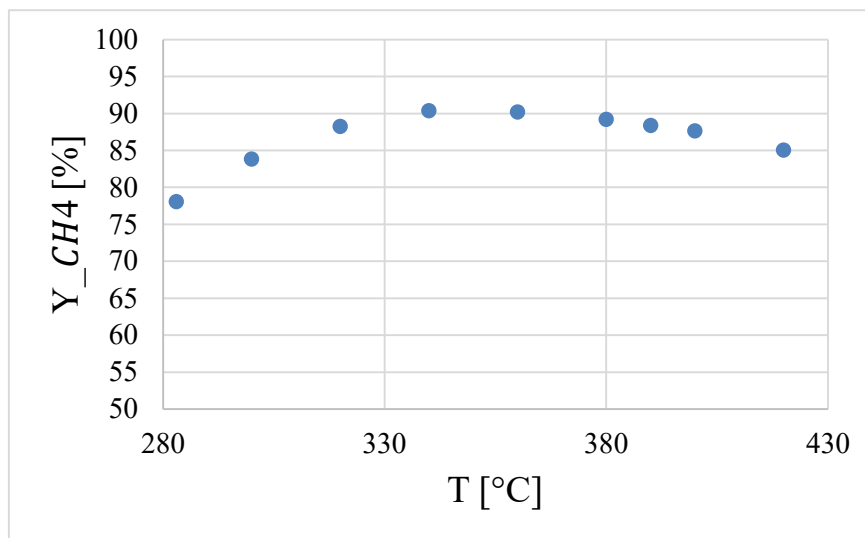


Figure 79: temperature vs methane yield of test run 7.

Table 37: methane yield at different temperatures of test run 7

T [°C]=	280	300	320	340	360	380	390	400	420
Y_CH4	[%]	[%]	[%]	[%]	[%]	[%]	[%]	[%]	[%]
Overall section	78.13	83.86	88.28	90.40	90.23	89.24	88.42	87.67	85.09

Methane yield has the same trend as methane amount, and therefore its maximum value is obtained for an intermediate temperature. Specifically, the maximum CH<sub>4</sub> yield is reached for  $T=340\text{ }^{\circ}\text{C}$  and it is equal to 90.40 %. Therefore, this temperature condition is the one which enhances more the methanation reaction and for which we have the highest methane productivity. This can be confirmed also by the CO and CO<sub>2</sub> conversions trends shown below.

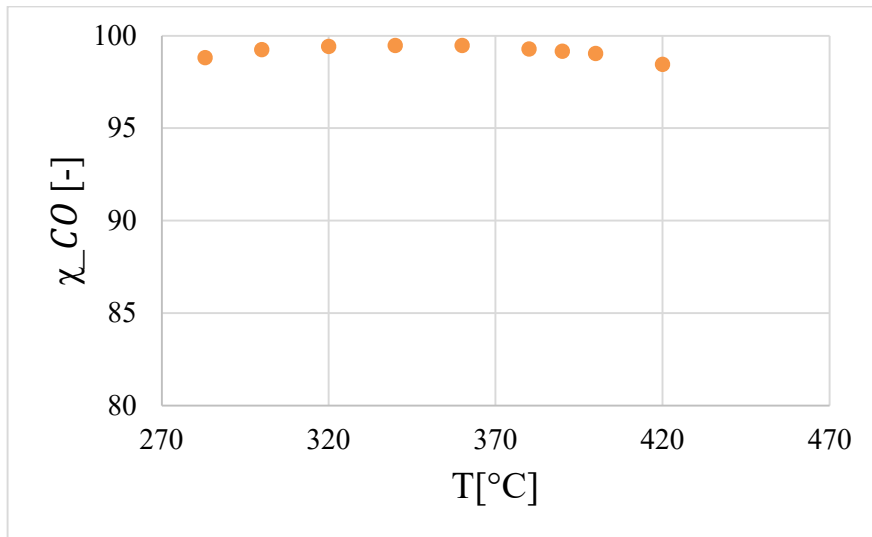


Figure 80: temperature vs carbon monoxide conversion of test run 7.

Table 38: carbon monoxide conversion at different temperatures of test run 7.

T [°C]=	280	300	320	340	360	380	390	400	420
χ <sub>CO_2</sub>	[%]	[%]	[%]	[%]	[%]	[%]	[%]	[%]	[%]
Overall section	98.83	99.26	99.45	99.50	99.49	99.31	99.18	99.06	98.47

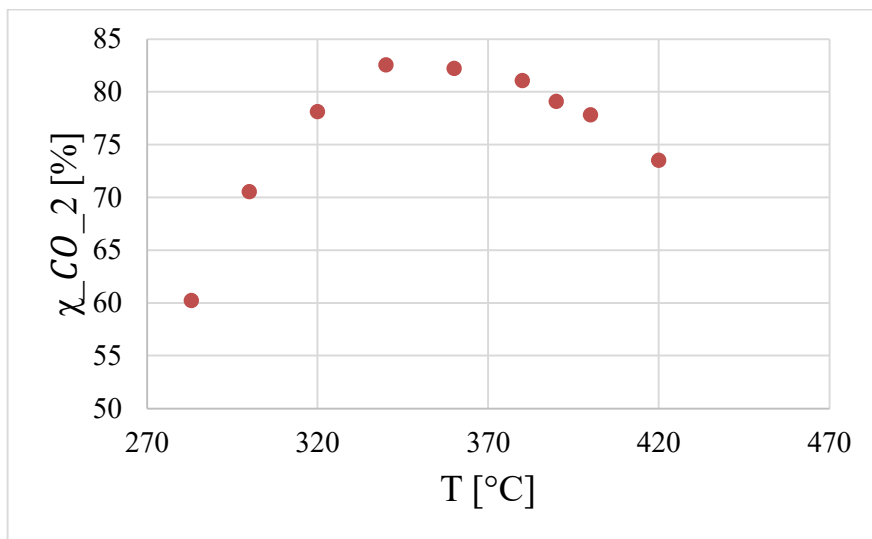


Figure 81: temperature vs carbon dioxide conversion of test run 7.

Table 39: carbon dioxide conversion at different temperatures of test run 7.

T [°C]=	280	300	320	340	360	380	390	400	420
χ <sub>CO_2</sub>	[%]	[%]	[%]	[%]	[%]	[%]	[%]	[%]	[%]
Overall section	60.23	70.55	78.13	82.53	82.22	81.08	79.10	77.82	73.52

Both carbon monoxide and carbon dioxide conversions have trends with a maximum with increasing temperature. Both the maximum values are reached for  $T=340\text{ }^{\circ}\text{C}$ , which we can consider as the optimal temperature for methanation for this feed composition. The maximum CO conversion is equal to 99.50 % and the maximum  $\text{CO}_2$  conversion is equal to 82.53 %. As we can notice, the CO conversion profile with increasing temperature is almost flat. Specifically, CO is almost completely converted for all the temperature conditions and its conversion is higher than  $\text{CO}_2$  one. This means that CO methanation is more favoured than  $\text{CO}_2$  methanation.

#### 4.8 Test run 8: Combined stoichiometric CO and $\text{CO}_2$ methanation with variable temperature and $\text{WHSV}=1.5\text{ NI}\cdot\text{h}^{-1}\cdot\text{g}_{\text{cat}}^{-1}$

In this test run, a mixture with  $\text{H}_2/\text{CO}/\text{CO}_2$  equal to 7 is implemented. This mixture has an SN equal to 1 and it corresponds to the condition for the combined CO and  $\text{CO}_2$  stoichiometric methanation. The pressure is kept constant and equal to 1 bar and the WHSV is  $1.5\text{ NI}\cdot\text{h}^{-1}\cdot\text{g}_{\text{cat}}^{-1}$ . This WHSV condition corresponds to an overall flowrate equal to  $2.4\text{ Nm}^3/\text{h}$  and 1.6 kg of catalyst are used. A fluidization ratio equal to 1 is implemented. The temperature is the varying parameter, and it is varied from  $280\text{ }^{\circ}\text{C}$  to  $420\text{ }^{\circ}\text{C}$ . The inlet composition of this test run is reported in Table 40.

**Table 40: inlet composition of test run 8.**

Component	[vol-%]
CO	11.51
$\text{H}_2$	77.11
$\text{CO}_2$	11.38
$\text{CH}_4$	0
$\text{H}_2\text{O}$	0

With this feed, the reactions mainly observed are CO methanation (Eq. 2.2) and RWGS (Eq. 2.8) Moreover, the combination of these two reactions gives the  $\text{CO}_2$  methanation. The values of temperatures at which the reaction is investigated are  $280\text{ }^{\circ}\text{C}$ ,  $300\text{ }^{\circ}\text{C}$ ,  $310\text{ }^{\circ}\text{C}$ ,  $320\text{ }^{\circ}\text{C}$ ,  $360\text{ }^{\circ}\text{C}$ ,  $380\text{ }^{\circ}\text{C}$ ,  $400\text{ }^{\circ}\text{C}$  and  $420\text{ }^{\circ}\text{C}$ . The outlet compositions trends as function of temperature are reported in the following Figures (84-88).

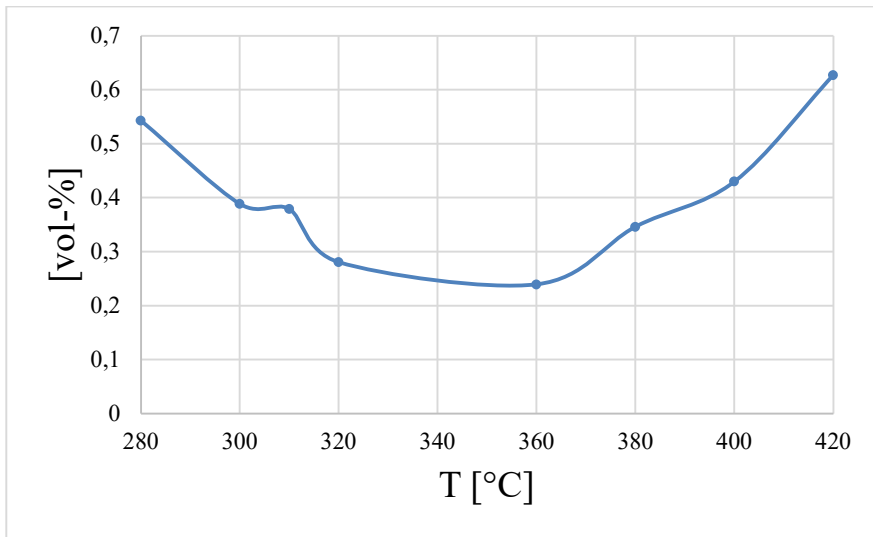


**Figure 82: temperature vs CO outlet percentage by volume of test run 8.**

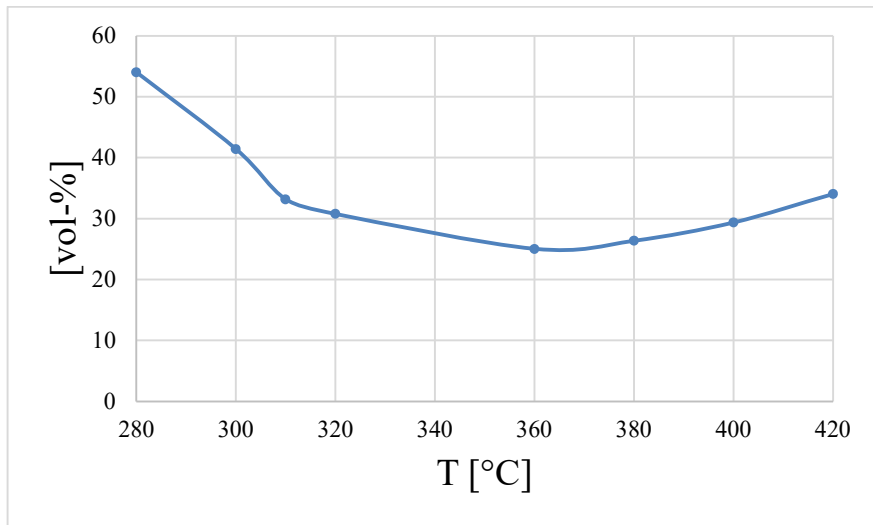


**Figure 83: temperature vs H<sub>2</sub> outlet percentage by volume of test run 8.**

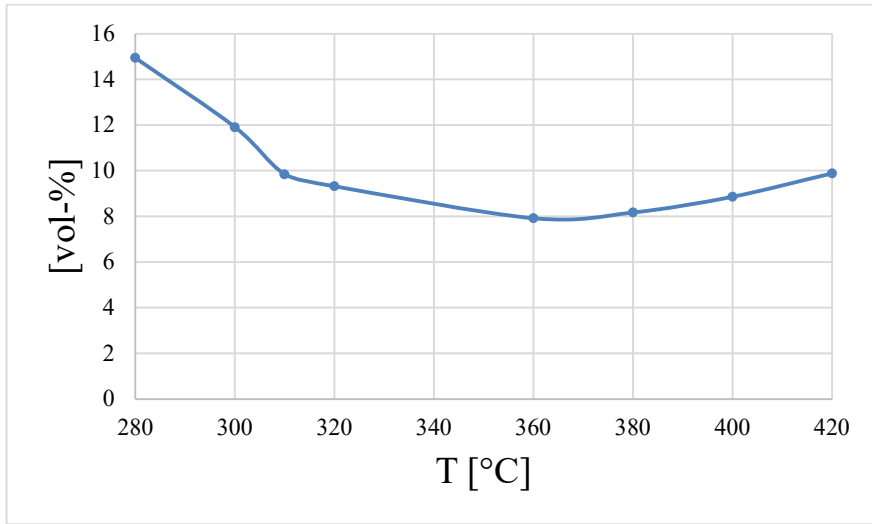


**Figure 84: temperature vs CO<sub>2</sub> outlet percentage by volume of test run 8.**

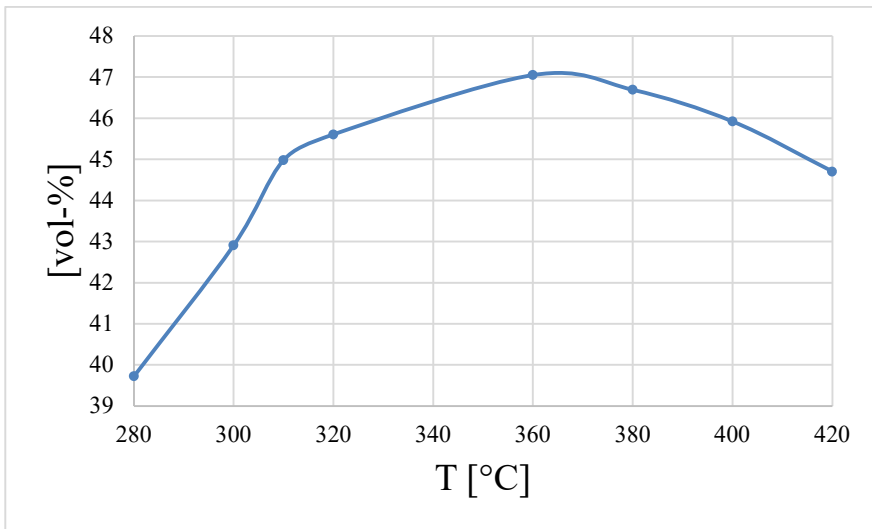


**Figure 85: temperature vs CH<sub>4</sub> outlet percentage by volume of test run 8.**

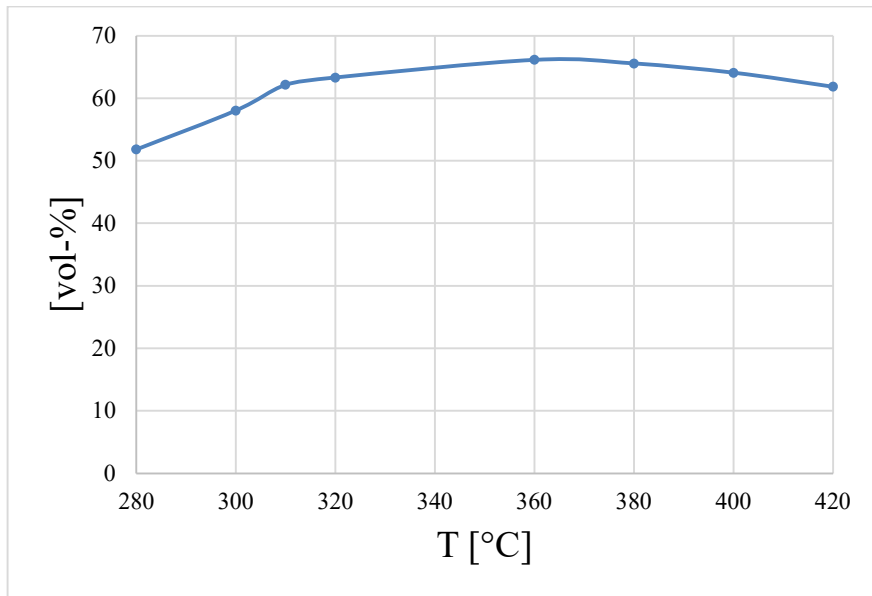


**Figure 86: temperature vs H<sub>2</sub>O outlet percentage by volume of test run 8.**

Carbon monoxide, hydrogen and carbon dioxide profiles have a minimum at intermediate temperatures. This is explained by the fact that they are the reactants and CO<sub>2</sub> methanation is an exothermic reaction and it is favoured thermodynamically at low temperatures and kinetically at high temperatures. Specifically, their minimum amount is observed at T=360 °C. On the other hand, methane and water, which are the products of methanation, have a trend with a maximum.

The explanation of this trend is the same that we reported for the reactants profiles. In particular, the maximum amounts for water and methane are reached for the same temperature at which the minimum for H<sub>2</sub> and CO is obtained: T=360 °C. For this feed compositions, in addition to the methane yield, both CO and CO<sub>2</sub> conversions are calculated. The specific values at all the different temperatures analysed, are reported in Table 41, Table 42 and Table 43. Moreover, their trend with temperature is shown in Figure 89, Figure 90 and Figure 91.

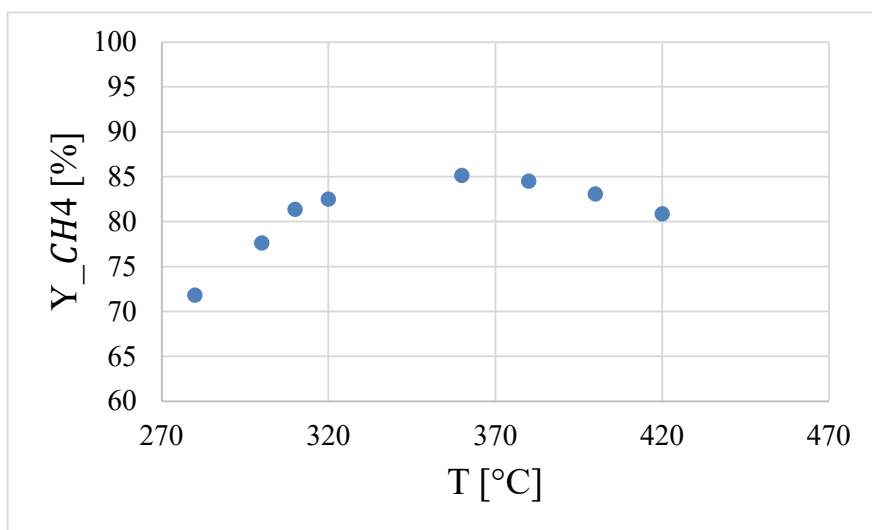


Figure 87: temperature vs methane yield of test run 8.

Table 41: methane yield at different temperatures of test run 8.

T [°C]=	280	300	310	320	360	380	400	420
Y <sub>CH4</sub>	[%]	[%]	[%]	[%]	[%]	[%]	[%]	[%]
Overall section	71.81	77.61	81.37	82.51	85.14	84.49	83.08	80.86

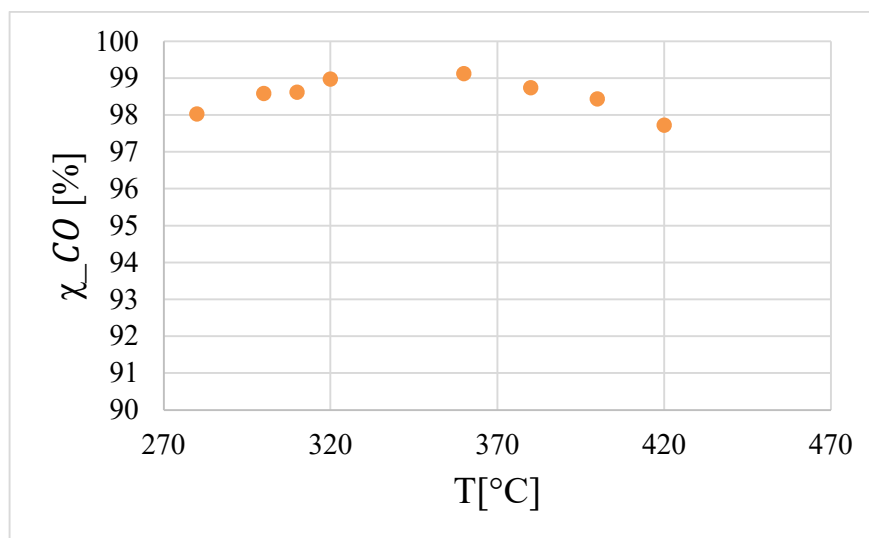


Figure 88: temperature vs carbon monoxide conversion of test run 8.

Table 42: carbon monoxide at different temperatures of test run 8.

T [°C]=	280	300	310	320	360	380	400	420
χ <sub>CO</sub>	[%]	[%]	[%]	[%]	[%]	[%]	[%]	[%]
Overall section	98.03	98.59	98.63	98.98	99.13	98.74	98.44	97.73



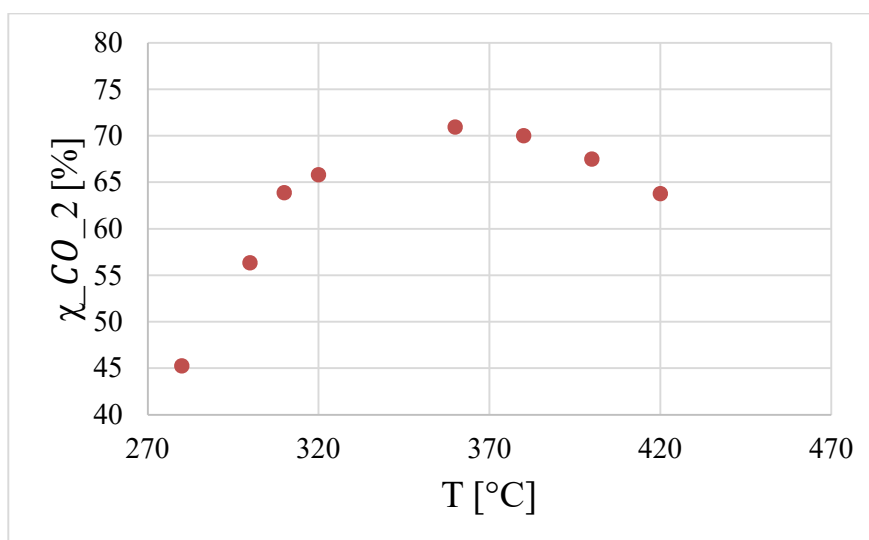


Figure 89: temperature vs carbon dioxide conversion of test run 8.

Table 43: carbon dioxide at different temperatures of test run 8.

T [°C]=	280	300	310	320	360	380	400	420
χ <sub>CO<sub>2</sub></sub>	[%]	[%]	[%]	[%]	[%]	[%]	[%]	[%]
Overall section	45.27	56.38	63.92	65.84	70.98	70.06	67.54	63.80

Methane yield, carbon monoxide and carbon dioxide conversions have trends with a maximum with increasing temperature. The maximum values are reached for  $T=360$  °C, which we can consider as the optimal temperature for methanation for this feed composition and this WHSV. The maximum methane yield is 85.14%, the maximum CO conversion is equal to 99.13 % and the maximum CO<sub>2</sub> conversion is equal to 70.98%. As we can notice, the CO conversion profile with increasing temperature is almost flat. Specifically, CO is almost completely converted for all the temperature conditions and its conversion is higher than CO<sub>2</sub> one. This means that CO methanation is more favoured than CO<sub>2</sub> methanation.

## 5 Discussion of results and summary

The experimental data reported in chapter 4 are analysed with the main objective to identify the optimal parameters for CO and CO<sub>2</sub> methanation in a bench-scale ICFB reactor at TU Wien. Different parameters have been varied and their variation effects are discussed in this chapter by comparing the results of the different experimental tests. The first parameter that has been changed is the Weight Hourly Space Velocity (WHSV) [ $\text{Nl}\cdot\text{h}^{-1}\cdot\text{g}_{\text{cat}}^{-1}$ ]. In particular, an increase of this value means the decrease of the

residence time in the reactor. As explicative examples, it is possible to analyse the two CO methanation experiments which have been realized with two different WHSV at  $T=320\text{ }^{\circ}\text{C}$  and with fluidization ratio equal to 2. Methane yield values of these two conditions for all the reactor sections are shown in Table 44 and CO conversion values in Table 45.

**Table 44: methane yield at different WHSV with  $T=320\text{ }^{\circ}\text{C}$  and fluidization ratio equal to 2**

WHSV [ $\text{Nl}\cdot\text{h}^{-1}\cdot\text{g}_{\text{cat}}^{-1}$ ]	1.3	1.8
$Y_{\text{CH}_4}$	[%]	[%]
Overall section	90.73	84.37
Annular region	90.10	88.98
Draft tube	90.27	82.84

**Table 45: CO conversion at different WHSV with  $T=320\text{ }^{\circ}\text{C}$  and fluidization ratio equal to 2**

WHSV [ $\text{Nl}\cdot\text{h}^{-1}\cdot\text{g}_{\text{cat}}^{-1}$ ]	1.3	1.8
$\chi_{\text{CO}}$	[%]	[%]
Overall section	98.91	95.19
Annular region	99.82	93.31
Draft tube	98.17	94.77

With a higher WHSV, both the methane yield and the carbon monoxide conversion are reduced in all the reactor sections. This result coincides with the ones found in literature [31]. Another interesting parameter to analyse at different values of the WHSV, is the temperature profile. Figure 84 shows the temperature level of the experiment with a  $\text{WHSV}=1.3\text{ Nl}\cdot\text{h}^{-1}\cdot\text{g}_{\text{cat}}^{-1}$  and Figure 85 shows the one of the experiment with a  $\text{WHSV}=1.8\text{ Nl}\cdot\text{h}^{-1}\cdot\text{g}_{\text{cat}}^{-1}$ .

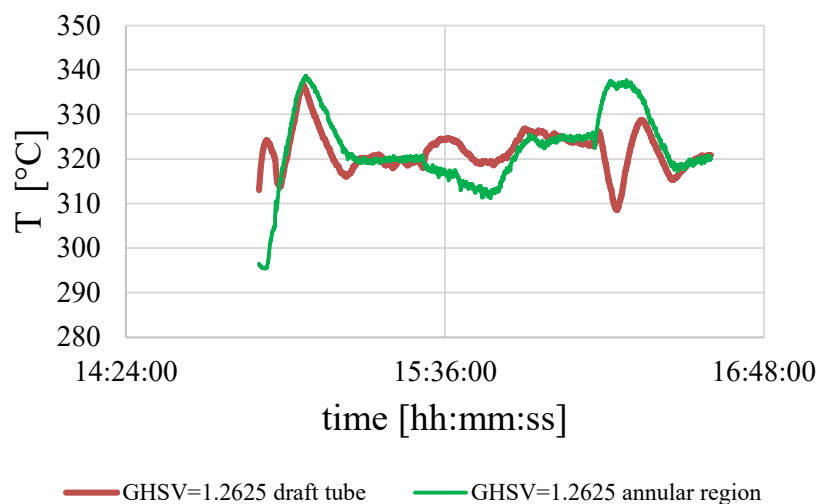


**Figure 90: time vs temperature in the different reactor regions for  $\text{WHSV}=1.3\text{ Nl}\cdot\text{h}^{-1}\cdot\text{g}_{\text{cat}}^{-1}$**

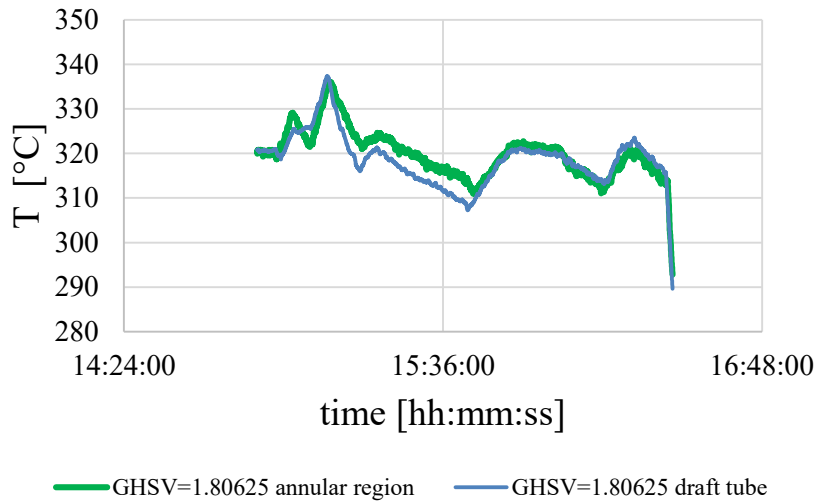


**Figure 91: time vs temperature in the different reactor regions for  $WHSV=1.8 \text{ NI}\cdot\text{h}^{-1}\cdot\text{g}_{\text{cat}}^{-1}$**

For the higher value of  $WHSV$ , there is a slightly higher homogeneity between the temperature profile of draft tube and that of the annular region for all the time span. Moreover, we can also notice that we have a slightly higher exothermicity for a  $WHSV$  equal to  $1.3 \text{ NI}\cdot\text{h}^{-1}\cdot\text{g}_{\text{cat}}^{-1}$  and a resulting smoother profile for a  $WHSV$  equal to  $1.8 \text{ NI}\cdot\text{h}^{-1}\cdot\text{g}_{\text{cat}}^{-1}$ . This is valid for both reactor regions. Anyway, we do not use a too high  $WHSV$  because of the maximum fluidization velocity limit and because we would obtain a lower methane yield. Flowrates higher than the maximum fluidization velocity, would cause the solid particles of catalyst to be dragged out of the reactor. Specifically, a maximum inlet overall flowrate of  $5.88 \text{ Nm}^3/\text{h}$  is allowed [52].

Moreover, also combined  $\text{CO}$  and  $\text{CO}_2$  stoichiometric methanation has been experimented at two different  $WHSV$  values and with a fluidization ratio equal to 1. Specifically, their ratio is such as to obtain the same fluidization conditions in the two reactor regions and the outputs are equal for the three point of measurement: outlet of the overall section, outlet of the annular region and outlet of the draft tube. Table 47 shows methane yield, carbon monoxide and carbon dioxide conversions obtained for the case of  $WHSV=1.2 \text{ NI}\cdot\text{h}^{-1}\cdot\text{g}_{\text{cat}}^{-1}$  and Table 48 shows the same parameters for the case with  $WHSV=1.5 \text{ NI}\cdot\text{h}^{-1}\cdot\text{g}_{\text{cat}}^{-1}$ .

**Table 46: parameters for combined  $\text{CO}$  and  $\text{CO}_2$  stoichiometric methanation with  $WHSV=1.2 \text{ NI}\cdot\text{h}^{-1}\cdot\text{g}_{\text{cat}}^{-1}$ .**

$T [^\circ\text{C}] =$	280	300	320	360	380	400	420
$WHSV[\text{NI}\cdot\text{h}^{-1}\cdot\text{g}_{\text{cat}}^{-1}] = 1.2$	[%]	[%]	[%]	[%]	[%]	[%]	[%]
$Y_{\text{CH}_4}$	78.13	83.86	88.28	90.23	89.24	87.67	85.09
$\chi_{\text{CO}}$	98.83	99.26	99.45	99.49	99.31	99.06	98.47
$\chi_{\text{CO}_2}$	60.23	70.55	78.13	82.22	81.08	77.82	73.52

**Table 47: parameters for combined  $\text{CO}$  and  $\text{CO}_2$  stoichiometric methanation with  $WHSV=1.5 \text{ NI}\cdot\text{h}^{-1}\cdot\text{g}_{\text{cat}}^{-1}$ .**

T [°C]=	280	300	320	360	380	400	420
WHSV[Nl·h <sup>-1</sup> ·g <sub>cat</sub> <sup>-1</sup> ]=1.5	[%]	[%]	[%]	[%]	[%]	[%]	[%]
Y_CH4	71.81	77.61	82.51	85.14	84.48	83.08	80.86
χ_CO	98.03	98.59	98.98	99.13	98.74	98.44	97.73
χ_CO_2	45.27	56.38	65.84	70.98	70.06	67.54	63.80

Also for combined CO and CO<sub>2</sub> stoichiometric methanation, as confirmed from the literature results, a higher methane yield, CO conversion and CO<sub>2</sub> conversions are obtained with a lower WHSV for all the temperatures investigated.

Another important parameter to discuss about, is temperature. Specifically, it is considered as a varying parameter in mostly of the test runs. In general, we can notice that the maximum methane yield is obtained for intermediate temperatures in all the experiments. Being CO and CO<sub>2</sub> methanations both strongly exothermic reactions, the methane production is enhanced for low temperatures from a thermodynamic point of view and for high temperatures for a kinetic point of view.

Furthermore, also the inlet composition strongly influences the methane production capacity. In particular, it is interesting to compare the results obtained for the different stoichiometric methanations. The maximum CH<sub>4</sub> yield value and the temperature at which it is obtained for CO stoichiometric methanation and combined CO and CO<sub>2</sub> stoichiometric methanation with a WHSV=1.2 Nl·h<sup>-1</sup>·g<sub>cat</sub><sup>-1</sup> are shown in Table 49.

**Table 48: maximum methane yield for different inlet compositions with WHSV=1.2 Nl·h<sup>-1</sup>·g<sub>cat</sub><sup>-1</sup>**

	Stoichiometric CO methanation	Combined CO and CO <sub>2</sub> stoichiometric methanation
	[%]	[%]
Y_CH4 [%]	92.31	90.40
T [°C]	340	340

The highest yield obtained is the one for stoichiometric CO methanation, which therefore results to be more favoured than combined stoichiometric methanation for this WHSV. The problem is that this composition is difficult to obtain industrially: it would mean a too expensive gas cleaning of the product gas obtained from woody biomass gasification. Essentially, stoichiometric CO methanation is not an option for industrial processes but this composition is investigated because it is interesting from the scientific point of view. On the other hand, CO<sub>2</sub> methanation is more easily obtained from hydrogen produced by electrolysis and biogas obtained by anaerobic digestion of biomasses. Anyway, a very high methane yield is also obtained for combined methanation with this WHSV.

At the same way, the maximum methane yield values and the temperature at which they occur are shown in Table 50 for stoichiometric CO<sub>2</sub> methanation, and combined CO and CO<sub>2</sub> stoichiometric methanation

realized with a  $WHSV=1.5 \text{ NI}\cdot\text{h}^{-1}\cdot\text{g}_{\text{cat}}^{-1}$ .

**Table 49: maximum methane yield for different inlet compositions with  $WHSV=1.5 \text{ NI}\cdot\text{h}^{-1}\cdot\text{g}_{\text{cat}}^{-1}$**

	<b>Stoichiometric CO<sub>2</sub> methanation</b>	<b>Combined CO and CO<sub>2</sub> stoichiometric methanation</b>
	[%]	[%]
<b>Y<sub>CH4</sub> [%]</b>	85.10	85.14
<b>T [°C]</b>	360	360

The highest yield with this WHSV value, is obtained from the combined CO and CO<sub>2</sub> methanation which therefore results to be more favoured than stoichiometric CO<sub>2</sub> methanation. In general, we can observe that maximum yield values are obtained between 340 °C and 360 °C for all the inlet stoichiometric compositions.

Being CO<sub>2</sub> methanation of greater industrial interest, both for the ease with which this inlet composition can be obtained and for the necessity to reduce the release of CO<sub>2</sub> to the atmosphere, it has been experimented with three different H<sub>2</sub>/CO ratios and stoichiometric numbers (SNs). Specifically, under-stoichiometric CO<sub>2</sub> methanation with an SN=0.9, stoichiometric CO<sub>2</sub> methanation with an SN=1 and over-stoichiometric CO<sub>2</sub> methanation with an SN=1.1 have been experimented. Moreover, under-stoichiometric CO<sub>2</sub> methanation is investigated with a  $WHSV=1.2 \text{ NI}\cdot\text{h}^{-1}\cdot\text{g}_{\text{cat}}^{-1}$ , while the other two conditions with a  $WHSV=1.5 \text{ NI}\cdot\text{h}^{-1}\cdot\text{g}_{\text{cat}}^{-1}$ . Table 51 shows the maximum yield and the CO<sub>2</sub> conversions which are obtained for these three inlet compositions, which is obtained for T=360 °C.

**Table 50: maximum methane yield for different inlet CO<sub>2</sub> methanation compositions**

<b>T=360 °C</b>	<b>Under-stoichiometric CO<sub>2</sub> methanation</b>	<b>Stoichiometric CO<sub>2</sub> methanation</b>	<b>Over-stoichiometric CO<sub>2</sub> methanation</b>
	[%]	[%]	[%]
<b>Y<sub>CH4</sub> [%]</b>	80.59	85.10	91.94
<b>χ<sub>CO_2</sub></b>	80.89	85.29	92.15

The highest CH<sub>4</sub> yield, and CO<sub>2</sub> conversion are obtained with an over-stoichiometric mixture H<sub>2</sub>-CO<sub>2</sub>. Anyhow, being hydrogen an expensive gas, this situation is disadvantageous from the economical point of view. However, an excellent methane yield value of 80.59% and a pretty high CO<sub>2</sub> conversion value of 80.89 % is obtained also with an under-stoichiometric mixture H<sub>2</sub>-CO<sub>2</sub> which is a more affordable condition.

## 6 Conclusion and outlook

The thesis work is part of the project ReGas4Industry funded by the “Klima- und Energiefonds” and carried out under the “Energieforschung” program. The project is based on the current knowledge in biomass gasification, gas cleaning and production of synthetic biofuels. The principal aim is to use low-cost feedstocks for the production of synthetic biofuels. For this purpose, residues from industries are gasified through the dual bed gasifier, previously built at TU Wien, by using steam as gasification agent. Moreover, several investigations are currently underway regarding synthesis reactions. Specifically, productions of hydrogen ( $H_2$ ), methane ( $CH_4$ ), hythane ( $H_2$  &  $CH_4$ ) as well as other gaseous and liquid products, are investigated.

In this thesis, the results of part of the investigations concerning synthetic methane production are reported. Synthetic methane, also defined as synthetic natural gas (SNG), is an alternative and clean energy carrier which can substitute part of the non-renewable natural gas (NG). In this way, greenhouse emissions and the global warming problem can be significantly reduced. The experimental investigation is carried out in a newly bench-scale fluidized bed methanation reactor in the facilities of Vienna University of Technology. Fluidized bed methanation is advantageous, with respect to fixed bed methanation, because of the improved heat and mass transfers and the reduced risk of carbon deposition over the catalyst.

In particular, the reactor used is an Internal Circulating Fluidized Bed (ICFB) with an internal draft tube which allows the possibility to achieve internal circulation of the catalyst, so that its height and construction costs can be reduced. The used catalyst is nickel based on alumina ( $Ni/Al_2O_3$ ), with alumina in its  $\alpha$  configuration. Additional alumina besides the catalyst support is also added to the reactor in order to reach the required filling level in the reactor and improve fluidization quality. Different parameters have been investigated and the effect of their variations is evaluated. Specifically, the experiments have been carried out with different temperatures, inlet compositions, Weight Hourly Space Velocities (WHSV) and fluidization ratios.

Temperatures between 280 °C and 420 °C have been investigated and it has been found that for all the compositions investigated, the maximum methane production is reached at intermediate temperatures between 340 and 360 °C. The fact that the maximum methane yield is obtained at intermediate temperatures, can be explained by methanation reaction nature. In particular, it is a strongly exothermic reaction, and thus it is thermodynamically favoured at low temperatures and kinetically favoured at high temperatures. The desired level of temperature can be controlled by removing heat. The heat removal is realized by using pressurized air as cooling fluid which flows in an external jacket and an internal coil. Moreover, a homogeneous temperature in the different regions of the reactor is desired.

The different experiments operated showed that it is possible to keep the temperature approximately

constant and that the temperature level is about the same in the draft tube and in the annular region for all the experiments. Specifically, the sudden temperature increase that is verified when the reaction starts, is counteracted by the cooling realized with pressurized air and it is possible to re-establish the previous conditions. Furthermore, the different thermocouples, which are located at different heights of the reactor, give us information about the temperature profile along the reactor. It has been observed that for all the experiments, the temperature increases with the height in the annular region, while it decreases with it in the draft tube.

Different inlet compositions have been experimented and for this purpose bottled gas have been used. Specifically, stoichiometric conditions for CO methanation, CO<sub>2</sub> methanation and combined CO and CO<sub>2</sub> methanation have been experimented. Moreover, CO<sub>2</sub> methanation has also been investigated with under-stoichiometric and over-stoichiometric inlet mixtures. It has been deduced that the feed gas composition strongly influences the methanation efficiency. Between the compositions analysed, the most efficient one, which gives a maximum methane yield equal to 92.31%, is the CO stoichiometric mixture. This is due by the fact that, as noticed by the performed thermodynamic calculations, CO<sub>2</sub> methanation is thermodynamically limited with respect to CO methanation. Therefore, CO<sub>2</sub> methanation can never reach the same yields and conversions as the CO methanation.

CO methanation inlet composition is actually not an industrial option, due to the difficulty with which it is possible to be obtained at the outlet of gasification processes. It is investigated because it is interesting from a scientific point of view and so that to create solid basis for the methanation of the product gas obtained by gasification processes. On the other hand, the inlet composition of CO<sub>2</sub> methanation is easily obtained from hydrogen produced by electrolysis and biogas from anaerobic digestion of biomass. However, this inlet mixture gives the lowest methane yield. In particular, between the three mixtures investigated for CO<sub>2</sub> methanation, the highest methane yield obtained for CO<sub>2</sub> methanation is produced by the over-stoichiometric mixture. This composition is not convenient from an economical point of view, because of the high-energy expenditure to produce hydrogen. The advantage of this composition is given by the fact that, converting more CO<sub>2</sub>, it will not be necessary to separate it before feeding the SNG to the natural gas grid. Moreover, a very good methane yield value is obtained also for the under-stoichiometric mixture, which is the most economically convenient. Combined CO and CO<sub>2</sub> methanation gives intermediate results.

Weight Hourly Space Velocity (WHSV) has been also varied and its influence on the methane production has been analysed. In particular, it is defined as the ratio between the volumetric inlet flowrate at standard conditions and the weight of the catalyst used. This parameter indicates how many volumes of feed can be treated in a unit of time, and when it increases the residence time in the reactor decreases. Concerning this parameter, values between 1.2 and 1.8  $\text{NI}\cdot\text{h}^{-1}\cdot\text{g}_{\text{cat}}^{-1}$  have been analysed. Furthermore, it has been observed that with a higher WHSV, methane yield and reactants conversions

are reduced.

The last variable parameter that has been considered, is the ratio between the WHSV to the draft tube and the one to the annular region of the reactor, defined as fluidization ratio. Specifically, a maximum methane yield has been obtained for a ratio approximately equal to 2 for different values of the overall WHSV. Higher and lower fluidization ratios give lower methane yield and reactants conversions. Moreover, the same fluidization conditions in the two sections are obtained with a fluidization ratio equal to 1. Specifically, with that value a gas with the same compositions at the outlet of the draft tube and of the annular region is produced.

These experimental tests, constitute a solid basis and an excellent starting point for the research in the field of methanation in Vienna University of Technology. Still numerous aspects will have to be investigated. In particular, more experiments with multiple WHSV values can be performed in the future so that to find its optimum value, that is a compromise between high methane yield and reactor size. Moreover, other compositions entering the methanation step should be analysed. Specifically, different typical Product Gas (PG) compositions, derived from different gasification and gas cleaning technologies should be experimented. The final objective is to establish a downstream technology suitable for the methanation of the outlet product gas from the Dual Fluidized Bed (DFB) gasifier of TU Wien. Furthermore, extensive experimental data will be collected in order to allow an interpretation of a potential large-scale demonstration.

## Notation

### Symbols

CH <sub>4</sub>	Methane	mol
H <sub>2</sub>	Hydrogen	mol
N <sub>2</sub>	Nitrogen	mol
CH <sub>3</sub> OH	Methanol	mol
CO	Carbon monoxide	mol
CO <sub>2</sub>	Carbon dioxide	mol
H <sub>2</sub> O	Water	mol
Ni	Nickel	mol



Al <sub>2</sub> O <sub>3</sub>	Alumina	mol
CaCO <sub>3</sub>	Calcite	mol
CaO	Calcium oxide	mol
CrO	Chromium oxide	mol
NiO	Nickel oxide	mol
MgO	Magnesium oxide	mol
SO <sub>2</sub>	Sulphur dioxide	mol
COS	Carbonyl sulphide	mol
H <sub>2</sub> S	Hydrogen sulphide	mol
HCl	Hydrochloric acid	mol
NH <sub>3</sub>	Ammonia	mol
HCN	Hydrocyanic acid	mol
NO <sub>x</sub>	Nitrogen oxides	mol
Zn	Zinc	mol
Fe	Iron	mol
Cu	Copper	mol
Mn	Manganese	mol
Co	Cobalt	mol
Mo	Molybdenum	mol
Pt	Platinum	mol
Pd	Palladium	mol
Ag	Silver	mol
Au	Gold	mol
Ru	Ruthenium	mol
Rh	Rhodium	mol
Re	Rhenium	mol

$\text{Fe}_2\text{O}_3$	Iron oxide	mol
$\text{NH}_4\text{Cl}$	Ammonium chloride	mol
$\text{SiO}_2$	Silica	mol
$\text{TiO}_2$	Titanium oxide	mol
$\text{ZrO}_2$	Zirconium oxide	mol
$\text{V}_2\text{O}_3$	Vanadium oxide	mol
C	Carbon	mol
T	Temperature	$^{\circ}\text{C}$
$\Delta H_R$	Standard enthalpy of reaction	$^{\circ}\text{C}$
$Y_{\text{CH}_4}$	Methane yield	%
$\chi_{\text{CO}}$	Carbon monoxide conversion	%
$\chi_{\text{CO}_2}$	Carbon dioxide conversion	%
$S_{\text{CO}/\text{CH}_4}$	Selectivity from carbon monoxide to methane	%
$S_{\text{CO}_2/\text{CH}_4}$	Selectivity from carbon dioxide to methane	%
WHSV	Weight hourly space velocity	$\text{NI}\cdot\text{h}^{-1}\cdot\text{g}_{\text{cat}}^{-1}$
$\varepsilon$	Porosity	-
$\nu$	Kinematic gas viscosity	$\text{m}^2/\text{s}$
$\rho_b$	Bulk density	$\text{kg}/\text{m}^3$
$\rho_p$	Particle density	$\text{kg}/\text{m}^3$
$\rho_g$	Gas density	$\text{kg}/\text{m}^3$
$\mu$	Viscosity	$\text{Pa}\cdot\text{s}$
$\phi$	Shape factor	-
$G_s$	Solid circulation rate	$\text{kg}/\text{m}^2/\text{s}$
$V_a$	Particle downward velocity in the annular region	$\text{m}/\text{s}$
$\rho_s$	Solid density	$\text{kg}/\text{m}^3$
$h_{\text{mf}}$	Gas holdup at minimum fluidization state	-

$V_p$	Particle volume	$m^3$
$S_p$	Particle surface	$m^3$
$M_p$	Particle mass	$m^3$
H	height	m
$d_p$	Particle size	m
$d_i, x_i (d_m, \sigma)$	Particle size distribution	m, -
$N_i$	Number of particles of mesh i	-
$\Delta P$	Pressure drops	bar
$U_L$	Minimum fluidization velocity	m/s
$U_s$	Terminal fluidization velocity	m/s
g	Standard gravity	$m/s^2$
x	Molar fractions	-
Re	Reynolds number	-
Ar	Archimedes number	-
SN	Stoichiometric number	-

## Abbreviations

NG	Natural gas
SNG	Synthetic natural gas
CNG	Compressed natural gas
CHP	Combined heat and power
PG	Product gas
PtG	Power to gas
FT	Fischer-Tropsch

DME	Dimethylether
DFB	Dual fluidized bed
PtG	Power to gas
WGS	Water gas shift
CFB	Circulating fluidized bed
ICFB	Internal circulating fluidized bed
WGS	Water Gas Shift
RWGS	Reverse Water Gas Shift
Nm <sup>3</sup>	Gas cubic meter according to standard conditions (0 °C, 1.013 bar <sub>abs</sub> )
SER	Sorption enhanced reforming
CR	Combustion reactor
GR	Gasification reactor
PID	Proportional Integral Derivative
TIC	Temperature Indicator Controller
SN	Stoichiometric Number
P&I	Piping and instrumentation diagram
TIR	Temperature indicator and report
TREMP	Topsøe Recycle Energy-efficient Methanation Process
vol-%	Percentage by volume
HICOM	High Combined Shift Methanation
RMP	Ralph M. Parsons

## List of tables

Table 1: Typical methanation feed gas compositions [7].....	6
Table 2: Gasification agents and the resulting PG compositions [18].....	8

Table 3: Most relevant reactions in the gasification process [19].	8
Table 4: Different gasification products obtained with different bed materials [12].	15
Table 5: Analysed input methanation compositions.	20
Table 6: Catalysts ratings [30].	25
Table 7: Possible definitions of the equivalent diameter of a particle [47].	40
Table 8: Inlet composition test run 1.	49
Table 9: Overall outlet composition of test run 1.	49
Table 10: Outlet compositions of test run 1 for the two different outlet sections.	50
Table 11: Methane yields for test run 1.	51
Table 12: Carbon monoxide conversion for test run 1.	52
Table 13: Selectivity to methane for test run 1.	53
Table 14: Inlet composition of test run 2.	56
Table 15: Overall outlet composition of test run 2.	56
Table 16: Outlet compositions of test run 2 for the two different outlet sections.	57
Table 17: Methane yields for test run 2.	58
Table 18: Carbon monoxide conversion for test run 1.	58
Table 19: Selectivity from carbon monoxide to methane of test run 2.	59
Table 20: Inlet composition of test run 3.	61
Table 21: methane yield at different temperatures of test run 3.	63
Table 22: carbon monoxide conversion at different temperatures of test run 3.	64
Table 23: selectivity from carbon monoxide to methane at different temperatures of test run 3.	64
Table 24: Inlet composition of test run 4.	65
Table 25: methane yield at different temperatures of test run 4.	69
Table 26: carbon dioxide conversion at different temperatures of test run 4.	70
Table 27: selectivity from CO <sub>2</sub> to CH <sub>4</sub> at different temperatures of test run 4.	70
Table 28: inlet composition of test run 5.	71

Table 29: methane yield at different temperatures of test run 5.....	74
Table 30: carbon dioxide conversion at different temperatures of test run 5.....	75
Table 31: selectivity from CO <sub>2</sub> to CH <sub>4</sub> at different temperatures of test run 5.....	75
Table 32: inlet composition of test run 6.....	76
Table 33: : methane yield at different temperatures of test run 6.....	80
Table 34: carbon dioxide conversion at different temperatures of test run 6.....	80
Table 35: selectivity from CO <sub>2</sub> to CH <sub>4</sub> at different temperatures of test run 6.....	81
Table 36: Inlet composition of test run 7.....	82
Table 37: methane yield at different temperatures of test run 7.....	85
Table 38: carbon monoxide conversion at different temperatures of test run 7.....	86
Table 39: carbon dioxide conversion at different temperatures of test run 7.....	86
Table 40: inlet composition of test run 8.....	87
Table 41: methane yield at different temperatures of test run 8.....	91
Table 42: carbon monoxide at different temperatures of test run 8.....	91
Table 43: carbon dioxide at different temperatures of test run 8.....	92
Table 44: methane yield at different WHSV with T=320 °C and fluidization ratio equal to 2.....	93
Table 45: CO conversion at different WHSV with T=320 °C and fluidization ratio equal to 2.....	93
Table 46: parameters for combined CO and CO <sub>2</sub> stoichiometric methanation with WHSV=1.2 NI·h <sup>-1</sup> ·g <sub>cat</sub> <sup>-1</sup> .....	94
Table 47: parameters for combined CO and CO <sub>2</sub> stoichiometric methanation with WHSV=1.5 NI·h <sup>-1</sup> ·g <sub>cat</sub> <sup>-1</sup> .....	94
Table 48: maximum methane yield for different inlet compositions with WHSV=1.2 NI·h <sup>-1</sup> ·g <sub>cat</sub> <sup>-1</sup> .....	95
Table 49: maximum methane yield for different inlet compositions with WHSV=1.5 NI·h <sup>-1</sup> ·g <sub>cat</sub> <sup>-1</sup> .....	96
Table 50: maximum methane yield for different inlet CO <sub>2</sub> methanation compositions.....	96

## List of figures

Figure 1: Different SNG production routes.....	4
Figure 2: Processes during gasification of a single particle [12].....	7
Figure 3 : Typical arrangement for an updraft fixed bed gasifier [12].....	9
Figure 4: Entrained flow gasifier standard configuration [12].....	10
Figure 5: Typical cross-sectional view of a bubbling fluidized bed gasifier [12]. <b>Fehler! Textmarke nicht definiert.</b>	
Figure 6: Fast fluidized bed configuration [12].....	12
Figure 7: Dual fluidized bed scheme [12].....	13
Figure 8: Basic principles of a classic DFB gasifier [10].....	13
Figure 9: SER process [12]. ....	14
Figure 10: Temperature vs molar fractions – stoichiometric CO methanation .....	20
Figure 11: Temperature vs molar fractions – stoichiometric CO <sub>2</sub> methanation.....	21
Figure 12: Temperature vs molar fractions – SER product gas methanation.....	21
Figure 13: Temperature vs molar fractions - typical product gas methanation.....	21
Figure 14: Temperature vs CH <sub>4</sub> yield.....	22
Figure 15: Lurgi methanation process scheme [42]. ....	27
Figure 16: TREMP methanation process scheme [42].....	28
Figure 17: HICOM methanation process scheme [9].....	29
Figure 18: RMP methanation process scheme [9].....	30
Figure 19: ICI/Koppers methanation process scheme [9]. ....	31
Figure 20: Linde methanation process [9].....	31
Figure 21: multiple feed Bureau of Mines fluidized reactor [9].....	33
Figure 22: Bi-gas fluidized bed methanation reactor [9].....	34
Figure 23: COMFLUX methanation process scheme [9].....	35
Figure 24: Possible states of a fluidized bed reactor [45].....	36

Figure 25: Circulating fluidized beds [45].	37
Figure 26: Scheme of an internally circulating bed reactor [50].	38
Figure 27: Solid circulation between two beds [45].	39
Figure 28: Pressure – velocity diagram [47].	42
Figure 29: ICFB reactor in TU Wien research laboratory.	43
Figure 30: P&I diagram of the methanation process.	44
Figure 33: time vs T during catalyst activation by reduction.	47
Figure 34: fluidization ratio vs methane yield of test run 1.	51
Figure 35: fluidization ratio vs CO conversion of test run 1.	52
Figure 36: fluidization ratio vs selectivity to CH <sub>4</sub> of test run 1.	53
Figure 37: time vs average temperature of test run 1.	54
Figure 38: time vs temperature at different height in the draft tube.	55
Figure 39: time vs temperature at different height in the annular region.	55
Figure 40: fluidization ratio vs methane yield of test run 2.	57
Figure 41: fluidization ratio vs CO conversion of test run 2.	58
Figure 42: fluidization ratio vs selectivity from CO to CH <sub>4</sub> of test run 2.	59
Figure 43: time vs average temperature of test run 2.	60
Figure 44: temperature vs outlet CO percentage by volume of test run 3.	61
Figure 45: temperature vs outlet H <sub>2</sub> percentage by volume of test run 3.	61
Figure 46: temperature vs outlet CO <sub>2</sub> percentage by volume of test run 3.	62
Figure 47: temperature vs outlet CH <sub>4</sub> percentage by volume of test run 3.	62
Figure 48: temperature vs outlet H <sub>2</sub> O percentage by volume of test run 3.	62
Figure 49: temperature vs methane yield of test run 3.	63
Figure 50: temperature vs carbon monoxide conversion of test run 3.	64
Figure 51: temperature vs selectivity from carbon monoxide to methane of test run 3.	64
Figure 52: temperature vs outlet CO percentage by volume of test run 4.	66



Figure 53: temperature vs outlet H <sub>2</sub> percentage by volume of test run 4. ....	66
Figure 54: temperature vs outlet CO <sub>2</sub> percentage by volume of test run 4.....	67
Figure 55: temperature vs outlet CH <sub>4</sub> percentage by volume of test run 4.....	67
Figure 56: temperature vs outlet H <sub>2</sub> O percentage by volume of test run 4. ....	68
Figure 57: temperature vs methane yield of test run 4. ....	69
Figure 58: temperature vs carbon dioxide conversion of test run 4. ....	69
Figure 59: temperature vs selectivity from CO <sub>2</sub> to methane of test run 4. ....	70
Figure 60: temperature vs outlet CO percentage by volume of test run 5.....	71
Figure 61: temperature vs outlet H <sub>2</sub> percentage by volume of test run 5. ....	72
Figure 62: temperature vs outlet CO <sub>2</sub> percentage by volume of test run 5.....	72
Figure 63: temperature vs outlet CH <sub>4</sub> percentage by volume of test run 5.....	73
Figure 64: temperature vs outlet H <sub>2</sub> O percentage by volume of test run 5. ....	73
Figure 65: temperatures vs methane yield of test run 5.....	74
Figure 66: temperatures vs carbon dioxide conversion of test run 5.....	75
Figure 67: temperature vs selectivity from CO <sub>2</sub> to methane of test run 5. ....	75
Figure 68: temperature vs outlet CO percentage by volume of test run 6.....	77
Figure 69: temperature vs outlet H <sub>2</sub> percentage by volume of test run 6. ....	77
Figure 70: temperature vs outlet CO <sub>2</sub> percentage by volume of test run 6.....	78
Figure 71: temperature vs outlet CH <sub>4</sub> percentage by volume of test run 6.....	78
Figure 72: temperature vs outlet H <sub>2</sub> O percentage by volume of test run 6. ....	79
Figure 73: temperatures vs methane yield of test run 6.....	80
Figure 74: temperatures vs carbon dioxide conversion of test run 6.....	80
Figure 75: temperatures vs selectivity from CO <sub>2</sub> to CH <sub>4</sub> of test run 6. ....	81
Figure 76: temperature vs CO outlet percentage by volume of test run 7.....	82
Figure 77: temperature vs H <sub>2</sub> outlet percentage by volume of test run 7. ....	83
Figure 78: temperature vs CO <sub>2</sub> outlet percentage by volume of test run 7.....	83

Figure 79: temperature vs CH <sub>4</sub> outlet percentage by volume of test run 7.....	84
Figure 80: temperature vs H <sub>2</sub> O outlet percentage by volume of test run 7. ....	84
Figure 81: temperature vs methane yield of test run 7. ....	85
Figure 82: temperature vs carbon monoxide conversion of test run 7. ....	86
Figure 83: temperature vs carbon dioxide conversion of test run 7. ....	86
Figure 84: temperature vs CO outlet percentage by volume of test run 8.....	88
Figure 85: temperature vs H <sub>2</sub> outlet percentage by volume of test run 8. ....	88
Figure 86: temperature vs CO <sub>2</sub> outlet percentage by volume of test run 8.....	89
Figure 87: temperature vs CH <sub>4</sub> outlet percentage by volume of test run 8.....	89
Figure 88: temperature vs H <sub>2</sub> O outlet percentage by volume of test run 8. ....	90
Figure 89: temperature vs methane yield of test run 8. ....	91
Figure 90: temperature vs carbon monoxide conversion of test run 8. ....	91
Figure 91: temperature vs carbon dioxide conversion of test run 8. ....	92
Figure 92: time vs temperature in the different reactor regions for WHSV=1.3 NI·h <sup>-1</sup> ·g <sub>cat</sub> <sup>-1</sup> .....	93
Figure 93: time vs temperature in the different reactor regions for WHSV=1.8 NI·h <sup>-1</sup> ·g <sub>cat</sub> <sup>-1</sup> .....	94

## References

- [1] Christof Rühl, 'BP: statistical review of world energy, June 2010', *Vopr. Ekon.*, vol. 2010, no. 10, pp. 101–112, 2010.
- [2] Eurostat, 'Energy balance flow for IT 2018.pdf', 2018. [Online]. Available: [https://ec.europa.eu/eurostat/cache/sankey/energy/sankey.html?geos=IT&year=2018&unit=GJ&fuels=TOTAL&highlight=\\_&nodeDisagg=0101000000000&flowDisagg=true&translateX=0&translateY=0&scale=1&language=EN](https://ec.europa.eu/eurostat/cache/sankey/energy/sankey.html?geos=IT&year=2018&unit=GJ&fuels=TOTAL&highlight=_&nodeDisagg=0101000000000&flowDisagg=true&translateX=0&translateY=0&scale=1&language=EN).
- [3] Eurostat, 'Energy balance flow for AT 2018.pdf', 2018. [Online]. Available: [https://ec.europa.eu/eurostat/cache/sankey/energy/sankey.html?geos=AT&year=2018&unit=GJ&fuels=TOTAL&highlight=\\_&nodeDisagg=0101000000000&flowDisagg=true&translateX=0&translateY=0&scale=1&language=EN](https://ec.europa.eu/eurostat/cache/sankey/energy/sankey.html?geos=AT&year=2018&unit=GJ&fuels=TOTAL&highlight=_&nodeDisagg=0101000000000&flowDisagg=true&translateX=0&translateY=0&scale=1&language=EN).
- [4] A. Duret, C. Friedli, and F. Maréchal, 'Process design of Synthetic Natural Gas (SNG) production using wood gasification', *J. Clean. Prod.*, vol. 13, no. 15, pp. 1434–1446, 2005, doi: 10.1016/j.jclepro.2005.04.009.
- [5] A. Kakoei and A. Gharehghani, 'Carbon oxides methanation in equilibrium; a thermodynamic approach', *Int. J. Hydrogen Energy*, vol. 45, no. 55, pp. 29993–30008, 2020, doi: 10.1016/j.ijhydene.2020.08.073.
- [6] J. Kopyscinski, T. J. Schildhauer, and S. M. A. Biollaz, 'Fluidized-bed methanation: Interaction between kinetics and mass transfer', *Ind. Eng. Chem. Res.*, vol. 50, no. 5, pp. 2781–2790, 2011, doi: 10.1021/ie100629k.
- [7] T. J. Schildhauer and S. M. A. Biollaz, *Synthetic Natural Gas: From Coal, Dry Biomass, and Power-to-Gas Applications*, vol. 2016, no. 8. 2016.
- [8] M. Gassner and F. Maréchal, 'Thermo-economic optimisation of the polygeneration of synthetic natural gas (SNG), power and heat from lignocellulosic biomass by gasification and methanation', *Energy Environ. Sci.*, vol. 5, no. 2, pp. 5768–5789, 2012, doi: 10.1039/c1ee02867g.
- [9] J. Kopyscinski, T. J. Schildhauer, and S. M. A. Biollaz, 'Production of synthetic natural gas (SNG) from coal and dry biomass - A technology review from 1950 to 2009', *Fuel*, vol. 89, no. 8, pp. 1763–1783, 2010, doi: 10.1016/j.fuel.2010.01.027.

- [10] J. C. Schmid, F. Benedikt, J. Fuchs, A. M. Mauerhofer, S. Müller, and H. Hofbauer, ‘Syngas for biorefineries from thermochemical gasification of lignocellulosic fuels and residues—5 years’ experience with an advanced dual fluidized bed gasifier design’, *Biomass Convers. Biorefinery*, 2019, doi: 10.1007/s13399-019-00486-2.
- [11] J. Li *et al.*, ‘Enhanced fluidized bed methanation over a Ni/Al<sub>2</sub>O<sub>3</sub> catalyst for production of synthetic natural gas’, *Chem. Eng. J.*, vol. 219, pp. 183–189, 2013, doi: 10.1016/j.cej.2013.01.005.
- [12] H. Hofbauer, ‘Biomass Gasification for Electricity and Fuels, large scale’, 2013, pp. 459–478.
- [13] A. Bartik, F. Benedikt, A. Lunzer, C. Walcher, S. Müller, and H. Hofbauer, ‘Thermodynamic Investigation of SNG Production Based on Dual Fluidized Bed Gasification of Biogenic Residues’, *Icps 2019*, 2019.
- [14] P. Biegger, F. Kirchbacher, A. Roza Medved, M. Miltner, M. Lehner, and M. Harasek, ‘Development of honeycomb methanation catalyst and its application in power to gas systems’, *Energies*, vol. 11, no. 7, pp. 1–17, 2018, doi: 10.3390/en11071679.
- [15] R. Y. Chein, C. T. Yu, and C. C. Wang, ‘Numerical simulation on the effect of operating conditions and syngas compositions for synthetic natural gas production via methanation reaction’, *Fuel*, vol. 185, pp. 394–409, 2016, doi: 10.1016/j.fuel.2016.07.123.
- [16] S. Chopra and A. K. Jain, ‘A Review of Fixed Bed Gasification Systems for Biomass’, *E-Journal - Int. Kommission für Agrartechn.*, vol. 9, no. 5, pp. 1–23, 2007.
- [17] J. Gil, J. Corella, M. P. Aznar, and M. A. Caballero, ‘Biomass gasification in atmospheric and bubbling fluidized bed: Effect of the type of gasifying agent on the product distribution’, *Biomass and Bioenergy*, vol. 17, no. 5, pp. 389–403, 1999, doi: 10.1016/S0961-9534(99)00055-0.
- [18] E. Shayan, V. Zare, and I. Mirzaee, ‘Hydrogen production from biomass gasification; a theoretical comparison of using different gasification agents’, *Energy Convers. Manag.*, vol. 159, no. August 2017, pp. 30–41, 2018, doi: 10.1016/j.enconman.2017.12.096.
- [19] A. Habibollahzade, P. Ahmadi, and M. A. Rosen, ‘Biomass gasification using various gasification agents: Optimum feedstock selection, detailed numerical analyses and tri-objective grey wolf optimization’, *J. Clean. Prod.*, vol. 284, p. 124718, 2021, doi:

10.1016/j.jclepro.2020.124718.

- [20] M. Siedlecki, W. de Jong, and A. H. M. Verkooijen, ‘Fluidized bed gasification as a mature and reliable technology for the production of bio-syngas and applied in the production of liquid transportation fuels-a review’, *Energies*, vol. 4, no. 3, pp. 389–434, 2011, doi: 10.3390/en4030389.
- [21] J. Fuchs, J. C. Schmid, S. Müller, and H. Hofbauer, ‘Dual fluidized bed gasification of biomass with selective carbon dioxide removal and limestone as bed material: A review’, *Renew. Sustain. Energy Rev.*, vol. 107, no. August 2018, pp. 212–231, 2019, doi: 10.1016/j.rser.2019.03.013.
- [22] P. J. Woolcock and R. C. Brown, ‘A review of cleaning technologies for biomass-derived syngas’, *Biomass and Bioenergy*, vol. 52, pp. 54–84, 2013, doi: 10.1016/j.biombioe.2013.02.036.
- [23] M. Asadullah, ‘Biomass gasification gas cleaning for downstream applications: A comparative critical review’, *Renew. Sustain. Energy Rev.*, vol. 40, pp. 118–132, 2014, doi: 10.1016/j.rser.2014.07.132.
- [24] J. R. Rostrup-Nielsen, K. Pedersen, and J. Sehested, ‘High temperature methanation. Sintering and structure sensitivity’, *Appl. Catal. A Gen.*, vol. 330, no. 1–2, pp. 134–138, 2007, doi: 10.1016/j.apcata.2007.07.015.
- [25] X. Bai, S. Wang, T. Sun, and S. Wang, ‘Influence of operating conditions on carbon deposition over a Ni catalyst for the production of synthetic natural gas (SNG) from coal’, *Catal. Letters*, vol. 144, no. 12, pp. 2157–2166, 2014, doi: 10.1007/s10562-014-1379-1.
- [26] A. Kambolis, T. J. Schildhauer, and O. Kröcher, ‘CO methanation for synthetic natural gas production’, *Chimia (Aarau)*, vol. 69, no. 10, pp. 608–613, 2015, doi: 10.2533/chimia.2015.608.
- [27] N. Pernicone and F. Traina, ‘Catalyst activation by reduction’, *Pure Appl. Chem.*, vol. 50, no. 9–10, pp. 1169–1191, 1978, doi: 10.1351/pac197850091169.
- [28] I. Chen and D. W. Shiue, ‘Reduction of nickel-alumina catalysts’, *Ind. Eng. Chem. Res.*, vol. 27, no. 3, pp. 429–434, 1988, doi: 10.1021/ie00075a011.
- [29] R. P. W. J. Struis, T. J. Schildhauer, I. Czekaj, M. Janousch, S. M. A. Biollaz, and C.

Ludwig, 'Sulphur poisoning of Ni catalysts in the SNG production from biomass: A TPO/XPS/XAS study', *Appl. Catal. A Gen.*, vol. 362, no. 1–2, pp. 121–128, 2009, doi: 10.1016/j.apcata.2009.04.030.

- [30] I. Kuznecova and J. Gusca, 'Property based ranking of CO and CO<sub>2</sub> methanation catalysts', *Energy Procedia*, vol. 128, pp. 255–260, 2017, doi: 10.1016/j.egypro.2017.09.068.
- [31] A. Lazdans, E. Dace, and J. Gusca, 'Development of the Experimental Scheme for Methanation Process', *Energy Procedia*, vol. 95, pp. 540–545, 2016, doi: 10.1016/j.egypro.2016.09.082.
- [32] T. J. Prins, 'UCLA UCLA Electronic Theses and Dissertations Title', 2019.
- [33] J. Wambach, A. Baiker, and A. Wokaun, 'CO<sub>2</sub> hydrogenation over metal / zirconia catalysts CO CO hydrogenation over metal / zirconia catalysts', *Phys. Chem. Chem. Phys.*, vol. 1, pp. 5071–5080, 1999.
- [34] G. A. Mills and F. W. Steffgen, 'Catalytic Methanation', *Catal. Rev.*, vol. 8, no. 1, pp. 159–210, Jan. 1974, doi: 10.1080/01614947408071860.
- [35] 'Daily Metal Spot Prices- Ruthenium Price (USD / Kilogram) for the Last Day', 2021. .
- [36] 'Daily Metal Spot Prices - Nickel Price (USD / Kilogram) for the Last Week', 2021. .
- [37] S. Rönsch *et al.*, 'Review on methanation - From fundamentals to current projects', *Fuel*, vol. 166, pp. 276–296, 2016, doi: 10.1016/j.fuel.2015.10.111.
- [38] S. Rahmani, M. Rezaei, and F. Meshkani, 'Preparation of highly active nickel catalysts supported on mesoporous nanocrystalline  $\gamma$ -Al<sub>2</sub>O<sub>3</sub> for CO<sub>2</sub> methanation', *J. Ind. Eng. Chem.*, vol. 20, no. 4, pp. 1346–1352, 2014, doi: 10.1016/j.jiec.2013.07.017.
- [39] J. Gao *et al.*, 'Ni/Al<sub>2</sub>O<sub>3</sub> catalysts for CO methanation: Effect of Al<sub>2</sub>O<sub>3</sub> supports calcined at different temperatures', *J. Energy Chem.*, vol. 22, no. 6, pp. 919–927, 2013, doi: 10.1016/S2095-4956(14)60273-4.
- [40] D. Hu *et al.*, 'Enhanced investigation of CO methanation over Ni/Al<sub>2</sub>O<sub>3</sub> catalysts for synthetic natural gas production', *Ind. Eng. Chem. Res.*, vol. 51, no. 13, pp. 4875–4886, 2012, doi: 10.1021/ie300049f.
- [41] M. Götz, A. M. D. Koch, and F. Graf, 'State of the art and perspectives of CO<sub>2</sub>

methanation process concepts for power-to-gas applications’, *Int. Gas Res. Conf. Proc.*, vol. 1, no. January, pp. 314–327, 2014.

- [42] A. Bolt, I. Dincer, and M. Agelin-Chaab, ‘A critical review of synthetic natural gas production techniques and technologies’, *J. Nat. Gas Sci. Eng.*, vol. 84, no. October, p. 103670, 2020, doi: 10.1016/j.jngse.2020.103670.
- [43] B. Liu and S. Ji, ‘Comparative study of fluidized-bed and fixed-bed reactor for syngas methanation over Ni-W/TiO<sub>2</sub>-SiO<sub>2</sub> catalyst’, *J. Energy Chem.*, vol. 22, no. 5, pp. 740–746, 2013, doi: 10.1016/S2095-4956(13)60098-4.
- [44] M. C. Seemann, T. J. Schildhauer, S. M. A. Biollaz, S. Stucki, and A. Wokaun, ‘The regenerative effect of catalyst fluidization under methanation conditions’, *Appl. Catal. A Gen.*, vol. 313, no. 1–2, pp. 14–21, 2006, doi: 10.1016/j.apcata.2006.06.048.
- [45] D. Kunii and O. Levenspiel, *1991 Fluidization Engineering, Kunii - Levenspiel.pdf*.
- [46] R. Cocco, S. B. R. Karri, and T. Knowlton, ‘Introduction to fluidization’, *Chem. Eng. Prog.*, vol. 110, no. 11, pp. 21–29, 2014.
- [47] H. Hofbauer, ‘Lecture from the course: Fluidization Technology’, 2017.
- [48] D. Kunii and O. Levenspiel, ‘Circulating fluidized-bed reactors’, vol. 52, no. 15, pp. 2471–2482, 1997.
- [49] A. Atta, S. A. Razzak, K. D. P. Nigam, and J. X. Zhu, ‘(Gas) - Liquid - Solid circulating fluidized bed reactors: Characteristics and applications’, *Ind. Eng. Chem. Res.*, vol. 48, no. 17, pp. 7876–7892, 2009, doi: 10.1021/ie900163t.
- [50] S. K. B. Song, Y. Kim, ‘Circulation of solids and gas bypassing in an internally circulating fluidized bed with a draft tube’, vol. 14, no. 4, p. 2500, 1997.
- [51] J. H. Jeon, S. D. Kim, S. J. Kim, and Y. Kang, ‘Solid circulation and gas bypassing characteristics in a square internally circulating fluidized bed with draft tube’, *Chem. Eng. Process. Process Intensif.*, vol. 47, no. 12, pp. 2351–2360, 2008, doi: 10.1016/j.cep.2008.01.011.
- [52] A. Bartik *et al.*, ‘Development of an internally circulating fluidized bed for catalytic methanation of syngas’, 2020.
- [53] F. Cheng and V. Dupont, ‘Nickel catalyst auto-reduction during steam reforming of bio-

oil model compound acetic acid', *Int. J. Hydrogen Energy*, vol. 38, no. 35, pp. 15160–15172, 2013, doi: 10.1016/j.ijhydene.2013.09.111.

- [54] C. Li and Y. W. Chen, 'Temperature-programmed-reduction studies of nickel oxide/alumina catalysts: effects of the preparation method', *Thermochim. Acta*, vol. 256, no. 2, pp. 457–465, 1995, doi: 10.1016/0040-6031(94)02177-P.